

The Evolution of Galaxies in Groups



Rhea-Silvia Remus

The Evolution of Galaxies in Groups

Diploma Thesis

at the
Ludwig–Maximilians–Universität (LMU) München

submitted by

Rhea-Silvia Remus

born on April 22nd 1983 in Hamburg

supervised by

Prof. Dr. Andreas Burkert

Munich, March 10th 2009

1st Evaluator: Prof. Dr. Andreas Burkert

2nd Evaluator: Prof. Dr. Ralf Bender

Contents

| | | |
|----------|--|-----------|
| 1 | Introduction | 7 |
| 2 | Theoretical Background | 9 |
| 2.1 | Dark Matter | 9 |
| 2.2 | The Friedman Universe | 11 |
| 2.3 | The Hubble Parameter | 13 |
| 2.4 | Density Perturbations | 13 |
| 2.5 | Hierarchical Growth | 16 |
| 2.5.1 | Top-Hat Collapse of Dark Matter Structures | 17 |
| 2.5.2 | Press-Schechter Mass Function | 18 |
| 3 | Observations | 19 |
| 3.1 | WMAP - Cosmic Microwave Background Survey | 19 |
| 3.2 | Galaxy Groups in Observations | 20 |
| 3.2.1 | X-Ray Luminous Galaxy Groups and Intra Group Light | 21 |
| 3.2.2 | Observational Group Classification | 23 |
| 3.2.3 | Supergroup SG1120-1202: A Protocluster | 27 |
| 3.3 | Galaxy Surveys at Intermediate Redshift | 27 |
| 3.3.1 | CNOC2 (Canadian Network for Observational Cosmology) | 27 |
| 3.3.2 | SDSS (Sloan Digital Sky Survey) | 30 |
| 3.3.3 | 2dF | 31 |
| 3.4 | Galaxy Groups in Theoretical Discussion | 31 |
| 4 | Methods | 34 |
| 4.1 | The Simulation | 34 |
| 4.2 | The Friends-of-Friends-Algorithm (FOF) | 34 |
| 4.3 | The SUBFIND-Algorithm | 35 |
| 4.4 | Merger Tree Construction | 35 |
| 5 | The Group Halos | 40 |
| 5.1 | The SUBFIND Sample | 40 |
| 5.1.1 | Mass Accretion History | 40 |
| 5.1.2 | The Special Case of Disturbed Halos | 43 |
| 5.2 | The FOF-Sample | 44 |
| 5.2.1 | Differences between FOF and SUBFIND | 44 |
| 5.2.2 | Mass Accretion History | 46 |
| 5.3 | Global Properties of the Groups | 48 |

Contents

| | | |
|----------|---|-----------|
| 5.3.1 | Formation Redshift | 50 |
| 5.4 | Mergers | 53 |
| 5.4.1 | Group Mergers | 54 |
| 5.4.2 | Multiple Merger Events | 55 |
| 5.5 | Discussion | 59 |
| 6 | Subhalos | 61 |
| 6.1 | Subhalo Abundance | 61 |
| 6.2 | Subhalo Mass Function at $z = 0$ | 62 |
| 6.3 | Phenomenological Description of Subhalo Evolution | 65 |
| 6.4 | Subhalo-Subhalo Mergers | 65 |
| 6.5 | Projected Velocity Dispersion | 69 |
| 6.5.1 | Comparison with Observed Velocity Dispersions | 69 |
| 6.6 | Discussion | 72 |
| 7 | Comparison with Observations | 73 |
| 7.1 | Fossil groups | 74 |
| 7.1.1 | The Most Fossil Group | 76 |
| 7.2 | Compact Groups | 78 |
| 7.3 | Luminosity of the Most Luminous Group Member | 79 |
| 7.4 | Discussion | 81 |
| 8 | Summary: the Evolution of Groups of Galaxies | 82 |
| 9 | Outlook | 85 |
| A | The SUBFIND Groups | 86 |
| B | The FOF Groups | 88 |
| C | Calculating the Group Radius | 90 |
| | Bibliography | 91 |

1 Introduction

Studies of the large scale structure of the universe revealed that galaxies live in several different environments. Some galaxies live in the field, that is they show no signs of interaction with neighbouring galaxies and the distances between the galaxy and its nearest massive neighbour are large compared to their size. Most of the field galaxies are spiral galaxies. In contrast a cluster consists of more than 100 galaxies within between 2 – 10 Mpc and therefore is therefore a very dense region. Galaxies in these environments have very high relative velocities and show signs of interactions. The fraction of elliptical galaxies is high compared to the field.

Galaxy groups are less massive and less dense than clusters. They normally consist of a few to 100 members with intermediate velocities. Galaxies in groups usually show signs of strong interactions and mergers. The galaxy group environment is a highly active environment (Mamon, 1992) with observable changes in the morphology of a galaxy and starburst phenomena. Observations have shown that about 50-70% of all galaxies live in a galaxy group environment (Wilman et al., 2005c; Eke et al., 2004). If we want to understand the formation and evolution of galaxies we have to better understand galaxy evolution in the group environment.

There has been a wide range of observations of galaxy groups since Abell detected galaxy overdensities in 1958. Groups of galaxies have been cast into three broad categories: Compact groups are groups with four or more bright members in an isolated environment, fossil groups are groups dominated by a single luminous, giant elliptical and loose groups are groups of galaxies spread about 1Mpc but nevertheless showing signs of distortion by tidal forces. A catalogue of compact groups has been provided by Hickson (1982) which is used in many studies dealing with this kind of groups (for example Da Rocha and Mendes de Oliveira, 2005; Da Rocha et al., 2008; Hunsberger et al., 1998), a sample of fossil groups has been presented by Jones et al. (2003) or by La Barbera et al. (2008).

It is difficult to identify galaxy groups in observations since they are medium overdensities of galaxies in two dimensions and therefore it is difficult to distinguish between galaxy groups and accumulations of galaxies caused by projectional effects.

Recently several studies using various galaxy surveys like SDSS and 2dF at intermediate redshifts have been published (for example Wilman et al., 2005b,a, 2008; McConnachie et al., 2008; Eke et al., 2006). These surveys include the possibility to identify the redshifts of galaxies and therefore they provide the possibility to distinguish better between projectional effects and real galaxy groups. They also provide better statistics and therefore the analysis of global group properties.

It is still an open question whether galaxy groups have a global dark matter halo or not. Simulations by Athanassoula et al. (1997) predict that the lifetime of

1 Introduction

compact groups grows significantly assuming a global group dark matter halo, so that the observed amount of compact groups can be explained. On the other hand studies of intra group light (Da Rocha and Mendes de Oliveira, 2005) predict that there is a fraction of groups, especially loose groups, that do not show any signs of a global halo and therefore can simply be an assembly of galaxies interacting with each other, building a global dark matter halo in the future.

In the standard cosmology assumed today, the Λ Cold Dark Matter (Λ CDM) scenario, galaxies form at the center of dark matter halos. These dark matter halos grow by assembling smaller dark matter structures, while the galaxies within these accreted dark matter halos become satellite galaxies (White and Rees, 1978). For the study of galaxy formation it is therefore necessary to first understand the evolution of dark matter halos.

Numerical simulations have shown that there are several processes for the mass assembly of a dark matter halo: merger events between two nearly equally massive halos, called major merger, merger between a massive halo and a small satellite halo, called minor merger, and the accretion of material that is not correlated with the assembly of a halo, for example in the course of a flyby event. The mass accretion history of halos is important for studying the substructure, the environment, the formation time and other statistical halo properties.

With increasing availability of cosmological simulations a lot of studies of general properties of dark matter halos of various masses have been published (for example Li et al., 2007; Angulo et al., 2008; Genel et al., 2008). While those results are not directly targeted at groups we will be able to compare our results with them as far as possible.

In this work we will analyze dark matter halos of galaxy group mass in a Λ CDM dark matter only simulation of a $100^3 h^{-3} \text{Mpc}^3$ box with 512^3 particles in each direction and with $\Omega_0 = 0.26$, $\Omega_\Lambda = 0.74$ and $h = 0.72$.

One of the major motivations for this work was to be able to compare simulated results with observations, because observers are only able to see one snapshot in the evolution of a special galaxy group. Ultimately it should be possible to approximately identify an observed group with a group in our simulation. Since we are able to follow a group halo through cosmological time in simulations we can predict galaxy group properties at different stages of their evolution.

In the process to reach this goal we will first investigate the mass accretion history, the formation time and the merger history of galaxy group halos in chapter 5, in chapter 6 we will analyze substructures within these group halos and in chapter 7 we will show a first attempt to populate the dark matter halos with baryons and compare our results with observations by Wilman et al. (2005b,a). A discussion of our findings is presented in chapter 8.

2 Theoretical Background

Since this work will deal with halos from a cosmological dark matter only simulation it is necessary to study the theoretical basis for structure formation in the universe. The main point of this chapter is to introduce dark matter, especially cold dark matter, and the formation of structure in a cold dark matter scenario. This scenario is important for our study of the mass accretion history and the subhalo assembly, as the results depend strongly on the choice of this model.

2.1 Dark Matter

It is known from Kepler's law

$$v^2(R) = \frac{GM(R)}{R}$$

that the velocity, at which a satellite orbits a central mass, decreases with increasing orbital distance. Since most of the visible matter of a spiral galaxy is concentrated at its center, this law should also apply to its outer parts. Therefore, if we measure rotational velocities of stars in the Milky Way around the galactic center, we expect a steep rise for these velocities at low radial distances, where the local density is not yet significantly lower than at the center, followed by a slow decrease towards higher radial distances.

However, observations revealed a different scenario. For the Milky Way the effect described in the following was measured by Clemens (1985) (see Fig. 2.1). While the description given above is right for the more central regions of the galaxy, after attaining a maximum close to the galactic center the rotational velocity of the stars decreases to a local minimum at about 3kpc followed by a slow increase of rotational velocities. Since we do not find any visible matter to explain this increase in velocities, it has been suggested that there exists mass causing this phenomenon, which is hidden from the observers' view. It has therefore been called dark matter.

In order to cause the observed effect, dark matter has to be more evenly distributed within the galaxy than the visible matter. It turns out that the density of the dark matter halo of a spiral galaxy is proportional to R^{-2} , that is the mass inside R increases linearly with the distance R . Due to this fact it is not possible to determine the dark matter mass of a galaxy without knowing the limits of the surrounding dark matter halo. It is very difficult to observe this limit, since there are less and less objects surrounding a galaxy for which the rotational velocity can be estimated.

2 Theoretical Background

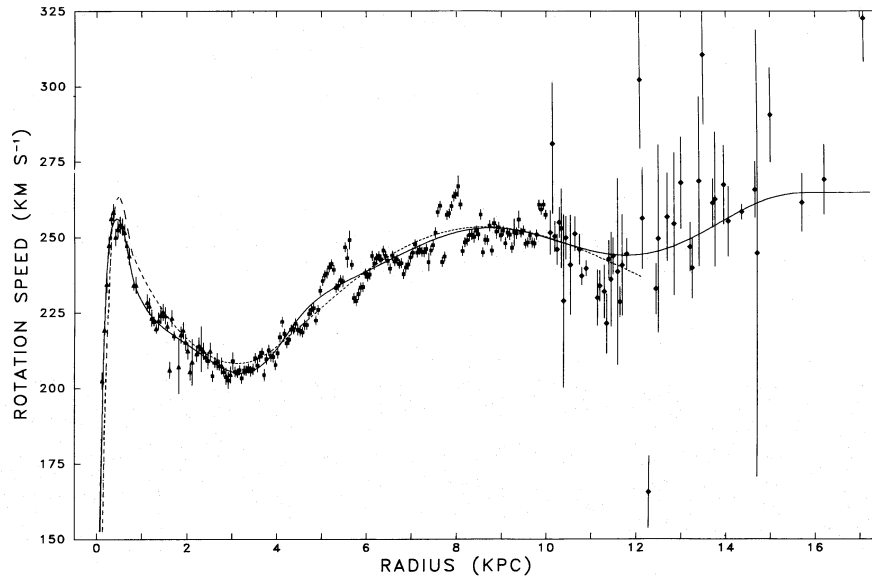


Figure 2.1: Figure 3 taken from Clemens (1985): The rotation curve of the Milky Way. For the outer parts the measurements have larger errors since the rotational velocity is more difficult to detect.

As we have seen, it is possible to detect dark matter in spiral galaxies using the rotation of stars. Since stellar orbits are much more complicated in elliptical galaxies this approach is not feasible for these galaxies. Nevertheless, dark matter has been observed in some elliptical galaxies that contain a bright X-ray luminous gas halo. The temperature of this gas is a good estimate for the depth of the potential well and therefore an indicator for the dark mass.

Despite those observational efforts, the nature of dark matter is still unknown today. It most likely cannot be explained by cold baryonic matter (e.g. brown dwarves), since this would imply a significantly higher density of baryonic matter in the universe. In that case the ratio of deuterium D to helium He^4 in the primordial medium (measured in Quasars) would be lower than actually measured because more deuterium would be destroyed during the primordial nucleosynthesis (see Schneider, 2006). Therefore, dark matter must be different from common baryons. Since such dark matter particles have not been detected by now it is assumed that they do not couple with any elementary force except gravitation.

There are two different candidates for dark matter, characterized by their different mass and velocity ranges:

- **Hot Dark Matter (HDM)** consists of particles that moved at very high speeds at the time of their decoupling¹ from the remaining matter during the formation of the universe. These particles have very low masses. Possible

¹i.e. the mean free path of a particle exceeds the event horizon of the universe

candidates are neutrinos, which most likely have small but nonzero masses and move with high speed.

- **Cold Dark Matter (CDM)** particles decoupled during an earlier stage of the early universe, thus the particles are slower and therefore are more massive than the HDM particles. Possible candidates are for example supersymmetric particles.

Of course a combination of these dark matter candidates might also be possible. The most likely candidate assumed today is the Cold Dark Matter.

2.2 The Friedman Universe

The Friedman model of the universe is one of the simplest models of cosmology. The universe is assumed to consist of self-gravitating matter of density ϱ that is homogeneous and isotropic² on large scales.

Since Einstein invented his general theory of relativity we know that by the equivalence of matter and energy radiation has to be considered when computing the gravitational field. Assuming that the universe is filled with a radiational field (for example the cosmic microwave background, see section 3.1), we have to add the mass density $\frac{3p}{c^2}$ of this field to the matter density ϱ . From observations by Riess et al. (1998) we know that there is a repulsive force in the universe, which is attributed to a cosmological constant Λ interpreted as the density of the vacuum.

Under these assumptions Einstein's field equations can be simplified to

$$\ddot{a} = -\frac{4\pi G}{3}a\left(\varrho + \frac{3p}{c^2}\right) + \frac{1}{3}\Lambda a; \quad (2.1)$$

$$\dot{a}^2 = \frac{8\pi G\varrho}{3}a^2 - \frac{c^2}{\mathfrak{R}^2} + \frac{1}{3}\Lambda a^2, \quad (2.2)$$

where a is the scale factor³ and \mathfrak{R} is the present-day radius of curvature of the universe. Here equation (2.2) is the first integral of equation (2.1) and $-\frac{c^2}{\mathfrak{R}^2}$ is the constant of integration representing the initial energy in the universe. These equations are called the Friedman-equations. For further details see for example Mukhanov (2005) or Longair (2008).

In the later stages of cosmic evolution, we can safely assume p to be 0. Since mass is conserved we have $\varrho = a^{-3}\varrho_0$, where ϱ_0 is the present-day density (this holds for all kinds of densities that will be introduced later).

In a universe with cosmological constant $\Lambda = 0$ the following holds: If the density of the universe is low, it will expand forever, whereas a dense universe will be governed by gravity and ultimately collapse. In the first case, the universe will have hyperbolic geometry ($\frac{c^2}{\mathfrak{R}^2} < 0$), while in the second case it will be spherical ($\frac{c^2}{\mathfrak{R}^2} > 0$).

²That is the universe looks the same from every point and in each direction.

³The scale factor gives the size of the universe normalized to a present-day value of 1.

2 Theoretical Background

The critical density, which differentiates between those two cases, is found by setting $\frac{c^2}{\mathfrak{R}^2} = 0$ in equation (2.2), resulting in

$$\varrho_c = \frac{3H_0^2}{8\pi G}, \quad (2.3)$$

where $H_0 = \frac{\dot{a}_0}{a_0}$ is the present-day value of the Hubble constant. We now define the density parameter

$$\Omega_0 = \frac{\varrho_0}{\varrho_c}. \quad (2.4)$$

Since our universe is made of several components, we define ϱ_B , ϱ_{DM} to be the densities associated to baryonic and dark matter respectively and set Ω_B and Ω_{DM} accordingly, which are included in Ω_0 .

Let us now assume that $\Lambda > 0$. Equation (2.1) shows that Λ causes an outward force even in an empty universe ($\varrho = 0$). Zeldovich showed in 1986 that this constant may then be an expression for the vacuum-energy-density. Defining ϱ_V via

$$\Lambda = 8\pi G\varrho_V,$$

we find that equation (2.1) at $t = t_0$ (thus $a = 1$) takes the form

$$\ddot{a}_0 = -\frac{4\pi G\varrho_0}{3} + \frac{8\pi G\varrho_V}{3}.$$

We can now define

$$\Omega_\Lambda = \frac{\varrho_V}{\varrho_c}$$

with ϱ_c as in equation (2.3).

The Friedman equations now take the following form:

$$\ddot{a} = -\frac{\Omega_0 H_0^2}{2a^2} + \Omega_\Lambda H_0^2 a; \quad (2.5)$$

$$\dot{a}^2 = \frac{\Omega_0 H_0^2}{a} - \frac{c^2}{\mathfrak{R}^2} + \Omega_\Lambda H_0^2 a^2. \quad (2.6)$$

At present-day we have $a = 1$ and $\dot{a} = H_0$, so from equation (2.6) it follows:

$$\frac{c^2}{\mathfrak{R}^2} = H_0^2(\Omega_0 + \Omega_\Lambda - 1). \quad (2.7)$$

Then for a flat ($\frac{c^2}{\mathfrak{R}^2} = 0$) universe we obtain

$$\Omega_0 + \Omega_\Lambda = 1.$$

2.3 The Hubble Parameter

When an object emits light of wavelength λ , this light is subjected to the universe's expansion. If the light was emitted at a time t , its wavelength has increased to

$$\lambda_{\text{present}} = \frac{\lambda}{a(t)}.$$

The redshift z is then defined as

$$z = \frac{\lambda_{\text{present}} - \lambda}{\lambda} = \frac{1}{a} - 1. \quad (2.8)$$

If we observe a photon with known redshift, it is possible, due to the constant speed of light, to determine the exact time and distance of its emission. Because of this it is often useful to state a redshift-value when referring to the time. Inserting equation (2.7) into equation (2.6) and using equation (2.8) we obtain

$$\frac{dz}{dt} = -H_0(1+z) \left((z+1)^2(\Omega_0 z + 1) - \Omega_\Lambda z(z+2) \right)^{\frac{1}{2}}.$$

Using the definition of the Hubble parameter, equations (2.6) and (2.7) also lead to an expression for the time dependent Hubble parameter $H(z)$:

$$H(z) = \frac{\dot{a}}{a} = H_0 \left((z+1)^2(\Omega_0 z + 1) - \Omega_\Lambda z(z+2) \right)^{\frac{1}{2}}.$$

The time that has passed since the emission of a photon from an object is

$$t = \int_0^z \frac{dz}{H(z)(1+z)},$$

which is also called the lookback time. On the other hand we also obtain a formula for the comoving distance

$$d = \frac{1}{a_0} \int_0^z \frac{dz}{H(z)}.$$

The comoving distance is the distance between two points taking the Hubble flow into account, i.e. the expansion of the universe with time is included. For a flat universe the comoving distance is equivalent to the real distance to an object.

2.4 Density Perturbations

So far we have studied a homogeneous universe. On a local scale however the universe is not homogeneous at all. The reason for this can be found in perturbations in the originally homogeneous universe. These perturbations have increased with time leading to concentrations of matter that would later form stars and galaxies.

The reason for these initial perturbations is found in the inflationary stage of our universe. During inflation the universe expanded rapidly so that vacuum fluctuations

2 Theoretical Background

were enlarged to form the perturbations that we see for example in the observations of the cosmic microwave background (see section 3.1).

We need to analyze the development of a perturbation with time. Therefore we assume the fundamental equations of hydrodynamics (Longair, 2008, page 313ff., page 377ff.):

$$\text{Equation of continuity:} \quad \frac{d\rho}{dt} = -\rho \nabla \cdot \mathbf{v}; \quad (2.9)$$

$$\text{Euler's Equation:} \quad \frac{d\mathbf{v}}{dt} = -\frac{1}{\rho} \nabla p - \nabla \phi; \quad (2.10)$$

$$\text{Poisson's Equation:} \quad \nabla^2 \phi = 4\pi G \rho, \quad (2.11)$$

Equation (2.9) describes the conservation of mass, equation (2.10) is the equation of motion for an element of the fluid and equation (2.11) is the equation for the gravitational potential caused by a density distribution ρ .

Let us assume an unperturbed ground state with first order perturbations, where $\mathbf{v} = \mathbf{v}_0 + \delta\mathbf{v}$, $\rho = \rho_0 + \delta\rho$, $p = p_0 + \delta p$ and $\phi = \phi_0 + \delta\phi$, where unperturbed quantities carry an index 0. As we expect our universe to be homogeneous and isotropic in its ground state, it follows that $\nabla \rho_0 = \nabla p_0 = 0$.

The unperturbed quantities satisfy equations (2.9) - (2.11). For the perturbations we obtain

$$\frac{d\Delta}{dt} = -\nabla \delta\mathbf{v}, \quad (2.12)$$

where $\Delta = \frac{\delta\rho}{\rho_0}$ is the density contrast. This describes the way in which the density contrast reacts to the velocity associated to the collapse of the perturbation. From equation (2.10) we get

$$\frac{d(\delta\mathbf{v})}{dt} + (\delta\mathbf{v} \cdot \nabla) \mathbf{v}_0 = -\frac{1}{\rho_0} \nabla \delta p - \nabla \delta\phi. \quad (2.13)$$

Finally equation (2.11) leads us to

$$\nabla^2 \delta\phi = 4\pi G \delta\rho. \quad (2.14)$$

Since we are dealing with an expanding universe it is convenient to introduce comoving coordinates defined by $\mathbf{x} = a(t)\mathbf{r}$ with usual spatial coordinate x and scale factor a . Then

$$\mathbf{v} = \frac{da}{dt} \mathbf{r} + a(t) \frac{d\mathbf{r}}{dt}.$$

We also introduce the perturbed comoving velocity \mathbf{u} with $\delta\mathbf{v} = a(t)\mathbf{u}$.

Equation (2.13) then becomes

$$\frac{d\mathbf{u}}{dt} + 2 \left(\frac{\dot{a}}{a} \right) \mathbf{u} = -\frac{1}{\rho_0 a^2} \nabla_c \delta p - \frac{1}{a^2} \nabla_c \delta\phi, \quad (2.15)$$

where ∇_c is the nabla operator in comoving coordinates.

We want to assume adiabatic perturbations, that is $\delta p = c_s^2 \delta \rho$. It has been shown by Coles and Lucchin (1995) that a good choice for c_s for dark matter is given by

$$v_s^{-2} = \frac{\int v^{-2} f(v) d^3 \mathbf{v}}{\int f(v) d^3 \mathbf{v}},$$

where $f(v)$ is the velocity distribution of the dark matter particles.

Taking divergence of equation (2.15) we obtain

$$\nabla_c \dot{\mathbf{u}} + 2 \left(\frac{\dot{a}}{a} \right) \nabla_c \mathbf{u} = -\frac{v_s^2}{\rho_0 a^2} \nabla_c^2 (\delta \rho) - \frac{1}{a^2} \nabla_c^2 (\delta \phi).$$

The time derivative of (2.12) is given as

$$\frac{d^2}{dt^2} \left(\frac{\delta \rho}{\rho} \right) = -\nabla \cdot \dot{\mathbf{u}}$$

Combining the last two equations and equation (2.14) we get

$$\frac{d^2 \Delta}{dt^2} + 2 \left(\frac{\dot{a}}{a} \right) \frac{d\Delta}{dt} = \frac{v_s^2}{\rho_0 a^2} \nabla_c^2 (\delta \rho) + 4\pi G \Delta \rho.$$

We are looking for wave solutions of the form $\Delta \propto \exp i(\mathbf{k}_c \cdot \mathbf{r} - \omega \mathbf{t})$ which leads us to

$$\frac{d^2 \Delta}{dt^2} + 2 \left(\frac{\dot{a}}{a} \right) \frac{d\Delta}{dt} = \Delta (4\pi G \rho_0 - k^2 v_s^2). \quad (2.16)$$

If we can neglect the internal pressure p then with $A = 4\pi G$ this equation becomes

$$\ddot{\Delta} + 2 \left(\frac{\dot{a}}{a} \right) \dot{\Delta} = \Delta A \rho. \quad (2.17)$$

Assume now that there are density waves both in the baryonic and dark matter. In that case we get two coupled equations

$$\ddot{\Delta}_B + 2 \left(\frac{\dot{a}}{a} \right) \dot{\Delta}_B = A \Delta_B \rho_B + A \Delta_{DM} \rho_{DM}; \quad (2.18)$$

$$\ddot{\Delta}_{DM} + 2 \left(\frac{\dot{a}}{a} \right) \dot{\Delta}_{DM} = A \Delta_B \rho_B + A \Delta_{DM} \rho_{DM}. \quad (2.19)$$

The right side of these equations, which expresses the gravitational influence, is exactly the same. Furthermore we assume the extreme case of $\rho_B \ll \rho_{DM}$, $\Omega_0 = 1$ and $\Lambda = 0$. This allows us to consider dark matter waves independently of baryonic matter. Therefore we get with the Friedman equations (2.1) and (2.2):

$$\Delta_{DM} = B a$$

with a constant B . Inserting this result into equation (2.18) we obtain

$$\ddot{\Delta}_B + 2 \left(\frac{\dot{a}}{a} \right) \dot{\Delta}_B = 4\pi G \rho_{DM} B a.$$

By substitution this yields

$$a^{\frac{3}{2}} \frac{d}{da} \left(a^{-\frac{1}{2}} \frac{d\Delta_B}{da} \right) + 2 \frac{d\Delta_B}{da} = \frac{3}{2} B.$$

This equation is solved by $\Delta_B = B(a - a_0)$. An important consequence of this result is, that even when $\Delta_B = 0$ the baryonic matter will follow the dark matter and therefore accumulate in the potential wells set up by perturbations of the dark matter. This justifies using a dark matter only simulation to understand the formation of galaxies and large scale structure.

2.5 Hierarchical Growth

The choice of the dark matter model has strong influence on the way how structure is formed out of the perturbations described in the previous section.

In the case of hot dark matter all smaller perturbations are quickly smoothed out since the dark matter particles move at very high speeds. Therefore only very large perturbations of at least $10^{15} M_\odot$ will live long enough in order to collapse and stabilize. Consequently during the evolution of the universe the large structures form first and the smaller structures appear by fragmentation at later stages. While this nicely explains the appearance of very large structures, it is in contradiction with observations of the early universe.

Cold dark matter on the other hand provides no mechanism that destroys smaller perturbations, since the cold dark matter particles are already non-relativistic at the time they decouple. Therefore, small perturbations collapse first and produce (virialized) dark matter halos, that accumulate baryons at the center, and thus smaller structures like globular clusters and galaxies are formed. The small dark matter halos cluster and build up the larger structures. This process is called the hierarchical growth, that is smaller structures collapse earlier than larger structures and the small structures aggregate successively into larger structures. Therefore, if we want to study galaxy formation we need to analyze and understand the assembly history and the structure of the dark matter halos.

Hierarchical growth and cold dark matter is actually the preferred mechanism of galaxy and large scale structure formation, as it is successfully reproducing the spectrum of fluctuations in the cosmic microwave background and the large-scale distribution of galaxies, which is why the Λ CDM models are the standard cosmological models used today as initial conditions for simulations.

2.5.1 Top-Hat Collapse of Dark Matter Structures

We assume a flat universe with $\Lambda = 0$. We study the collapse of a spherical homogeneous dark matter overdensity (top-hat) within this universe. Since this overdensity is spherical it is not influenced by the universe surrounding it, provided this universe is homogeneous. Therefore we can describe the overdensity using the Friedman equations (2.1) and (2.2) for a universe with $\Omega_0 > 1$.

As a solution we obtain

$$a_{\text{pert}} = A(1 - \cos(\theta)) \quad \text{with} \quad A = \frac{\Omega_0}{2(\Omega_0 - 1)}; \quad (2.20)$$

$$t_{\text{pert}} = B(\theta - \sin(\theta)) \quad \text{with} \quad B = \frac{\Omega_0}{2H_0(\Omega_0 - 1)^{3/2}}. \quad (2.21)$$

This implies that the perturbation will ultimately collapse.

Of course, the perturbation cannot collapse onto a point because it will fragment into smaller perturbations as separate areas satisfy the Jeans criterion. These small perturbations will settle in a virialized state following a process of violent relaxation as described by Lynden-Bell (1967). In the virialized state the kinetic energy E_{kin} given as

$$E_{kin} = \frac{3GM^2}{5r_{max}}$$

with r_{max} the maximal radius assumed by the perturbation during its development.

Using these results we can estimate the time an object needs in order to achieve a density ρ_{vir} of more than $100\rho_{bg}$ with ρ_{bg} the background density, that is

$$\rho_{vir} \geq 100 \times \frac{3\Omega_0 H_0^2}{8\pi G} (1 + z_{vir})^3$$

with z_{vir} the redshift at which the perturbation gets virialized.

If v^2 is the velocity dispersion of the perturbation the virial theorem provides us with the relation

$$\frac{1}{2}Mv^2 = \frac{GM^2}{2R},$$

with some suitably defined radius R . Then

$$\rho_{vir} \approx \frac{3M}{4\pi R^3} = \frac{3v^6}{4\pi G^3 M^2}.$$

This leads us to an estimate of z_{vir} :

$$z_{vir} \leq 0.47 \left(\frac{v}{100\text{km/s}} \right)^2 \left(\frac{M}{10^{12}M_\odot} \right)^{-2/3} (\Omega_0 h^2)^{-1/3} - 1. \quad (2.22)$$

This places a limit on the redshift of formation for a dark matter halo of mass M and velocity dispersion v . It also explains why smaller objects form first in the case of hierarchical growth.

2.5.2 Press-Schechter Mass Function

Press and Schechter presented in 1974 a formalism to describe the process of hierarchical growth (Press and Schechter, 1974).

They assumed that the primordial density perturbations are Gaussian fluctuations, that is the probability distribution of the amplitudes of the perturbations can be described by a Gaussian function

$$p(\Delta) = \frac{1}{\sqrt{2\pi}\sigma(M)} \exp\left(-\frac{\Delta^2}{2\sigma^2(M)}\right),$$

where M is the mass of the perturbation and $\sigma^2(M)$ its variance. Press and Schechter furthermore assumed that the perturbations had evolved into bound objects with mass M already, that is their amplitude got greater than the critical value Δ_c , and that the perturbations had a power-law power spectrum $P(k) = k^n$. The last assumption is the idealized case of an Einstein-de Sitter universe, that is $\Omega_0 = 1$ and $\Omega_\Lambda = 0$. In such a universe the perturbations grow proportional to the scale factor: $\Delta \propto a \propto t^{2/3}$ to the present epoch.

With the probability integral

$$\Phi(x) = \frac{2}{\sqrt{\pi}} \int_0^x e^{-t^2} dt$$

the fraction $F(M)$ of perturbations with mass M that become bound at each epoch is

$$F(M) = \frac{1}{\sqrt{2\pi}\sigma(M)} \int_{\Delta_c}^{\infty} \exp\left(-\frac{\Delta^2}{2\sigma^2(M)}\right) d\Delta = \frac{1}{2}(1 - \Phi(t_c)) \quad (2.23)$$

with

$$t_c = \frac{\Delta_c}{\sqrt{2}\sigma(M)} = \left(\frac{M}{M^*}\right)^{-(3+n)/3} \quad (2.24)$$

the time of the collapse. M^* is a time dependent reference mass.

In a linear regime, the mass of a perturbation is $M = \bar{\rho}V$ with $\bar{\rho}$ the mean density of the background model. Therefore, when the perturbation becomes nonlinear and the structure collapses, the space density $N(M)dM$ is

$$N(M)dM = \frac{1}{V} = -\frac{\bar{\rho}}{M} \frac{\partial F}{\partial M} dM. \quad (2.25)$$

Therefore, with equations (2.23), (2.24) and (2.25) we find the time dependent equation for the distribution of the mass:

$$N(M) = \frac{1}{2\sqrt{\pi}} \left(1 + \frac{n}{3}\right) \frac{\bar{\rho}}{M^2} \left(\frac{M}{M^*}\right)^{(3+n)/6} \exp\left[-\left(\frac{M}{M^*}\right)^{(3+n)/6}\right].$$

This way of predicting the mass distribution in the universe at a certain time is called the Press-Schechter mass function.

3 Observations

Groups of galaxies have been studied in observations with widely different instruments and at many different wavelengths. Observational results are important for our study of galaxy groups as we will test our results by comparison with them.

In this chapter we will present the observational data which is relevant to discuss the formation of groups of galaxies. The cosmic microwave background surveys provide us with constraints on cosmological parameters for setting up the simulation box. Studies of galaxy groups in the local universe and in X-Ray give an insight into the behaviour of galaxies in groups. Finally galaxy surveys at intermediate redshift provide statistics about the evolution of groups.

In the following sections we will shortly introduce the surveys and their results as far as they are relevant for this work.

3.1 WMAP - Cosmic Microwave Background Survey

The cosmic microwave background (CMB) is an echo of the earliest phases of structure formation and therefore it provides an insight into the fundamental structure of the universe. There have been several experiments in the past which measured the cosmic microwave background, the most recent being the Wilkinson Microwave Anisotropy Probe (WMAP). Its goal is to measure the fluctuations in the cosmic microwave background as precisely as possible in order to constrain fundamental cosmological parameters.

WMAP observes the full sky microwave background in five frequency bands from 23 to 94 GHz, measuring the temperature differences between two directions. Bennett et al. (2003) subtracted the foreground from the data and presented a map of the whole sky, as seen in Fig. 3.1.

The newest set of data, presented by Komatsu et al. (2008) provides a strong limit on the parameters of the Λ CDM models:

| | WMAP 5 Komatsu et al. (2008) | WMAP 3 Bennett et al. (2003) |
|------------------|-------------------------------------|-------------------------------------|
| Ω_Λ | 0.726 ± 0.015 | 0.73 ± 0.04 |
| Ω_b | 0.0456 ± 0.0015 | 0.044 ± 0.004 |
| Ω_c | 0.228 ± 0.013 | |
| H_0 | $70.5 \pm 1.3 \text{km/s/Mpc}$ | $71 \pm 4 \text{km/s/Mpc}$ |
| t_0^1 | $13.72 \pm 0.12 \text{Gyr}$ | $13.7 \pm 0.2 \text{Gyr}$ |

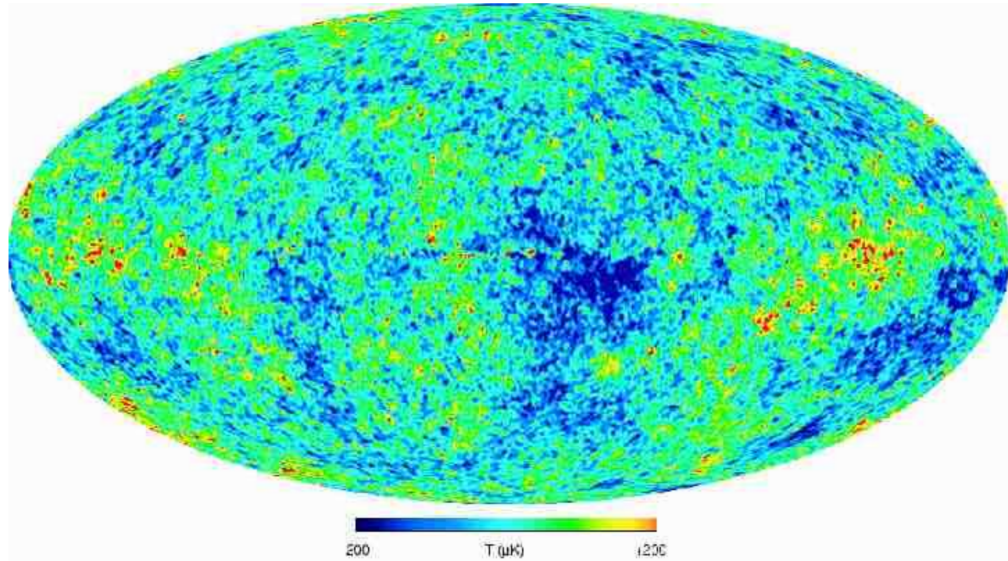


Figure 3.1: Plot taken from Bennett et al. (2003): This “internal linear combination” map combines the five band maps in such a way as to maintain unity response to the CMB while minimizing foreground contamination.

3.2 Galaxy Groups in Observations

We can observe local overdensities in the galaxy distribution. If a local overdensity contains more than 50 galaxies in an magnitude range of $m_3 < m < m_3 + 2$ with m_3 the magnitude of the third brightest galaxy and an observed angular radius of $\theta_A = \frac{1.47}{z}$, this overdensity was called a cluster by Abell in 1958. Local overdensities that do not fit this criterion were called galaxy groups. This distinction between galaxy clusters and galaxy groups is somewhat arbitrary, i.e. rich groups might be poor clusters or the other way around.

It is difficult to observe local overdensities: Since the observations usually deal only with two dimensional data, local overdensities might be a projectional effect. This is important especially for local overdensities that consist of only a few members, as the statistical error introduced by inclusion of background or foreground galaxies is more important for a small sample of galaxies. Thus galaxy groups are more difficult to detect than clusters. The situation improves by including spectroscopic data, as that allows to calculate the redshift of the assumed galaxy group members with higher accuracy than it was possible with photometric data.

Galaxies that form a group are assumed to be gravitationally bound and interact with each other. Since groups are intermediate overdensities, they have less mass and velocity dispersion (about $\sigma_v \simeq 300\text{km/s}$) than a cluster (about $\sigma_v \simeq 1000\text{km/s}$), but more than any galaxy in the field. From dynamical analysis it is known that the mass of a galaxy group is much higher as the sum of the masses of the galaxies they consist of (Longair, 2008). Together with the extended X-ray luminous hot halos

observed in several groups, this leads to the conclusion that groups might have a global dark matter halo. Low redshift groups show, like clusters, a much higher fraction of early type galaxies than field galaxies. At intermediate redshift we can only distinguish between star forming galaxies and passive galaxies by spectroscopic data, while their morphology is hard to observe. Although, as can be seen in Figure 3.2, the fraction of passive galaxies in groups is higher than in the field.

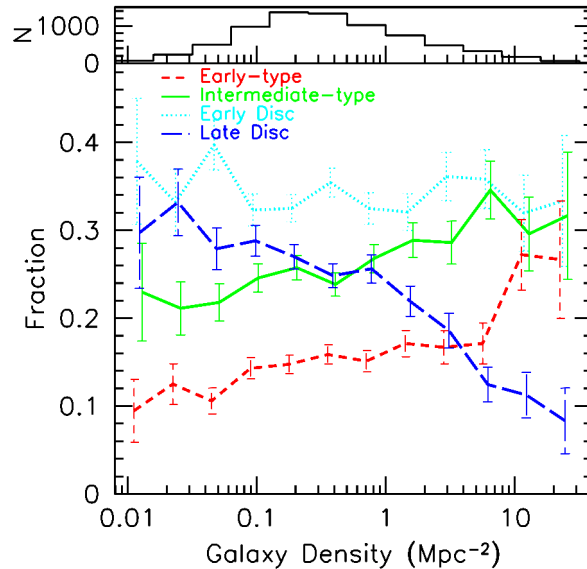


Figure 3.2: Plot taken from Goto et al. (2003): The authors show the morphology-density relation for four types of galaxies. The short-dashed, solid, dotted and long-dashed lines represent early-type, intermediate-type, early-disc and late-disc galaxies, respectively. The histogram in the upper panel shows the number of galaxies in each bin of local galaxy density.

Wilman et al. (2005c) and Eke et al. (2004) showed that about 50 – 70% of all galaxies are found in a group environment. Density and velocity of the group galaxies suggest that mergers and interactions are more common than in the field or in the cluster environment, see Mamon (1992). Because galaxies are more likely to interact in the group environment, they are interesting systems for studying the evolution of galaxies.

3.2.1 X-Ray Luminous Galaxy Groups and Intra Group Light

As mentioned above there is a huge amount of galaxy groups in which diffuse X-ray emission is observed. These emissions are strong evidence that galaxy groups are real gravitationally bound objects and not just an accumulation of galaxies.

The X-ray luminosity, temperature and surface brightness hold information about the depth of the potential and the distribution of mass in these systems. Helsdon

3 Observations

and Ponman (2003) studied several X-ray bright groups and found that most of these have a bright early-type galaxy at the central X-ray isophote and the dynamical center of the velocity distribution of the group members. They assume that this results from the fact that these early-type galaxies are formed by galaxy mergers soon after the initial collapse of the group (see also Governato et al., 1996). Since the X-ray properties of these central galaxies are stronger correlated with the group itself than with the optical light of the galaxy this indicates that the X-ray luminosity originates from the group itself and does not only result from the central galaxy. Additionally they found no hint that there exists a correlation between X-ray properties of the group and the degree of dominance the central galaxy has, measured by the magnitude difference between the two brightest group members.

Furthermore Helsdon and Ponman (2003) found a morphology-density relation, as they found a weak anticorrelation between the group temperature, measured from the X-ray luminosity, and the spiral galaxy fraction.

Intra Group Light is another source for studying the dynamical evolution of galaxies in groups, as it is supposed to result from tidal interaction, accretion and galaxy encounters, see Dressler (1984). When galaxies interact, material gets stripped. For a field galaxy the material would fall back to the galaxy, but in a dense environment like a group the stripped material forms a diffuse envelope around the group, related to the distribution of the dark matter. Since compact groups of galaxies are dense,

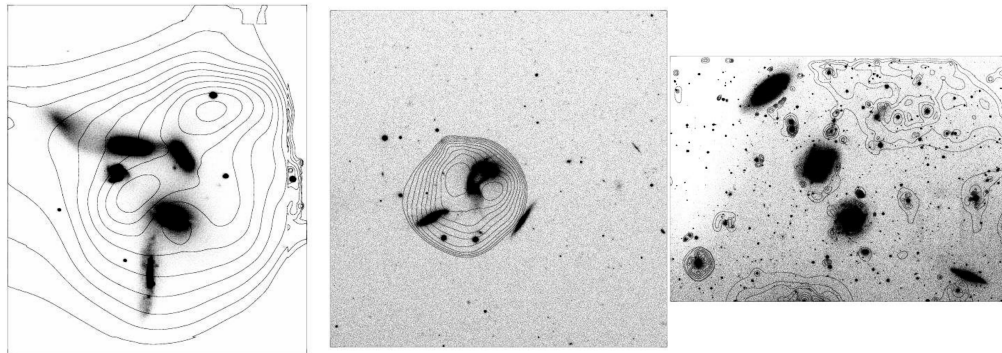


Figure 3.3: Plots taken from Da Rocha and Mendes de Oliveira (2005): Left: HCG 79 is the most evolved compact group tested in their sample. All group members interact, only one galaxy is a late-type galaxy. Its intra group light has a fraction of $46 \pm 11\%$ and is shown as contour curves with surface brightness levels ranging from 24.2 to 25.1 in B band. Center: HCG 95 is a group with an ongoing merger. The intra group light has a fraction of $11 \pm 26\%$ and is centered around this merger, as can be seen from the contour curves with surface brightness levels with range from 26.92 to 27.8 in B band. Right: HCG 88 consists of four late-type galaxies aligned in a filamentary structure. It has no intra group light.

they are preferred regions for galaxy interactions and therefore perfect objects for studying intra group light. Da Rocha and Mendes de Oliveira (2005); Da Rocha

et al. (2008) studied such compact groups and their intra group light in detail. Although their sample is not large, they found an evolutionary sequence: The more evolved compact groups show a brighter and more irregular intra group light halo, while the less evolved groups show no sign of interaction and do not have observable intra group light, see three examples for intra cluster light halos in Figure 3.3.

The fraction of intra group light increases with the state of evolution up to $46 \pm 11\%$ for the most evolved group HCG 79, while the crossing time² is decreasing from $8.7H_0^{-1}$ for HCG 88 to $0.004H_0^{-1}$ for HCG 79. Under the assumption that the intra group light traces the dark matter mass of the group the irregular shape of the intra group light suggests that these groups are not virialized systems.

3.2.2 Observational Group Classification

In general three types of groups are distinguished by observers which have their own difficulties in detection and provide different insight into the evolution of galaxies. Their characteristic features are laid out in the following.

Compact Groups

Following Hickson (1982) a compact group is defined by the following criteria:

1. Population criterion: A compact group consists of $N \geq 4$ galaxies within 3 mag of the brightest group member
2. Isolation criterion: There is no other galaxy in an angular diameter $\theta_N \geq 3\theta_G$ with θ_G the minimum circle containing the geometric centers of all group galaxies and θ_N the largest circle containing no other galaxies than the group galaxies.
3. Compactness criterion: The total magnitude μ_G of the group galaxies per arcsec² is $\mu_G < 26.0$

The second and third criterion exclude clusters since cluster galaxies cannot be isolated.

The first systematic sample of compact groups was created by Hickson (1982), the Hickson Compact Group catalogue (HCG). He found that there was no correlation between the group density and the magnitude difference between the first and second brightest member of the compact group. While there is no preferred morphological type for the first-ranked galaxy, Hickson (1982) found that all groups contain fewer spiral galaxies than a comparable sample of field galaxies. The fraction of spiral galaxies decreases with the compactness of the group, Hickson's least compact group has 60% spirals, the most compact one just 20%. Especially Hickson (1982) sees a correlation between compactness and morphology: groups that contain a bright spiral galaxy are about a factor of 2 less compact than the other groups.

²Time a galaxy needs to cross the group.

3 Observations

Compact groups are very dense environments with projected galaxy densities ranging from 300 to $10^3 h^2 \text{Mpc}^{-2}$ and low velocity dispersions around $\sigma_v \simeq 200 \text{km/s}$. Thus galaxy interactions should be numerous and stripping very efficient, which leads to extended intra group light (Da Rocha et al., 2008).

Hunsberger et al. (1998) determined a luminosity function for the HCG. They found that a single Press-Schechter function

$$\Psi(M)dM = \frac{2}{5} \psi^* \ln 10 (10^{0.4(M^*-M)})^{\alpha+1} \times \exp(-10^{0.4(M^*-M)}) dM$$

with M^* the magnitude at the exponential cut-off and α the slope of the power law at low luminosities (Longair, 2008, page 77) could not fit the detected luminosities, so they took a combination of two Schechter functions as can be seen in Figure 3.4. The bright end was best fitted by $M^* = -21.6$ and $\alpha = -0.52$, while the faint end slope was fitted best by $M^* = -16.1$ and $\alpha = -1.17$. Furthermore they found that

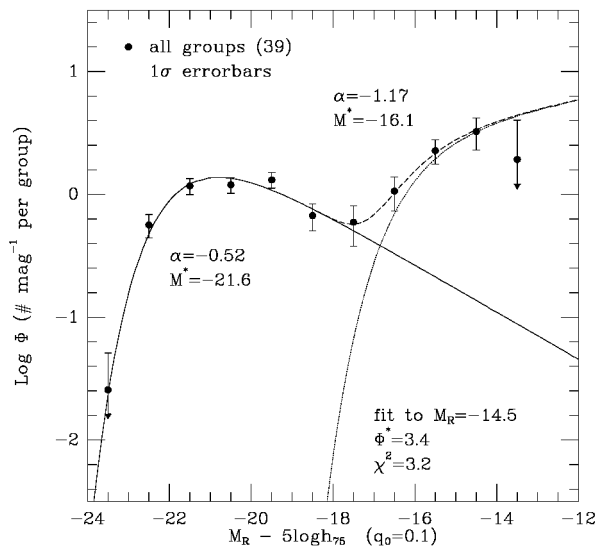


Figure 3.4: Figure 5 taken from Hunsberger et al. (1998): Luminosity function of HCG galaxies. Data points represent the average number of galaxies per group in each magnitude bin. The bright and faint populations are fitted separately using two Schechter-functions. The solid line is the bright end, the dotted line is the faint end, and the dashed line is the composite fit.

compact groups with X-Ray emissions have a large dwarf galaxy population, their dwarf-to-giant ratio is comparable to that of clusters. Also compact groups with a first-rank spiral galaxy have a smaller population of faint galaxies than the others.

Looking at the crossing time of a group, $t_{cross} \sim \frac{R}{\sigma_v} \sim 0.02 H_0^{-1}$ we see that it is much smaller than H_0^{-1} . Since the crossing time is so small, compact groups have a short lifetime. Thus we should find remnants of former compact groups today in form of large field elliptical galaxies. Sulentic and Rabaca (1994) have searched for

such remnants, but found a significantly lower rate of large field ellipticals that could be remnants of compact groups than expected. This leads to the conclusion that the evolutionary timescale of compact groups is somehow larger than predicted.³

Fossil Groups

A fossil group is defined as an extended source of X-Ray luminosity with a lower limit of $L_{X,bol} \geq 10^{42} h_{50}^{-2} \text{erg/s}$ that hosts a bound system of galaxies in the optical. This optical counterpart is dominated by a single bright elliptical galaxy and is characterized by a large magnitude gap of $\Delta m = 2 \text{mag}$ between the brightest and the second brightest galaxy within half the projected virial radius. By choosing this definition field ellipticals and large ellipticals in groups or clusters are excluded. Half the virial radius is chosen, because this is approximately the radius within which dynamical friction would cause any galaxy with mass to light ratio $\frac{M}{L} = 10 \frac{M_{\odot}}{L_{\odot}}$ to fall into the center of the halo within a Hubble time.

Jones et al. (2003) presented a sample of fossil groups, selected by the criterion above. They found giant ellipticals with total luminosities similar to the luminosities of the brightest galaxies in clusters. Nevertheless, most of their fossil ellipticals can be fitted by de Vaucouleurs $r^{1/4}$ profile and do not show any excess like cD galaxies. None of the selected fossil groups show any sign of merger activity.

This leads Jones et al. (2003) to the conclusion that fossil groups are old, undisturbed systems in which all L^* -galaxies within $r < r_{vir}$ have merged and formed the central luminous elliptical galaxy.

From their studies Jones et al. (2003) found that fossil groups represent 8 – 20% of all systems with the same X-ray luminosity, which is 2 – 4 times more numerous than compact groups. They are as numerous as all clusters combined which suggests that the bright cluster galaxies and the fossil group galaxies have the same origin. Jones et al. (2003) conclude that both have evolved from a $10^{13} - 10^{14} M_{\odot}$ system at $z \geq 1$.

Meanwhile La Barbera et al. (2008) have studied a sample of fossil groups identified in the SDSS survey (see the following section) by using the same detection criterion as Jones et al. (2003). They compared their sample with a similar sample of bright field ellipticals and found that there is no significant difference between their two samples. They conclude that fossil groups simply are objects formed by the merger of a few bright galaxies without gaining enough matter to form additional bright galaxies⁴.

Loose Groups

In general all groups that do not fit in the two categories mentioned above are called loose groups. They consist of a few bright galaxies and tens of small faint members,

³From simulations Athanassoula et al. (1997) found that a global dark matter halo for compact groups would lead to a much longer lifetime.

⁴That is similar to the results D’Onghia et al. (2005) found from simulations.

3 Observations

so the group contains $N \leq 50$ members. Following Girardi and Giuricin (2000) these groups are assumed to be collapsing systems, where the sample size is larger than the expected virialized region. Thus the bright member galaxies are separated by a few hundred kpc, spread about 1Mpc in total. Typical velocity dispersions for loose groups are $\sigma_v \simeq 200\text{km/s}$ and the bright galaxies show signs of distortion by tidal forces.

The galaxies belonging to a loose group are spread so wide, that they are difficult to identify as group members. Girardi and Giuricin (2000) studied a sample of loose groups and found that the observed mass function for the mass within the expected virial radius is fitted well by the Press-Schechter mass functions that also describe well the cluster data, see Fig. 3.5. They interpret this as an indication of

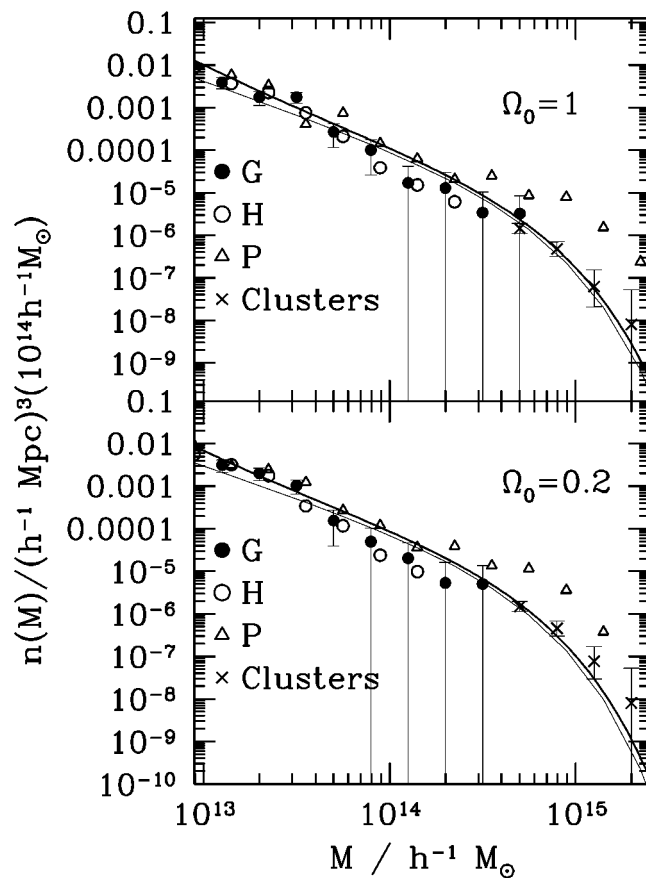


Figure 3.5: Figure 8 taken from Girardi and Giuricin (2000): For two reference cosmological models we show mass functions, where masses are computed within the virialized region with an overplotted Schechter function.

the continuity of clustering properties from poor groups to rich clusters.

3.2.3 Supergroup SG1120-1202: A Protocluster

The supergroup SG1120-1202 consists of four X-ray luminous groups at $z = 0.37$ that are gravitationally bound and whose dynamics indicate that they will assemble to a cluster of Coma mass by $z = 0$. Kautsch et al. (2008) studied the fraction of ellipticals for this object in order to figure out whether the cluster environment or the group environment causes the observed fraction of ellipticals in clusters.

They found that SG1120-1202 has the same fraction of ellipticals as clusters, which is at redshift $z = 0.37$ about 66%, while the mean value of the fraction of ellipticals in galaxy groups falls below this value (Jeltema et al., 2007). Therefore Kautsch et al. (2008) suggest that the galaxies in these groups are pre-processed in the group environment and the late infall of galaxy groups into a cluster does not change the cluster's fraction of early-type galaxies significantly.

3.3 Galaxy Surveys at Intermediate Redshift

Galaxy surveys provide information about the large scale structure of the universe, the evolution of galaxies with redshift and by spectroscopic data about the star formation history of galaxies. They even give some limits to the cosmological parameters, measuring the power spectrum of the galaxy distribution. There are several galaxy surveys at high and low redshifts available at the moment, three of them are presented in the following sections, because they are especially relevant for studying galaxy groups.

3.3.1 CNOC2 (Canadian Network for Observational Cosmology)

The Canadian Network for Observational Cosmology 2 (CNOC2) Field Galaxy Redshift Survey contains redshifts, photometry and velocities for about 5000 galaxies between $0.1 < z < 0.6$ covering an area of sky of 1.5 square degrees in total. The survey consists of four widely separated regions chosen under the aspects of avoiding low redshift clusters, bright stars with less than 12 mag and any other bright foreground object. Spectroscopy was performed for objects with R -band magnitude below 21.5. A more detailed description of the CNOC2 Survey is provided by Lin et al. (1998) and Yee et al. (1997).

The left panel of Figure 3.6 shows the amount of galaxies found in the CNOC2 survey at various redshifts by Lin et al. (1998). The right panel of Figure 3.6 shows the distribution of galaxies in redshift-space from Yee et al. (1997). The fraction of passive, non star forming groups f_p in the CNOC2 survey at a redshift range of $0.3 \leq z \leq 0.55$ have been studied by Wilman et al. (2005b) and Wilman et al. (2005a). For studying the star formation in a group galaxy they use the equivalent width of the $[OII]\lambda 3727$ emission line as it lies centrally in the visible window of the CNOC2 redshift range and at a wavelength of low sky emission. They found that the fraction of passive galaxies depends strongly on the following three quantities, as can be also seen in the left panel of Figure 3.7:

3 Observations

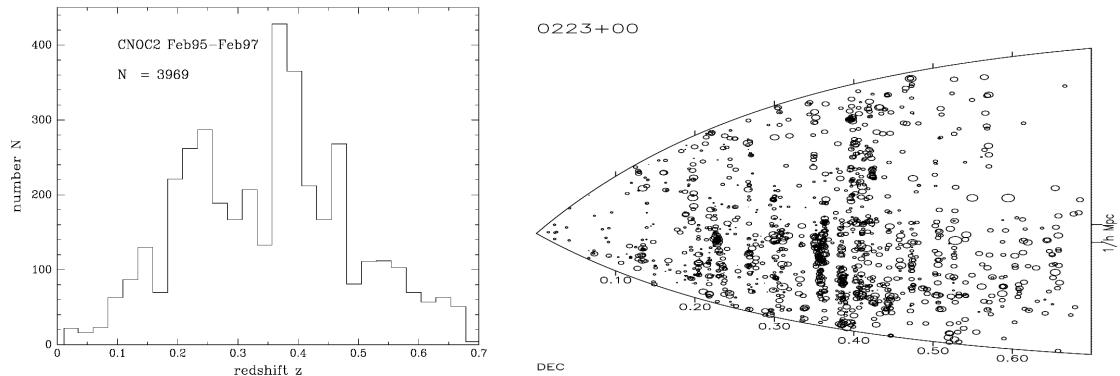


Figure 3.6: Left: Figure 2 taken from Lin et al. (1998): The CNOC2 survey redshift histogram. Right: Figure 2 taken from Yee et al. (1997): Wedge Diagram for CNOC2-patch 0223+00. The thick marks on the vertical axis denote $1h^{-1}\text{Mpc}$, while the horizontal axis shows redshift. Note the sheet-like structures spanning across the whole field in the Dec-axis. The unevenness of the density of points across the structures is due to an unequal number of fields projected.

1. Redshift: While the fraction of passive galaxies in cluster cores remains constant for redshifts between $0 \leq z \leq 1$ the fraction of passive galaxies declines strongly with redshift for groups as well as for the field. This is in agreement with the Butcher-Oemler effect⁵.
2. Environment: There is a significantly higher fraction of passive galaxies in the dense group environment than in the field at the same redshift.
3. Luminosity: The fraction of passive galaxies increases steeply with luminosity.

For a redshift of $z \sim 0.4$ Wilman et al. (2008) were able to classify the group galaxies by morphology. They tested the sample for the fraction of S0-galaxies, ellipticals and spirals and found an agreement with the previous morphology-density relations:

1. The fraction of S0-galaxies is significantly higher in groups than in the field, though S0s are less common within $0.3h_{75}^{-1}\text{Mpc}$ of the group centres than in the outer parts of the group. Together with the fact that the fraction of S0s in groups is as high as that in clusters they conclude that groups are the environment of S0 formation. The growth of the S0 fraction at late times indicates that their formation process is slow. The fact that they lie in the outer regions of the group implies that the formation mechanism takes places in lower density regions like group outskirts. Thus minor mergers, galaxy harassment and tidal interactions are possible formation scenarios.

⁵Butcher and Oemler found that, though the fraction of passive galaxies in cluster cores remains constant since $z \sim 1$ the fraction of star forming galaxies in the whole cluster environment is higher at higher redshifts.

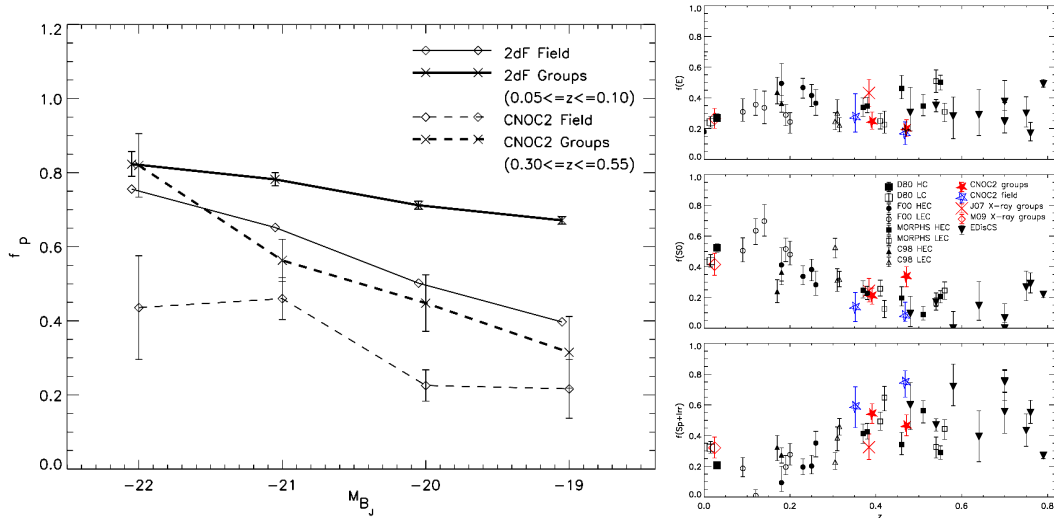


Figure 3.7: Left: Figure 3 taken from Wilman et al. (2005a): The fraction of passive galaxies in group and field environment as a function of the luminosity. For comparison the authors also plotted data from the 2dF survey (see below). Right: Figure 5 taken from Wilman et al. (2008): The fraction of ellipticals, S0s and spirals is plotted against the redshift. The results from Wilman et al. (2008) are highlighted in red for the group environment and blue for the field. The black symbols are results for cluster environment.

3 Observations

2. Although the fraction of spiral galaxies in groups is low compared with the field there is evidence for Sc+-spirals to be more common in the inner group regions than in the outer parts.
3. The fraction of elliptical galaxies in groups is similar to the fraction of ellipticals in the field, although bright ellipticals in the inner regions of groups are common.

3.3.2 SDSS (Sloan Digital Sky Survey)

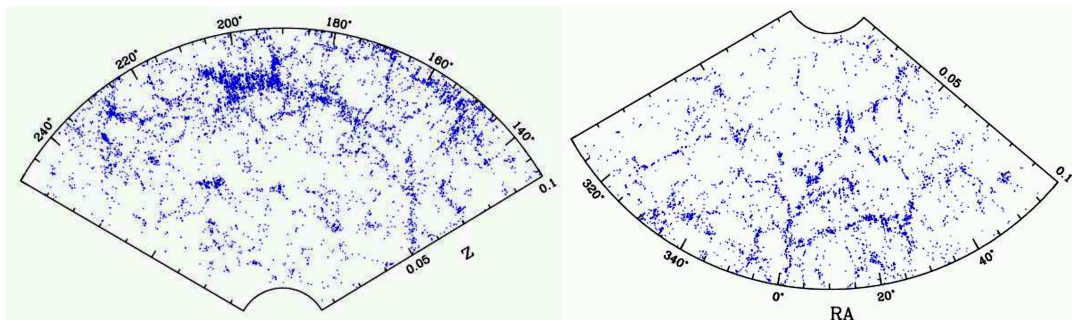


Figure 3.8: Figure 7 from Berlind et al. (2006): Equatorial slice through the SDSS volume-limited sample in the redshift range $0.015 - 0.1$. The slice is 4° thick and each point shows the RA and redshift of a galaxy in the sample.

The Sloan Digital Sky Survey (SDSS) is an imaging and spectroscopy survey of a large (two fifths) portion of the northern sky and a smaller area of the southern sky. It maps galaxies up to an R-band magnitude of 22.5. The sample contains about 300000 galaxies in 3495.1 square degrees of the sky. 98% of these galaxies are within a redshift range of $0 < z < 0.25$.

Figure 3.8 shows the distribution of galaxies in the observed portion of the sky.

Compact groups of galaxies in the SDSS survey have been studied by McConnachie et al. (2008). They used Hicksons criteria for compact groups (see Sec. 3.2.2) and found 2297 compact groups down to a magnitude $M = 18$ and 74791 compact groups down to $M = 21$. This represents 0.9% of all galaxies in the SDSS data release 6 at these magnitudes. The mean line of sight velocity dispersion for their groups is $\sigma_v = 220 - 259 \text{ km/s}$ which is consistent with other measurements. A histogram of the line-of-sight velocity dispersion for all compact groups can be seen in Figure 3.9 together with two examples of their group sample.

In agreement with previous studies by Hickson et al. (1988) they found that many galaxies are early type galaxies, although most of the groups contain at least one late-type galaxy. Actually they are working on a more detailed analysis of the morphology.

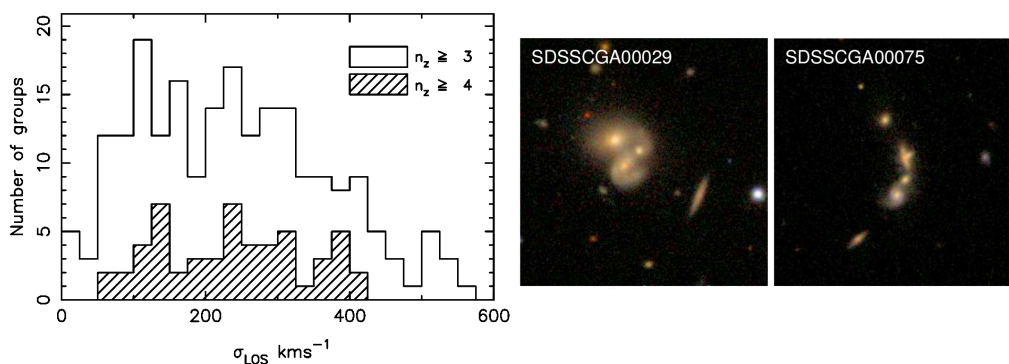


Figure 3.9: Figures taken from McConnachie et al. (2008): Left: Histogram for the line of sight velocity dispersion of the compact groups identified in the SDSS survey, with n_z the number of group galaxies for which a measure of redshift exists. The hatched histogram shows groups with $n_z \geq 4$, the blank one groups with $n_z \geq 3$. Right: Two examples of compact groups from the SDSS sample.

3.3.3 2dF

The 2dF Galaxy Redshift Survey (2dF) consists of 100 random 2 degree fields and two main rectangular strips, one in the southern galactic sky covering $75^\circ \times 15^\circ$ of the sky, the other in the northern hemisphere with an area of $75^\circ \times 7.5^\circ$. It provides spectroscopy and redshift data. The “bright” sample contains 250000 galaxies with B-band magnitude up to 19.5 at a mean redshift of $\bar{z} = 0.11$, the “faint” sample contains 10000 galaxies down to an R-band magnitude of 21 with a mean redshift of $\bar{z} = 0.3$.

The left panel of Fig. 3.10 shows the amount of galaxies found in the 2dF survey with the mean redshift peak at $z = 0.1$, the right panel of Fig. 3.10 shows the distribution of galaxies in redshift-space Colless (1999b).

Eke et al. (2006) measured the mass and luminosity functions of clusters and groups, as can be seen in Fig. 3.11. From this they created a mass-to-light ratio with a minimum value of $\sim 100hM_\odot/L_\odot$ at a group luminosity of $L_{bj} \sim 5 \times 10^9 h^{-2} L_\odot$. With this group mass-to-light ratio they concluded that the halo circular speed is a function of group luminosity. The mass function and the mass-to-light ratio can be seen in Fig. 3.11

3.4 Galaxy Groups in Theoretical Discussion

From observations we know, that the mass-to-light ratio of galaxies increases with distance r up to 100 – 200kpc, but it is flattening for groups and clusters up to 1.5Mpc (see Dekel and Ostriker, 1999, page 155). This suggests, that most of the

3 Observations

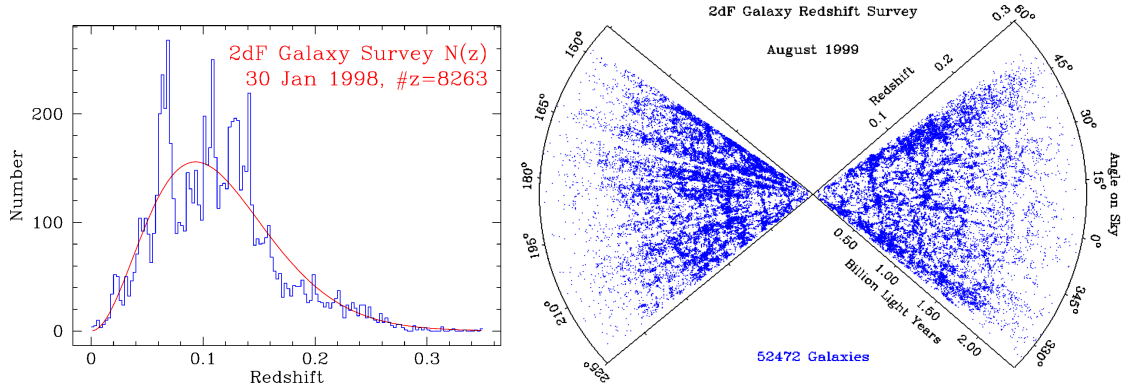


Figure 3.10: Left: Figure 4 from Colless (1999a): Redshift distribution from the 2dF survey. The smooth curve is the predicted redshift distribution neglecting clustering. Right: Figure 2 from Colless (1999b): Redshift cone diagram showing the distribution of objects from the 2dF galaxy survey.

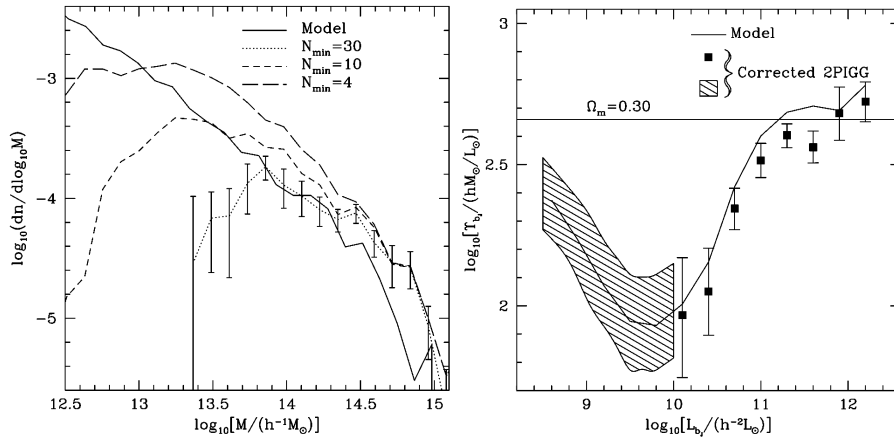


Figure 3.11: Figures taken from Eke et al. (2006): Left: Mass distribution for galaxy groups and clusters from the 2dF survey in comparison with the mass function of dark matter halos from the Λ CDM simulation by Jenkins et al. (1998). Right: Mass to light ratio as a function of group luminosity for the 2dF group sample (points).

dark matter is associated with the dark matter halos around galaxies, while groups or clusters do not show signs of an own global dark matter halo.

In contradiction there are simulations by Athanassoula et al. (1997) that show that the lifetime of compact groups, would not be long enough for the observed fraction of compact group without a global dark matter halo.

Therefore, it is still an open question whether galaxy groups and clusters possess a global dark matter halo or if they are an assembly of smaller dark matter halos linked together by gravity. Since this is still unknown it is not clear how to identify galaxy groups in cosmological dark matter only simulations for sure.

4 Methods

In the course of this work we are analysing a high resolution cosmological simulation set up by Ludwig Oser to study galaxy formation and the evolution of structure. For our analysis we use merger trees based on data created with FOF and SUBFIND algorithms from the simulation by Christian Maubetsch and Michaela Hirschmann. In the following we will describe the simulation and the construction of the merger trees in more detail as this is the groundwork of our analysis.

4.1 The Simulation

We use a Λ CDM Dark Matter only simulation with $\Omega_0 = 0.26$, $\Omega_\Lambda = 0.74$ and $H_0 = 72\text{km/s/Mpc}$. These parameters were chosen from the WMAP 3 data published by Bennett et al. (2003). The simulated box has a size of $100 \times 100 \times 100h^{-3}\text{Mpc}^3$ and contains 512^3 particles in each direction. Each particle has a mass of $M_{part} = 2 \times 10^8 M_\odot$. The simulation runs over 94 timesteps from $a = 0.07$ to $a = 1$.

The simulation was produced with the parallel TreeSPH code GADGET-2 designed by Volker Springel (Springel et al., 2001b; Springel, 2005). GADGET-2 models dark matter and stars as self-gravitating collisionless fluids and the intergalactic and interstellar medium as an ideal, inviscid gas.

4.2 The Friends-of-Friends-Algorithm (FOF)

The Friends-of-Friends (FOF) algorithm is a method to single out the groups of particles in a cosmological simulation that are likely to contain galaxies. FOF identifies a particle as part of a group of particles, if its distance to its nearest neighbour does not exceed a specified value, the linking length h_{link} . This linking length h_{link} is usually calculated as

$$h_{link} = bn^{-\frac{1}{3}},$$

where n is the number density of particles and b is called the linking parameter¹. A typical value for b is 0.2, since this has been found to give the best fit to the mass distribution predicted by the Press-Schechter theory (Götz et al., 1998).

¹ b is often referred to as the linking length, as it is the relevant value when comparing with other simulations.

In this way the FOF algorithm forms groups of particles contained within isodensity surfaces of a density

$$\varrho = \frac{2M_p}{\frac{4\pi}{3}h_{link}^3},$$

where M_p is the mass per particle (Warren et al., 2006; Frenk et al., 1988).

In order to suppress random gatherings of particles that have no physical significance, we require groups of particles to have at least a certain number of members. Nevertheless, FOF groups can still contain a significant amount of statistical noise. Furthermore FOF has a certain tendency to link disjoint structures via small bridges of connected particles.

In our simulation we used FOF with a linking parameter $b = 0.2$ corresponding to a linking length of 28.125pc and a lower particle limit of 20 particles.

4.3 The SUBFIND-Algorithm

In order to find smaller density structures within a larger structure like the groups identified with FOF, Springel et al. (2001a) devised the SUBFIND algorithm. These subhalos are defined as locally overdense, self-bound particle groups.

For identifying the local overdensities the particle lists are searched for saddle points in the density field, which mark the boundary of the subhalos. By testing the total energy of each particle and identifying the ones with positive values, the unbound particles, which were a problem in the FOF method, can be eliminated. Most FOF-halos consist of several SUBFIND-halos, the largest one contains most of the particles and is called the background halo, the smaller SUBFIND-halos are called subhalos. An example can be seen in Figure 4.1.

4.4 Merger Tree Construction

Since many properties of galaxies observed today are assumed to result from their mass assembly history, it is necessary to construct the accretion history of the halos and subhalos identified in the simulation at each timestep. For this it is necessary to follow a specific halo through all timesteps by identifying the progenitors and merger events for the halos.

A progenitor is defined as following: A halo H_2 (or subhalo) at timestep z_2 is assumed to be the progenitor of the halo H_1 at timestep $z_1 > z_2$ if H_1 contains more than half of the particles of H_2 . If there is more than one halo H_2 for which more than half of its particles end up in H_1 than the halo H_2 with the highest number of particles in H_1 is the progenitor. A merger is defined as following: A halo H_2 at timestep z_2 is assumed to merge into the halo H_1 at z_1 if it is not a progenitor but nevertheless more than half of its particles belong to the halo H_1 at z_1 .

Technically we construct the tree by the following procedure:

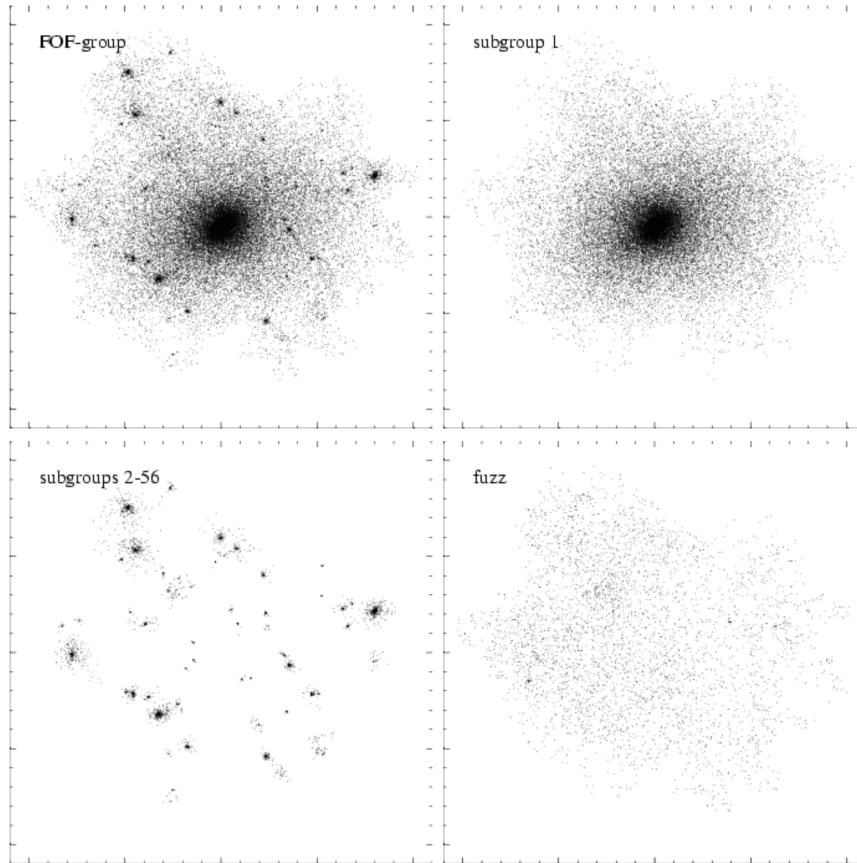


Figure 4.1: Figure 3 taken from Springel et al. (2001a): The author shows here an example for a subhalo identification with SUBFIND. The top left panel shows a small FOF-group (44800 particles), identified at $z = 0$. SUBFIND identifies 56 subhalos within this group, the largest one forms the background halo and is shown on the top right, while the other 55 subhalos are plotted on the lower left. In this example the total mass in all the “true” subhalos 2-56 is about 8% of the group mass. Particles not bound to any of the subhalos form “fuzz”, and are displayed on the lower right. These particles primarily lie close to the outer edge of the group.

1. For each halo at $z = 0$ the most massive progenitor in the previous timestep is identified. Then for this most massive progenitor again its most massive progenitor is identified. This is repeated until the smallest timestep available in the simulation, so that we create a complete most massive progenitor branch for all halos at $z = 0$. If there is no most massive progenitor in the previous timestep the four previous timesteps are searched for the most massive progenitor in case the most massive progenitor for a halo is not detected in one timestep.
2. After all halos at $z = 0$ have a progenitor we select from the next higher redshift step all halos that are not a progenitor. For these halos we create a merger tree up to the highest redshift available. This is repeated going backward in time for all halos that are not contained in any branch.
3. At this point every branch represents a single halo that is followed through time. If such a branch ends before $z = 0$, this halo most likely has merged into another halo². We check whether this happens and in that case we connect this branch to the branch of the halo it merges into at the timestep after the branch ends.

An example for such a merger tree can be found in Wechsler et al. (2002), Figure 1, as reproduced in Figure 4.2.

This method of constructing merger trees has been applied before in simulations, see for example Wechsler et al. (2002), Springel et al. (2001a), Maulbetsch et al. (2007).

In our simulation we use two different types of merger trees: One for isolated halos and one for all halos including the subhalos. These trees were constructed by Christian Maulbetsch (see Maulbetsch, 2007) and Michaela Hirschmann. In the isolated trees, halos are excluded if their center is within the virial radius of a larger halo, while in the subhalo trees all halos are included, whether they exist within the virial radius of another object or not. Our isolated-trees contain 41008 merger trees that begin at $z = 0$, the subhalo-trees contain 45101 merger trees at $z = 0$. (At $z = 0$ only halos with more than 100 particles are counted for both files). The trees contain the halo's number of particles, progenitor ID, virial mass, center of mass coordinates, center of mass velocities and the virial radius for each halo at each timestep.

There are some caveats in the construction of the merger trees. First there occur some double identifications which result in a fake halo. The tree of these halos only contains one timestep and these halos are skipped in order to avoid double identifications instead of being connected to another branch. Second there are some massive halos that have main branches of only a few timesteps which already start with a high mass. These ones are fake halos too, since it was most probably a double

²It also happens that a halo loses mass until it drops below the detection threshold. In that case we discard the branch.

4 *Methods*

identification during a merger event that lasted for several timesteps. These halos were ignored too. Third there are some halos with an extended main branch until a redshift higher than $z = 0$, where they get lost and no merger is found. This happens if the halo is next to another halo and its particles get stripped to this halo, but the halo does not merge. This problem is not solved in the merger trees we use.

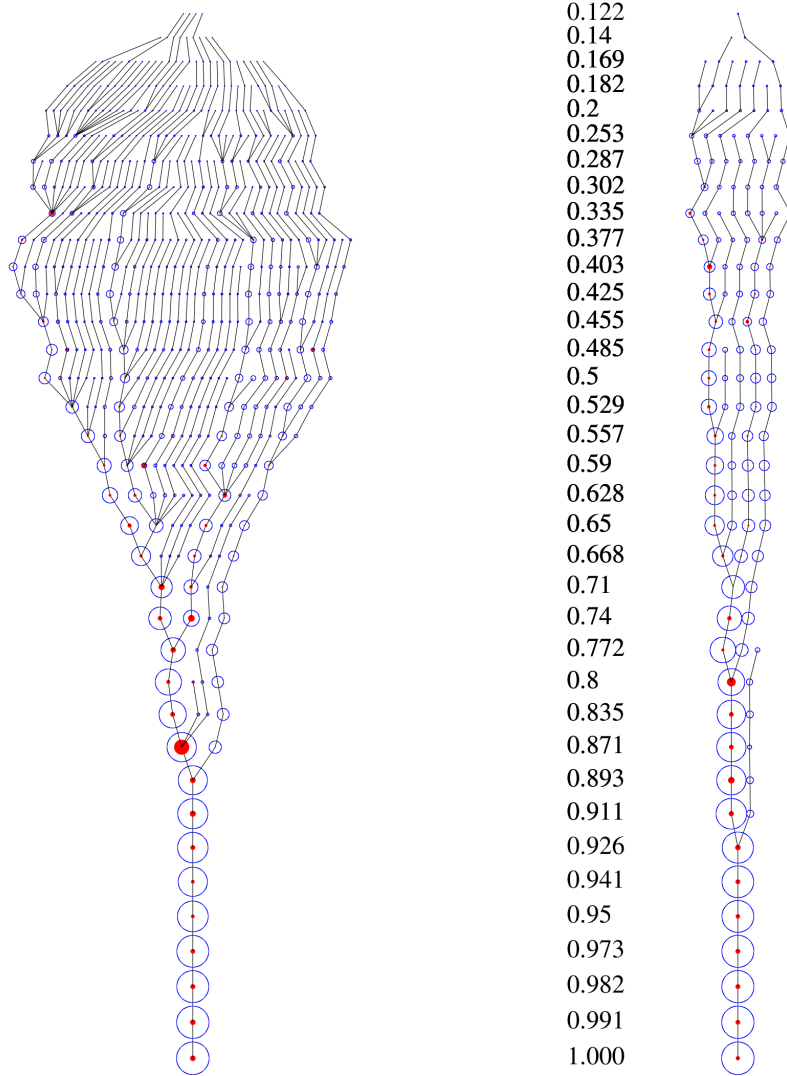


Figure 4.2: Figure 1 taken from Wechsler et al. (2002): The authors show the structural merger trees for two halos. The left side shows the merging history of a cluster mass halo ($M_{vir} = 2.8 \times 10^{14} h^{-1} M_{\odot}$ at $z = 0$), the right side shows a galaxy-mass halo ($M_{vir} = 2.9 \times 10^{12} h^{-1} M_{\odot}$ at $z = 0$). The scale factor a at the output time is listed at the center of the plot.

5 The Group Halos

As described in chapter 4 we select our sample of groups from a $100^3 h^{-3} \text{Mpc}^3$ cosmological dark matter only N-body simulation of ΛCDM with $\Omega_m = 0.26$, $\Omega_\lambda = 0.74$ and $H_0 = 72 \text{km/s/Mpc}$. The simulation box contains 512^3 particles. We will first consider a sample created using the SUBFIND algorithm and then a second sample selected using the FOF algorithm.

X-Ray observations by Zabludoff and Mulchaey (1998) show groups to have dark matter masses between $M_{vir} = 1 \cdot 10^{13} M_\odot - 1 \cdot 10^{14} M_\odot$, see section 3.2.1. Therefore we select halos within this mass range at $z = 0$ to study their evolution in time. In the following these halos will be referred to as groups. The more massive halos will be called clusters. No other restrictions were placed on the potential groups due to our limited knowledge of dark matter within groups of galaxies.

Figure 5.1 illustrates the locations of group halos within the simulated box. The groups are mostly located on filaments within the box, as can be seen in the lower left panel of Figure 5.1, although there are some separated group halos as well (central panel). Very mass rich structures like clusters can be found at the intersections of filaments (lower right panel).

5.1 The SUBFIND Sample

We assume our groups to have a global halo as this was done in earlier simulations. This appears to be true in the case of groups with bright intra group light (Da Rocha et al., 2008). Furthermore Athanassoula et al. (1997) have shown that a common halo would increase the lifetime of compact groups significantly so that the observed frequency of such groups can be explained. This is why in this section we examine the dark matter halos found by the SUBFIND algorithm, since SUBFIND selects halos by their overdensity and therefore we can be sure to only find isolated halos, that is halos that do not live within the virial radius of a larger halo, with embedded substructures within its virial radius.

At $z = 0$ SUBFIND found 41008 isolated halos of which 131 have masses within the specified mass range. 6 additional halos have a higher mass than $10^{14} M_\odot$. When necessary we will refer to these halos as SUBFIND-groups.

5.1.1 Mass Accretion History

Before examining the groups quantitatively we investigate the phenomenology of these halos. We follow the evolution of the most massive branch of the group

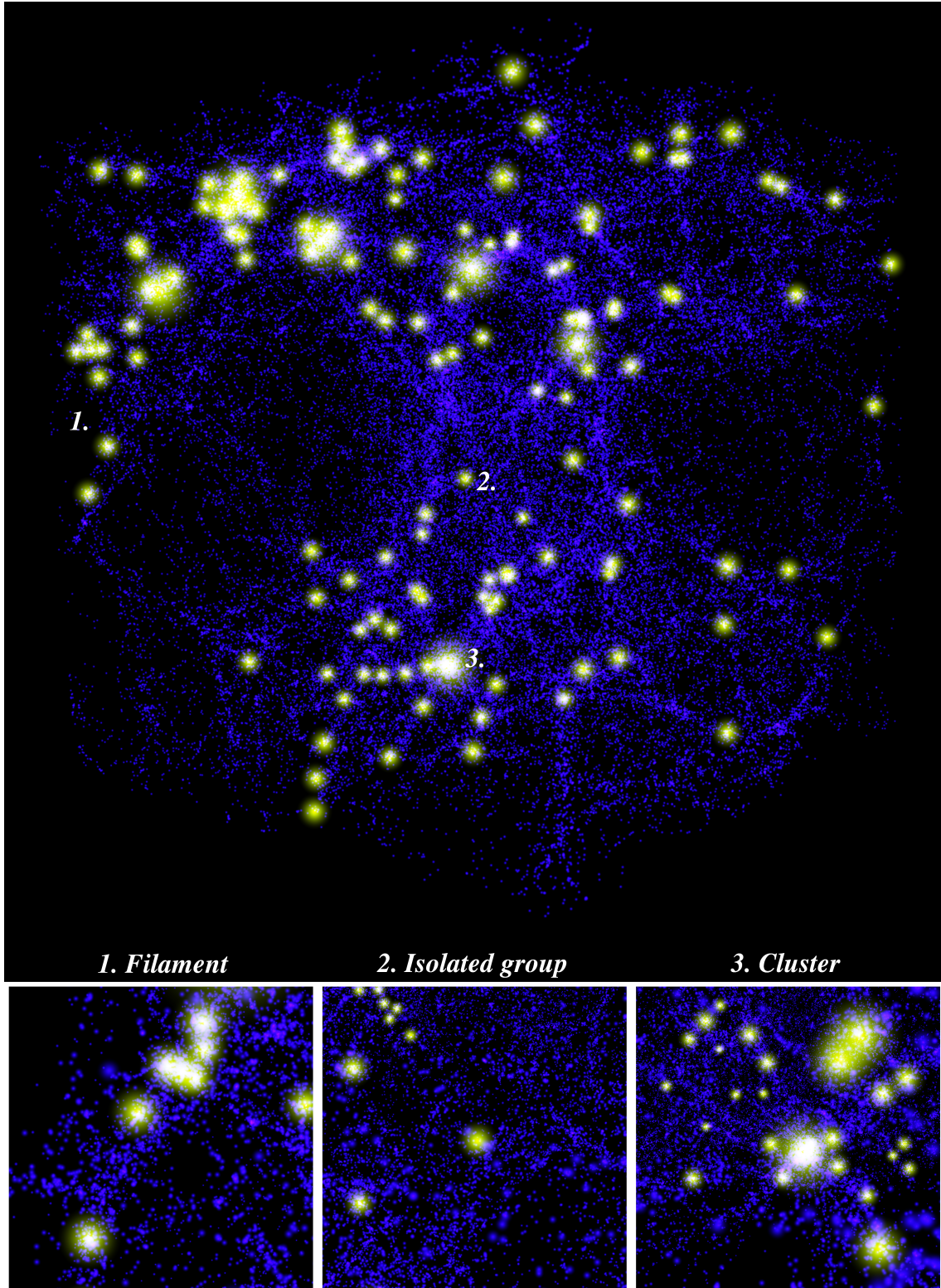


Figure 5.1: The whole simulation box at $z = 0$. Highlighted are the groups (small yellow spots) and the clusters (large yellow spots). Blue dots represent all halos with masses of at least $10^{10} M_{\odot}$. Lower panels show selected regions of the box with higher resolution.

halos. Looking at the mass accretion history we single out four archetypes of group assembly:

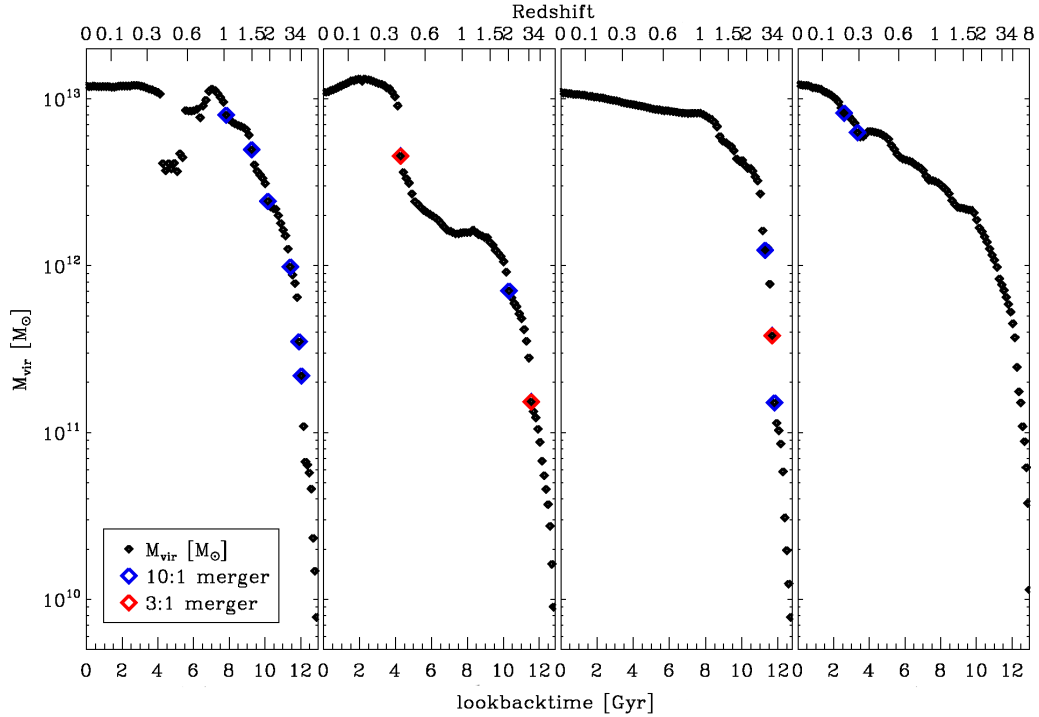


Figure 5.2: The figures show the four different archetypes of virial mass behaviour: Left: Disturbed group; Central left: Merger driven group; Central right: Starved group; Right: Smooth forming group

1. **Disturbed groups**, which have a spontaneous jump in the virial mass, they start growing and spontaneously lose a lot of their mass, but then jump back to higher masses, see Figure 5.2, left panel.
2. **Merger driven groups**, which experience a merger that causes a jump in the mass accretion history, as seen in Figure 5.2, central left panel.
3. **Starved groups**, which show a fast increase of the mass at high redshifts where they reached almost their final mass, as seen in Figure 5.2, central right panel.
4. **Smooth forming groups**, which show a smooth increase of the mass, see Figure 5.2, right panel.

Also shown in Figure 5.2 are merger events (into the main branch of the tree) with merger ratios below 3:1 (red) and 10:1 (blue). 43.5% of all groups experience at least

one major merger ($\frac{M}{m} \geq 3$), among them 14% had two major mergers (corresponding to 6% of all groups). 10:1 mergers are fairly common events for all groups.

In general the growth of the virial mass is connected with the continuous accretion of small halos, resulting in a smooth increase of the virial mass. This happens in the case of smooth forming groups. In the case of merger driven groups we see the strong influence a major merger can have on the mass evolution. If the infall stops early, the group does not grow anymore and we see a starved group.

Most groups in our sample show a mass accretion history that is a combination of smooth formation and starved behaviour at low redshifts.

5.1.2 The Special Case of Disturbed Halos

We can understand the case of disturbed mass accretion by looking at a series of density plots. In the example of Figure 5.3 we can first see another large halo falling into the group halo, which results in an increase of the virial mass. When this second halo does not merge with the group halo we can see a fly-by situation: The virial mass of the group decreases strongly because mass is transferred to the second halo. If the second halo comes back again as it happens in this example, the virial mass jumps up again. The virial radius shows a corresponding behaviour.

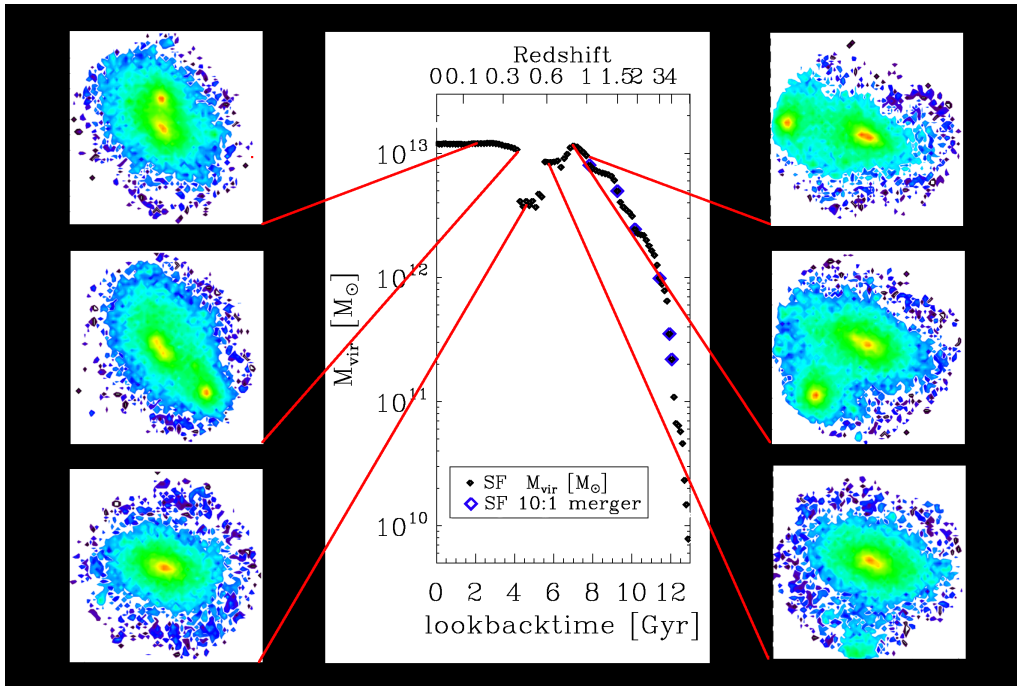


Figure 5.3: Fly-by event: Evolution of the virial mass (normalized to maximal mass). Also shown is the virial radius and the corresponding density plots at different redshifts.

5.2 The FOF-Sample

According to Girardi and Giuricin (2000) groups are not necessarily virialized systems and their extension is larger than the one expected for a virialized system of the same mass. Therefore we need a halo identification algorithm that does not search for systems cut at the virial radius of its massive central halo but for systems in close contact. The FOF algorithm offers exactly this as it connects particles that are within a specified linking length, as explained in section 4.2.

Using the FOF algorithm we find 150013 halos of which 140 are within the mass range specified for groups and 7 have a higher mass. It is not possible to find subhalos using the FOF algorithm, but we applied the SUBFIND algorithm to discern a substructure within the FOF halos. The subhalos identified in this way will from now on be called subhalos. Subhalos are called isolated, when they are part of the isolated merger trees, that is they are not members of a larger SUBFIND structure. A FOF group can consist of several isolated subhalos.

5.2.1 Differences between FOF and SUBFIND

First we compare the group halos found with the FOF and the SUBFIND algorithms. We see three different archetypes:

1. **Protocluster:** Protoclusters consist of several SUBFIND-groups that are linked into one large FOF group, i.e. interacting groups that are not yet joined into a single large system.
2. **Simple group:** A simple group is a FOF group that contains exactly one SUBFIND group, i.e. results of FOF and SUBFIND are mostly the same.
3. **Aggregation group:** An aggregation group is a FOF group that does not contain any SUBFIND group. It consists of several smaller SUBFIND halos, that do not reach group mass individually.

In the FOF sample we find 5 protoclusters, 21 aggregation groups and 82 simple groups. Examples for these archetypes can be seen in Figure 5.4.

The remaining 32 FOF groups are a combination of the simple and the aggregation group type. They consist of a single SUBFIND group and several SUBFIND halos with mass above $10^{12}M_{\odot}$. These groups have a variety of different mass constellations: In some, the mass of these less massive subhalos does not contribute a significant portion of the group mass, thus the group shows the same behaviour as a simple group. Other groups however draw a significant fraction of their mass from these less massive subhalos, thereby exhibiting the behaviour of an aggregation group.

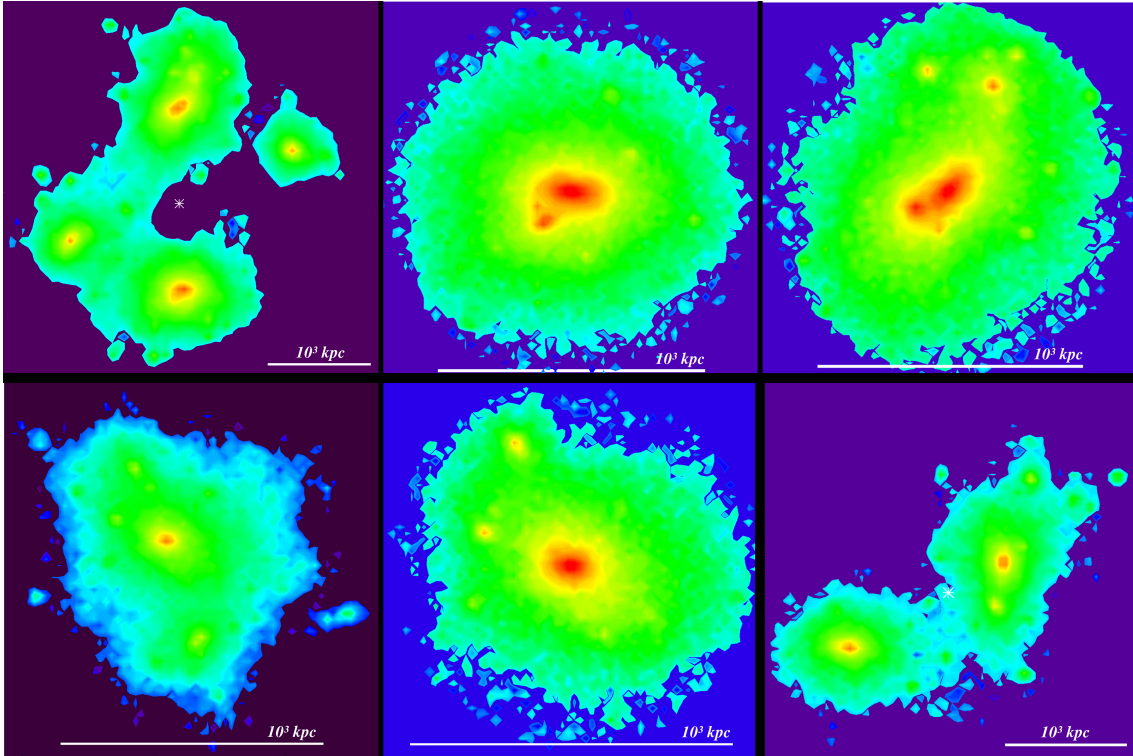


Figure 5.4: Top: The left panel shows a proto-cluster, the other panels show the two SUBFIND groups contained in the proto-cluster. The proto-cluster is also inhabited by two less massive SUBFIND halos. Bottom: The left panel shows a simple group, the central panel shows the according SUBFIND group. Note however the additional halo in the lower part of the FOF diagram. The right panel shows an aggregation group that is built up of two halos with about $5 \times 10^{12} M_{\odot}$.

5.2.2 Mass Accretion History

Comparing the mass evolution of FOF groups with their corresponding SUBFIND groups we find that the FOF mass is generally greater than the SUBFIND mass. These differences, however, are small for most of the time. Only at certain times does the FOF mass increase spontaneously when a new halo is linked, rising above the SUBFIND mass. In the following timesteps the SUBFIND mass usually slowly increases until it catches up with the FOF mass when the infalling halo passes the virial radius of the central halo. This behaviour can be seen in Figure 5.5. Furthermore, the effects that cause a sudden drop in the SUBFIND mass (disturbed groups) seem to have no effect on the FOF mass.

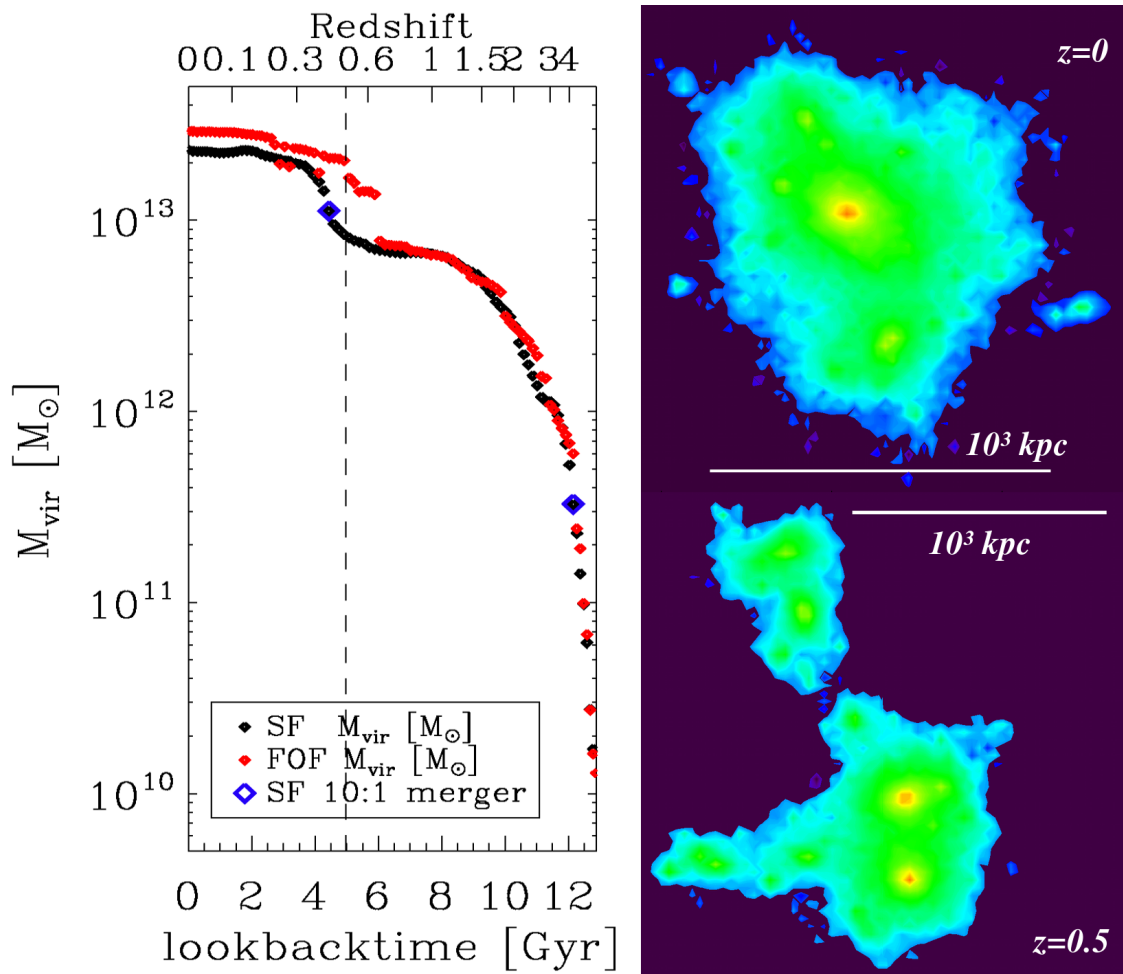


Figure 5.5: Left: Mass accretion history for a simple group. The black symbols show the mass of the whole FOF group, the blue ones show the mass of its most massive subhalo. Right: Densities at $z = 0$ (top) and $z = 0.5$ (bottom). We see that the group is changing from an aggregation group to a simple group with time.

The mass accretion history also provides us with clues towards the fate of aggre-

gation groups. We picked out a simple group at $z = 0$ and followed it back in time until $z = 0.5$. At $z = 0.5$ this group turns out to consist of three halos with masses of $9.1 \times 10^{12} M_\odot$, $3.4 \times 10^{12} M_\odot$ and $1.8 \times 10^{12} M_\odot$ respectively, i.e. it is an aggregation group.

The fact, that the SUBFIND mass tends to follow the FOF mass also supports the idea that aggregation groups are less evolved systems that will become more concentrated in the future and therefore actually are possible candidates for loose groups.

The mass assembly history of dark matter halos has also been studied by Li et al. (2007). They analyzed inter alia a $300^3 h^{-3} \text{Mpc}^3$ -box with 512^3 particles of $1.3 \times 10^{11} M_\odot$ with $\Omega_0 = 0.24$, $\Omega_\Lambda = 0.76$ and $h = 0.73$, for which they obtained halo statistics in the mass range we are looking at. Their cosmology is similar to the one used in our simulation, but their resolution is not as high as ours. They also used a FOF-algorithm with linking length $b = 0.2$ to identify the halos.

We compare our results with theirs and find that they are in good agreement, as can be seen in Figure 5.6. Therefore we can be sure that we established a group

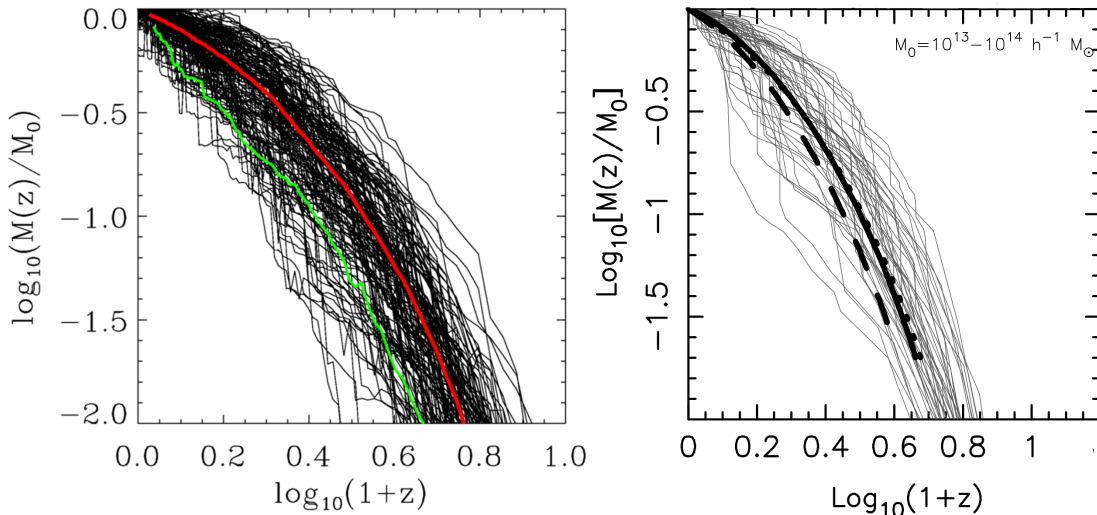


Figure 5.6: Mass accretion histories of dark matter halos with present day mass between $10^{13} M_\odot < M < 10^{14} M_\odot$. Left: The mass accretion histories for our 140 FOF group mass halos. The red curve is the average of all group mass accretion histories. The green curve is the average of the 7 cluster halos in our FOF sample. Right: Figure 2 taken from Li et al. (2007): Mass accretion histories for 40 random halos with group mass in the $300 h^{-3} \text{Mpc}^3$ -box. The dotted black line is the average of the mass accretion histories of all halos within this mass range. The dashed and solid lines show this average for different types of simulation.

sample comparable with statistics from other simulations. In this figure we have also shown the average mass accretion history for the 7 cluster halos in our FOF catalogue. It is not very smooth due to the bad statistics. Nevertheless we can

see that the clusters reach the same mass fractions at significantly lower redshifts compared to the average group. This is what was to be expected from the principle of hierarchical growth.

5.3 Global Properties of the Groups

After introducing the group samples we are analysing in this work we will now take a closer look at the global properties of our groups, especially the mass distribution and the number of groups generated throughout cosmic time.

Figure 5.7 shows the distribution of the group masses at $z = 0$. We can see that most of the mass in both samples is concentrated below $5 \times 10^{13} M_{\odot}$, although the FOF group sample has a significant amount of groups with higher masses than the SUBFIND group sample. This is due to the fact that FOF links more structures together than SUBFIND and therefore the halos are more massive. Indeed we just have two SUBFIND groups with more than $5 \times 10^{13} M_{\odot}$. We will come back to these two groups later when we analyze the mergers of the SUBFIND halos. The fact that

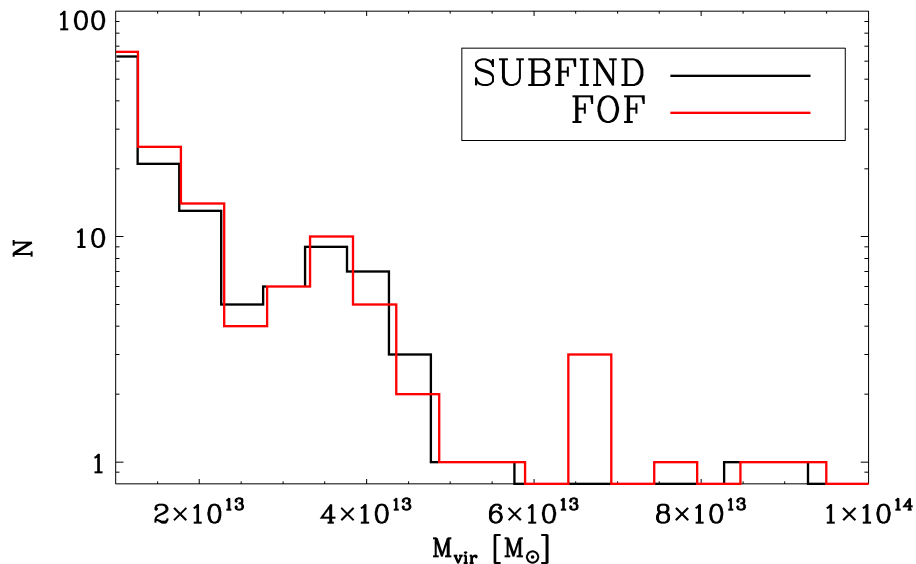


Figure 5.7: Histogram for the distribution of group mass in the SUBFIND and the FOF group samples. The black line shows the SUBFIND groups, the red line the FOF groups.

we have more halos for lower group masses than higher is explained by hierarchical growth. The smaller the mass, the more halos have already evolved. We will see this effect again when we analyze the formation redshift of all halos in the box.

In order to compare our sample with observations we need to be aware of the fact that observers see groups at various redshifts. We find that about 60% of the groups had already reached a mass of $10^{13} M_{\odot}$ at $z = 0.5$ for both samples. Figure

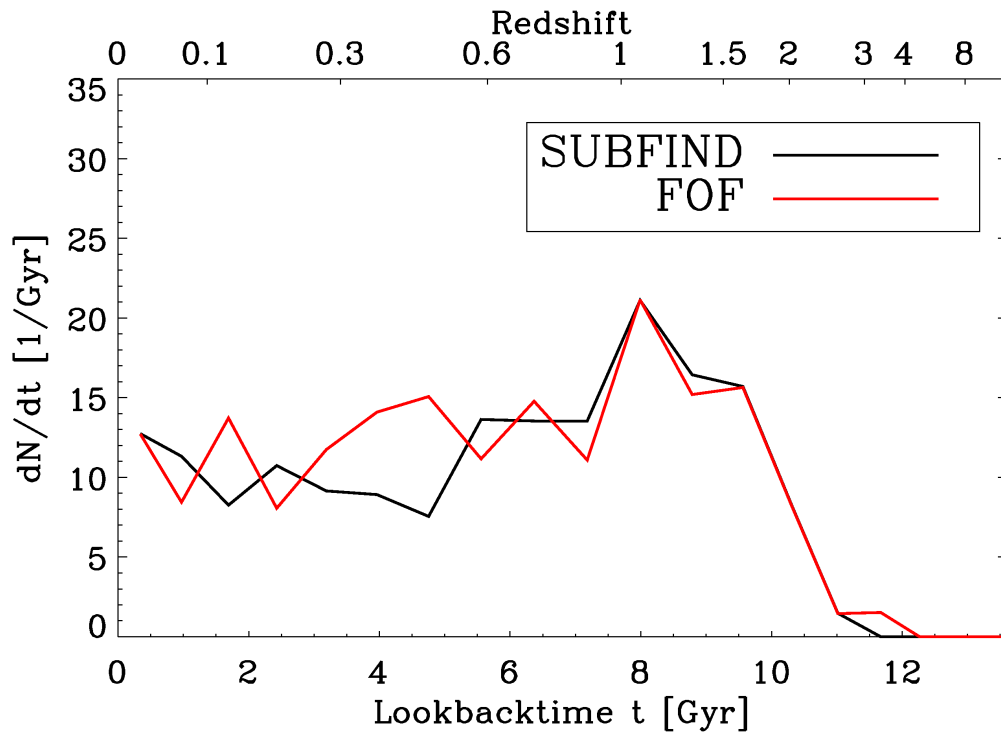


Figure 5.8: Number of newly formed groups per Gyr against time. The black line shows the results for the SUBFIND, the red line the FOF groups

5.8 therefore shows the number of new formed groups per Gyr. Obviously there is a peak at redshift $z \approx 1$ for both the SUBFIND and the FOF halos, but the FOF halos form with a higher rate at low redshifts than the SUBFIND groups. We see that there are only a few groups formed at higher redshifts than $z = 1$ and the rate increases dramatically between $z = 2$ and $z = 1.5$.

We can make rough estimate of the formation redshift using the spherical top-hat collapse approximation described in subsection 2.5.1. Choosing for example a galaxy group with a group velocity dispersion of $\sigma = 300\text{km/s}$ ¹ and a mass of $M = 1 \times 10^{13} M_{\odot}$ we calculate the redshift, at which this halo collapses, with equation (2.22). We find that a halo with these conditions cannot be virialized at redshifts higher than $z = 0.8$ and we would not expect the halo to form much earlier than this.

5.3.1 Formation Redshift

An interesting parameter for halos is their formation redshift. We define the formation redshift as the redshift at which a halo has accreted more than half of its mass at $z = 0$.

The upper left panel of Figure 5.9 illustrates the distribution of the formation redshift with halo mass for all virialized halos. As we would expect from halos in a Λ CDM cosmology, we see hierarchical growth, which means that small structures form earlier than large structures that are generated by aggregation of small structures. Looking closely at the top left diagram in Figure 5.9 we notice that there are only a few objects with high mass and very low formation redshift. In order to understand this effect we identified all SUBFIND halos that exist at $z = 0.5$, $z = 1$ and $z = 2$ and calculated their formation redshifts. The results are also shown in Figure 5.9. We see this effect for each of the samples, although it is less pronounced for the formation redshifts of halos at higher redshifts. Therefore the effect is not caused by a reduction in the formation of high mass halos but rather results from the fact that the halos simply need time to accumulate the same mass they have accumulated at the formation redshift. Only a merger with mass ratio $\frac{M}{m} \simeq 1$ would cause a very low formation redshift. As we will see in the section mergers with such a fraction are not very common for high mass halos.

It should also be noted that the amount of group mass halos at $z = 2$ is very low with only three groups. At $z = 1$ on the other hand we see already several more groups. This corresponds well with the predictions from Figure 5.8 that group halos do not form in a significant amount below $z \approx 1$.

We also find evidence for hierarchical growth by studying the histogram for the formation redshift, as can be seen in Figure 5.10. The number of halos strongly reduces with lower redshift as the halos accumulate to form larger halos. As expected we also found that the mean formation redshift is shifted towards higher redshifts for

¹This is a typical value for a group velocity dispersion according to SDSS data (see subsection 3.3.2).

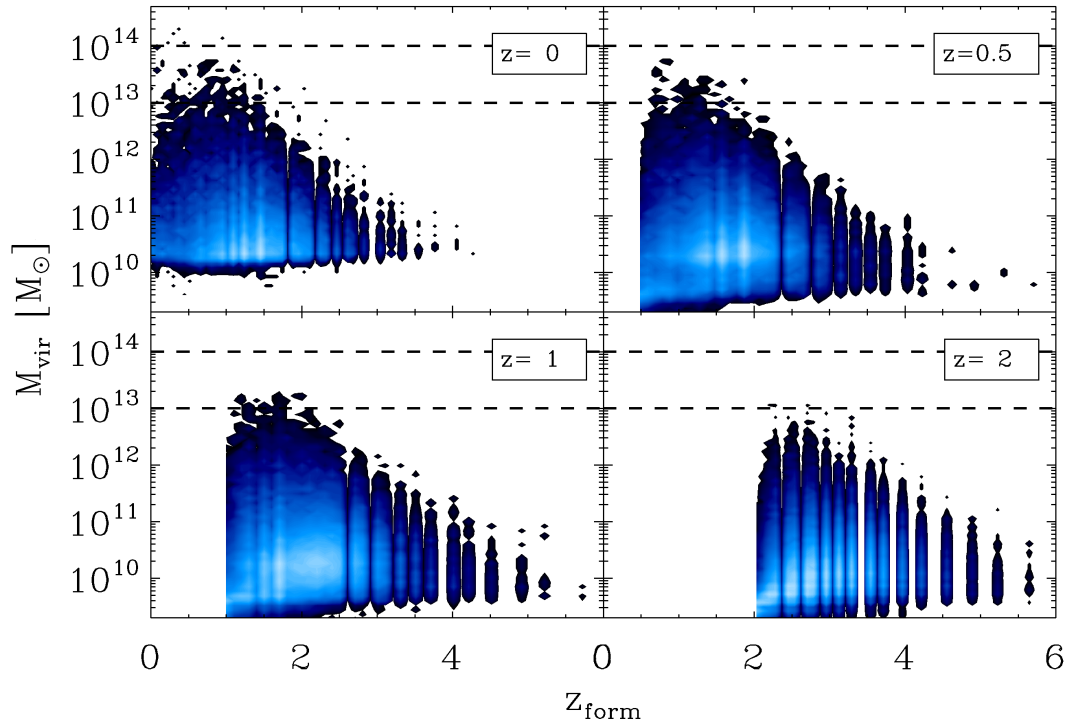


Figure 5.9: Formation redshift for SUBFIND halos in the simulation at different redshifts: Upper left: at $z = 0$; Upper right: at $z = 0.5$; Lower left: at $z = 1$; Lower right: at $z = 2$.

the high redshift samples. The mean formation redshift at $z = 0$ is $\bar{z}_{\text{form}} = 1.26$ for

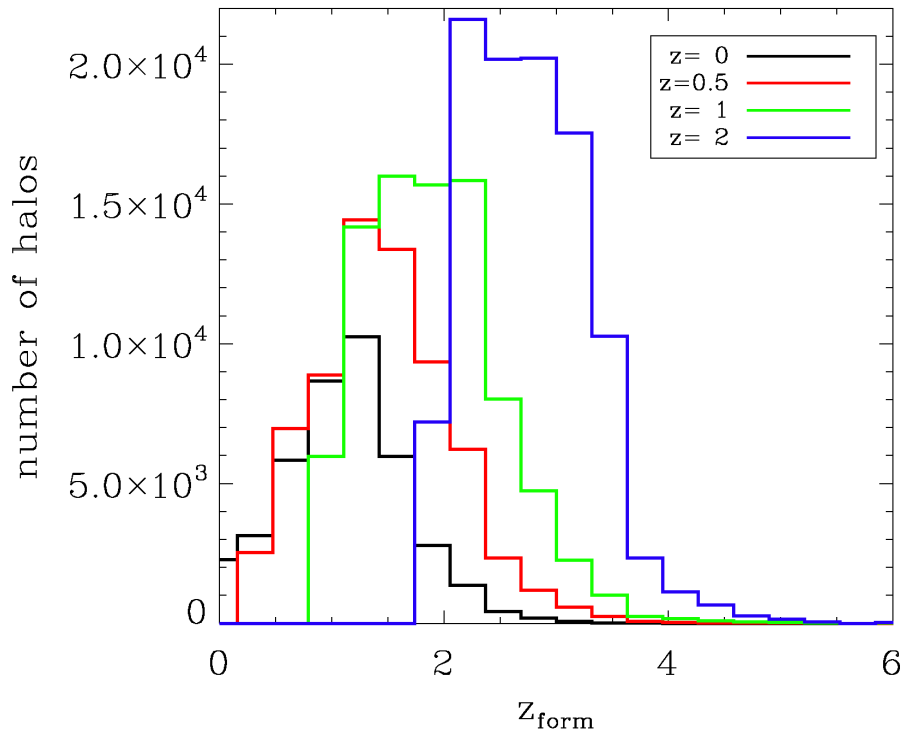


Figure 5.10: Histogram for the formation redshift of all SUBFIND halos in the simulation. The black histogram shows the distribution of formation redshifts for all present-day halos, the red (green, blue) histogram shows the distribution of formation redshifts for all halos at $z = 0.5$ ($z = 1$, $z = 2$).

all halos. When only group mass halos are considered, the mean formation redshift is $\bar{z}_{\text{form}} = 0.75$. This shows again that massive halos form during late stages of the universe.

Li et al. (2007) calculated formation redshifts which are identical to our definition, and they find the median in the formation redshift histogram at about $z = 0.75$ for present-day mass halos of $10^{13} M_{\odot} < M < 10^{14} M_{\odot}$ in their $300^3 h^{-3} \text{Mpc}^3$ box, which is in agreement with our result for present-day halos, as can be seen in Figure 5.11. Although their statistics is better than ours we find similar results, especially for the FOF groups. The SUBFIND groups form generally a bit earlier than the FOF groups, which is due to the fact that a larger fraction of FOF group halos show still ongoing accretion in their mass accretion histories while most of the SUBFIND groups only accrete small halos at high redshifts and therefore show a starved accretion history.

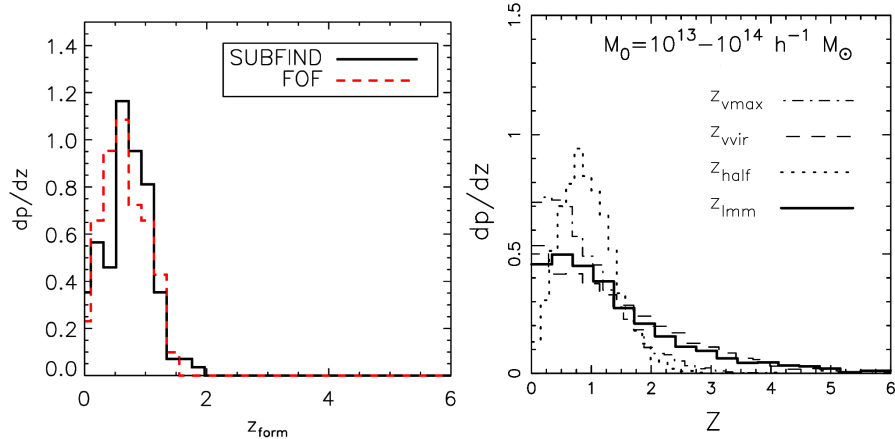


Figure 5.11: Formation redshift of halos with a present-day mass of $10^{13}M_{\odot} < M < 10^{14}M_{\odot}$. Left: The formation redshift of our group samples. The black histogram shows the distribution of formation redshift for SUBFIND groups, the red histogram shows the distribution of formation redshift for FOF groups. Right: Figure 7 taken from Li et al. (2007): The dotted line shows the formation redshift called z_{half} of group mass halos from their 300^3h^{-3}Mpc^3 -box. The other three curves show the results for other definitions for calculating the formation time.

5.4 Mergers

As we have seen in the phenomenological description of the mass accretion, mergers play a significant role in the mass evolution of a group. We were interested in whether the number of mergers correlates with the final mass of the halo. For this we especially distinguish between mergers into the main branch of a tree and the number of mergers occurring in the whole tree. Furthermore we consider major mergers with a mass ratio of the merging halos lower than 3:1, following Genel et al. (2008) and many others, since major mergers deepen the potential well of a halo significantly as they add a huge amount of mass to the halos mass at the time the merger occurs. The results are summarized in Figure 5.12. As we can see, there is no correlation between the number of major mergers in the main branch and the final mass of the group for the SUBFIND sample (left panel of Figure 5.12). About half of the groups do not even have a single major merger in their main branch. Nevertheless, there is an obvious correlation between the number of minor mergers and the final mass.

For the FOF group sample the results are shown in the right panel of Figure 5.12. Even though there are much more major mergers occurring in the main branch of the trees, there is no strong correlation between the present-day mass of a halo and its number of major mergers. As for the SUBFIND groups we see that there is a correlation between the number of minor mergers and the present-day mass of the FOF groups.

The difference between our two group samples results from the fact, that the halos

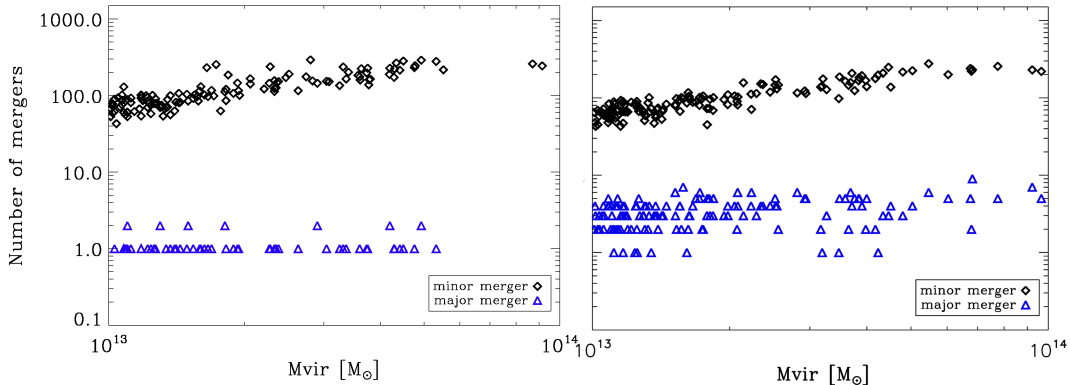


Figure 5.12: Number of mergers versus the present-day mass of the group halos. Left: Diagram for the SUBFIND group sample. The blue symbols show the number of major mergers of ratio less than 3 : 1 with the main branch of the group’s merger tree versus the groups virial mass at $z = 0$, while the black symbols show the total number of all mergers occurring with the main branch of the group’s merger tree. Right: the analogue plot for the FOF groups.

that merge into a group halo are found much earlier by the FOF algorithm than by SUBFIND, since SUBFIND detects the merger only after the infall into the virial radius. Therefore the infalling halo has been stripped much more at the time it passes the virial radius of the halo and so its mass is much lower. Furthermore the FOF halos have generally higher masses than the SUBFIND halos and this influences the merger ratio, too.

Li et al. (2007) analyzed the distribution of the number of major mergers with a ratio of 3 : 1 for FOF halos identified in their $300^3 h^{-3} \text{Mpc}^3$ -box described above. The results are shown in Figure 5.13 in comparison with the results from our FOF sample. As can be seen our results are in good agreement with theirs again, even though their statistics is better. The differences result from cosmic variances.

Like Li et al. (2007) we found that most of the major mergers occur at high redshifts, while major mergers are rare at low redshifts for group mass halos. This is due to the fact that the number of halos decreases with higher masses and therefore the probability of a major merger decreases with increasing mass.

5.4.1 Group Mergers

A group merger is an event in which two halos of masses between $10^{13} M_{\odot}$ and $10^{14} M_{\odot}$ merge. We were in particular interested in the question if there are groups in our simulation box that have undergone a group merger. We find that this is the case for the two most massive groups in our SUBFIND sample at $z = 0$. As we have seen in Figure 5.7 these two groups are almost twice as massive as any other SUBFIND group in the sample. We tested six halos that are identified as clusters in the SUBFIND catalogue and find that three of them had a group merger too, both

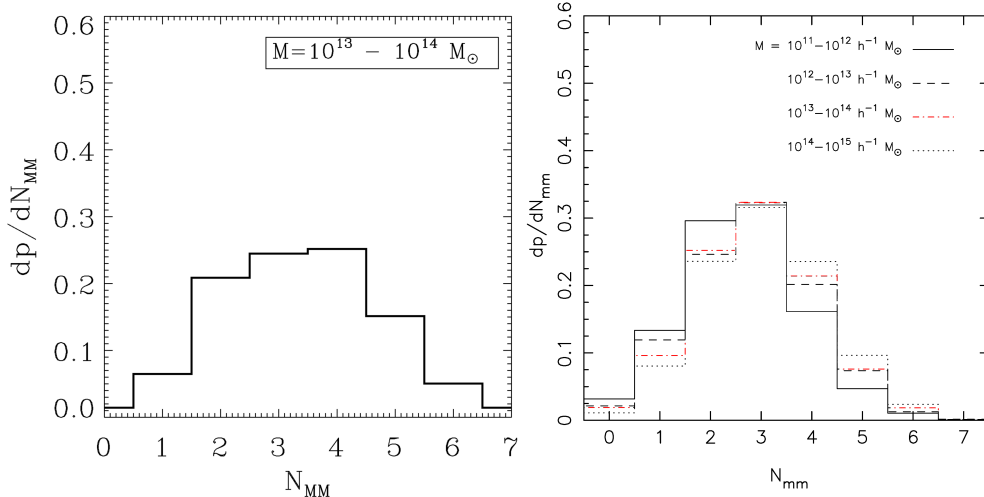


Figure 5.13: Distribution of the number of major mergers (mass ratio smaller than 3:1). Here $\frac{dp}{dN_{mm}}$ represents the relative frequency of galaxy groups with N_{mm} major mergers. Left: The distribution of number of major mergers in our FOF sample for group halos. Right: Figure 10 taken from Li et al. (2007): The distribution of number of major mergers in the $300^3 h^{-3} \text{Mpc}^3$ box for different mass bins. The histogram comparable with our group mass is the dashed-dotted line.

most massive clusters even had two group mergers.

This leads us to the conclusion that the two most massive groups are already poor clusters, as their mass accretion history is also similar to that of clusters as seen in Fig. 5.6. Though the group mergers are massive events they are not massive enough to count as major mergers, which shows that the classification of major and minor mergers in the case of high mass halos is not very meaningful.

5.4.2 Multiple Merger Events

Multiple mergers are merger events where more than one halo is falling into a host halo. We are interested in the question whether multiple mergers play a significant role in the formation of galaxy groups or not. Therefore we need to estimate the time a merger endures.

We follow Genel et al. (2008) who calculated the time T_{merg} a merger is going on by using the timescale of dynamical friction for (FOF) dark matter halos found by Boylan-Kolchin et al. (2008):

$$T_{\text{merg}} = 0.7 \text{Gyr} \frac{(M/m)^{1/3}}{\ln(1 + M/m)} \frac{H_0}{H(z)},$$

where M/m is the mass ratio of the merging partners with $M > m$. For comparison with the results from Genel et al. (2008) for the Millenium simulation, we plotted the merger fraction with redshift for halos in different mass bins. The result is

shown in Figure 5.14. Since the Millenium simulation has much better statistics our

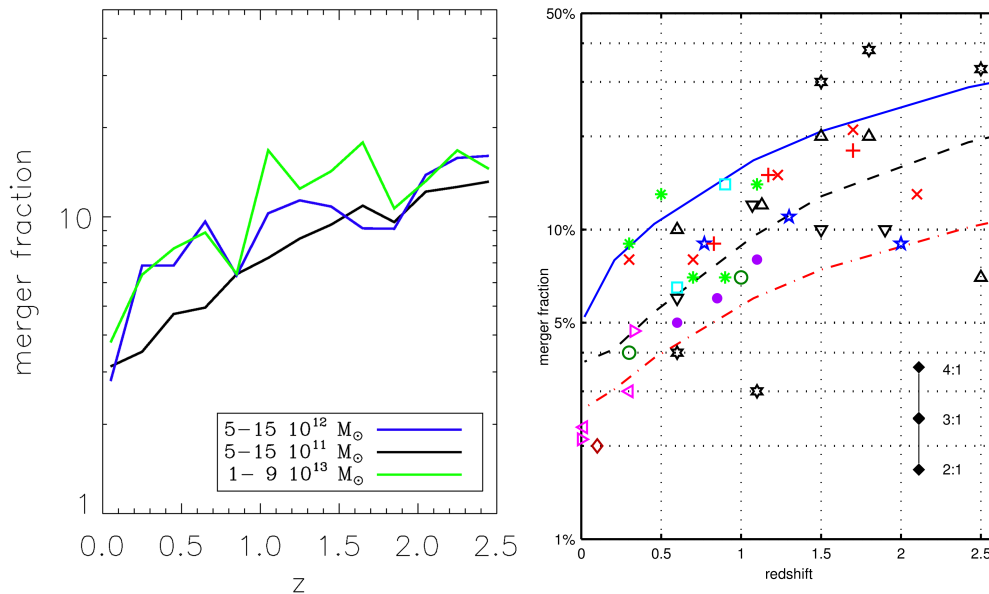


Figure 5.14: The merger fraction as a function of redshift. Left: Merger fraction for the FOF halos from our simulation box. The different lines show the fractions for halos in different mass bins. Right: Figure 8 taken from Genel et al. (2008): The different lines show the fractions for halos from the millenium simulation of different mass bins. The blue line shows halos with masses of $\log(M_{halo}[M_{\odot}]) = 13$, the black line shows halos with masses of $\log(M_{halo}[M_{\odot}]) = 11.5$, the red line shows halos with masses of $\log(M_{halo}[M_{\odot}]) = 10.9$. The symbols are observational data for comparison.

results are noisier especially for the group mass halos, but nevertheless in general agreement.

We now calculated the time at which a multiple merger event occurs. The results are shown in Figure 5.15 for different merger ratios. We see that a multiple major merger is a very rare event for group halos, and they only occur at high redshifts. This is in agreement with our result that major merger do not play a significant role in the evolution of group halos. While multiple major mergers with a ratio of less than 3 : 1 are rare, multiple mergers with mass ratios less than 10 : 1 are more common, even if their fraction decreases with lower redshifts. In the case of a merger ratio of less than 20 : 1 multiple merger are a fairly common event at all redshifts for group halos. We can even find a significant fraction of multiple mergers with three or more halos merging into the host halo.

We compared the fraction of multiple major mergers for groups with the one for halos in a present-day mass range of $5 \cdot 10^{11} M_{\odot} < M < 1.5 \cdot 10^{12} M_{\odot}$ and found that the fraction of multiple major mergers is a little bit higher, but they are not a common event even for low mass halos as can be seen in Figure 5.16. It would be

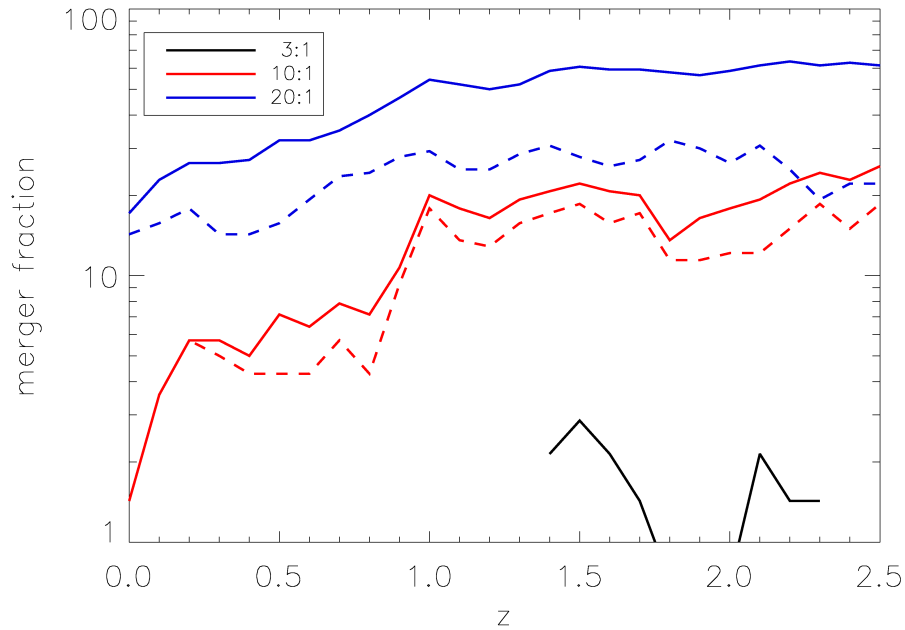


Figure 5.15: Multiple merger fractions for our group mass halos from the FOF sample. The different colors show the results for different merger ratios. The black line shows the fraction for multiple major merger, the red line is for multiple mergers with a mass ratio of less than 10:1 and the blue line for mergers with a mass ratio of less than 20:1. The dashed lines are the lines for the fraction of triple mergers, that is all multiple mergers with more than two infalling halos into a host halo are subtracted, while the solid lines show the fraction for all multiple mergers independent of the number of infalling objects.

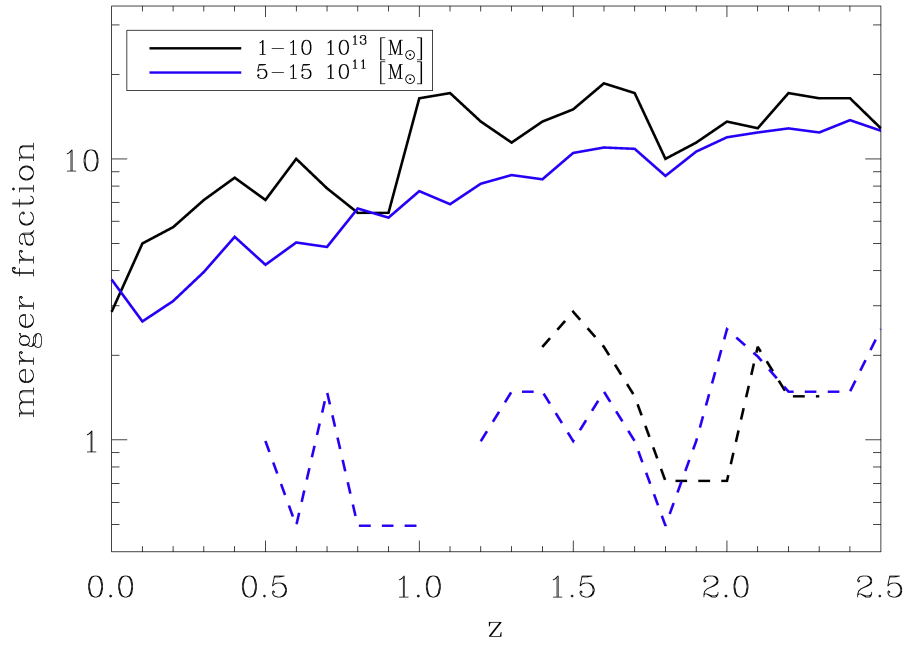


Figure 5.16: Multiple major merger fraction with redshift for halos within different mass bins. The solid lines show the general major merger fraction, the dashed lines show the major merger fraction for multiple mergers with two halos falling into a host halo. The black line shows halos with group mass, the blue lines show halos with a present-day mass of $5 \cdot 10^{11} M_{\odot} < M < 1.5 \cdot 10^{12} M_{\odot}$.

interesting to study the influence of multiple mergers on the mass accretion history of group halos, especially for minor mergers, in more detail, and we will address this in the future.

5.5 Discussion

In the preceding sections we have analyzed global properties of group halos. We find that these halos are mostly found on filaments within the box. Those that are in less dense regions of the simulation box often show starved behaviour in their mass accretion history with no significant mass infall for a prolonged period of time.

In our study of SUBFIND and FOF dark matter group mass halos we found that there is a big difference between these two kinds of groups.

It turns out that most of the isolated SUBFIND groups consist of one central halo, and a starved mass accretion at low redshifts. A few groups however have two or more larger halos within their virial radius, showing signs of interaction between them and an accretion history that is continuously increasing. In general isolated SUBFIND groups which end up with a starved mass accretion consist of a single main halo at $z = 0$. The whole sample of isolated SUBFIND groups is plotted in Appendix A.

On the contrary FOF groups show a large variety of substructures at $z = 0$ and in general more activity in their mass accretion history. We have also seen that the groups that are nearly identical with their SUBFIND pendant pass through less evolved and less concentrated states during their accretion history which indicates that these structures evolve from loose, less evolved systems to compact systems which are barely larger than the virial radius of the main halo. (Of course they do not have to stay in this compact state since new infall of halos is possible). The whole sample of FOF groups is plotted in Appendix B.

This is qualitatively consistent with observations, as the more concentrated groups are characterised by large X-ray halos and intra group light and are generally denser than the loose, wide-spread groups, which is exactly what we see in the SUBFIND group sample. Less concentrated group members are spread wide and this can be seen for the FOF groups in our sample, too, as these groups are generally more prolonged than the SUBFIND groups.

So far we see that our two samples of groups provide a good description of reality. Especially, we have identified a FOF group consisting of two isolated SUBFIND groups of medium mass and two small groups which resemble the observations of the protocluster made by Kautsch et al. (2008) (see section 3.2.3).

We also analyzed the merger history of virialized groups and compared it with results from Li et al. (2007) who studied mass accretion histories of halos in various mass ranges statistically. We studied the mass accretion and merger history for group halos in more detail and found that the most important mechanism for the mass accretion of groups is the continuous accretion of low mass halos. Most groups do not even have a single major merger, and if a group has a major merger it

generally happens long before $z = 0.5$, i.e. it occurs while the mass of the group is still low. This is the same for both the SUBFIND and the FOF sample, even if the number of major mergers for FOF halos is generally higher.

Nevertheless, we have also seen that the definition of major mergers as mergers with a fraction of $\frac{M}{m} \leq 3$ is not that representative for group halos as it does not include group mergers, i.e. the merger of a high mass group and a less massive group is not identified as major merger, even though group mergers increase the halo mass significantly. From our study we found that group mergers typically occur in clusters and not in galaxy groups and therefore can be assumed as a possible formation scenario for galaxy clusters.

Finally we investigated the fraction of multiple mergers by calculating the time span of a merger event using the timescale of dynamical friction for (FOF) dark matter halos found by Boylan-Kolchin et al. (2008). We found that multiple major mergers are very rare events and do not play a significant role in the evolution of a group halo, while they become more important for less massive halos. As seen before the multiple major merger events only occur at high redshifts. Multiple mergers with lesser merger ratios however are fairly common events for group mass halos even at present-day. There are even some multiple mergers still going on in most groups. Since a mass ratio of 10 : 1 is still a massive event in a group environment these multiple mergers are highly interesting and we will study them in the future in more detail.

6 Subhalos

Until now we have only studied global properties of the groups found in the simulation box. However, an important attribute of a group of galaxies is its substructure. In this chapter we will therefore look at subhalos within group halos and will examine the properties of galaxy group members from a dark matter only study.

We will first study the distribution and general properties of subhalos at $z = 0$. In section 6.3 we will compare the evolution of the number of subhalos to the mass accretion history of the host halo. Section 6.4 will deal with mergers between substructures and in section 6.5 we will study the mean velocity dispersion of the whole group. In section 6.6 we will discuss the results of this chapter.

A subhalo is a structure embedded into a larger, more massive structure. In the case of SUBFIND halos this means the subhalos lie within the virial radius of an isolated halo, in the case of FOF halos subhalos are all substructures within the FOF halo. Subhalos are generally detected using the SUBFIND algorithm even in the case of the FOF sample, as FOF is not able to detect subhalos on its own. The virial mass of the subhalos is limited by the resolution of the simulation, which means there are no subhalos with masses lower than $4 \cdot 10^9 M_\odot$. We will refer to halos which are not subhalos of a more massive structure as host halos.

6.1 Subhalo Abundance

In order to obtain a general overview we will investigate the number of subhalos at $z = 0$ for both group samples, the isolated SUBFIND halos and the FOF halos in the simulation box. Since we select our group halos only by their mass we compare the halo mass with their number of subhalos to see whether the different mass accretion types might cause a different behaviour in the number of subhalos at $z = 0$. Figure 6.1 shows the number of subhalos with the mass of the host halo (not restricted to groups) with a linear function fitted to the data. We find that there are no clearly separated areas but rather the number of subhalos is given approximately as a linear function of the mass:

$$N_{sub} = \alpha \cdot \frac{M_{vir}}{10^{12} M_\odot}, \quad (6.1)$$

where $\alpha = 1.4$ for SUBFIND host halos and $\alpha = 1.7$ for FOF host halos. The higher α in the case of FOF host halos results from the fact that FOF halos are generally larger than SUBFIND halos of the same mass, as we have seen in the previous chapter, and thus can contain more substructures. The linear function from equation (6.1) provides a good fit at higher masses. For low mass halos a

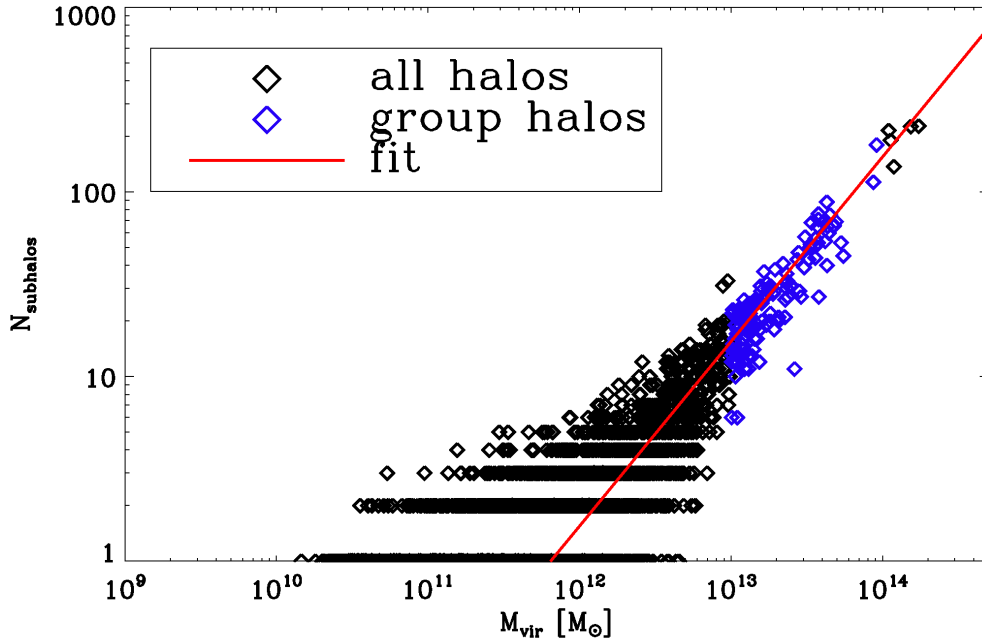


Figure 6.1: Number of subhalos versus host halo mass at $z = 0$. The group halos are highlighted in blue. The red line is the χ^2 -fitted line to the data with $N_{\text{sub}} = 1.4 \cdot \frac{M_{\text{vir}}}{10^{12} M_{\odot}}$.

systematic shift of subhalo numbers towards higher values is caused by the fact that subhalo numbers must be positive integers.

6.2 Subhalo Mass Function at $z = 0$

Some general properties of the subhalo population were studied by Angulo et al. (2008) for the millenium simulation and their own high resolution simulation. The high resolution Λ CDM simulation covers a comoving volume of $100^3 h^{-3} Mpc^3$ with 900^3 dark matter particles of $9.5 \cdot 10^7 h^{-1} M_{\odot}$. The cosmology is the same as the one in the millenium simulation, that is $\Omega_0 = 0.25$, $\Omega_{\Lambda} = 0.75$ and $h = 0.73$.

Angulo et al. (2008) used a FOF algorithm with a linking length $b = 0.2$ to identify dark matter halos in their simulation. The substructures within these FOF halos are identified using the SUBFIND algorithm. They also use SUBFIND to detect subhalos within subhalos.

They used the data from the millenium simulation and their own high resolution simulation to find a universal function that describes the behaviour of the subhalo mass function with host halo mass. The subhalo mass function they found is of the form

$$\frac{dN}{d \ln(M_{\text{sub}}/M_{\text{host}})} = A \left(\frac{M_{\text{sub}}}{M_{\text{host}}} \right)^{\alpha} \exp \left(-\frac{1}{\sigma^2} \left(\frac{M_{\text{sub}}}{M_{\text{host}}} \right)^2 \right), \quad (6.2)$$

where N is the number of subhalos per host halo and A , α , σ are free parameters, which fit the data best for $\log_{10} A = -2.05$, $\alpha = -0.9$, $\sigma = 0.16$. The exponential

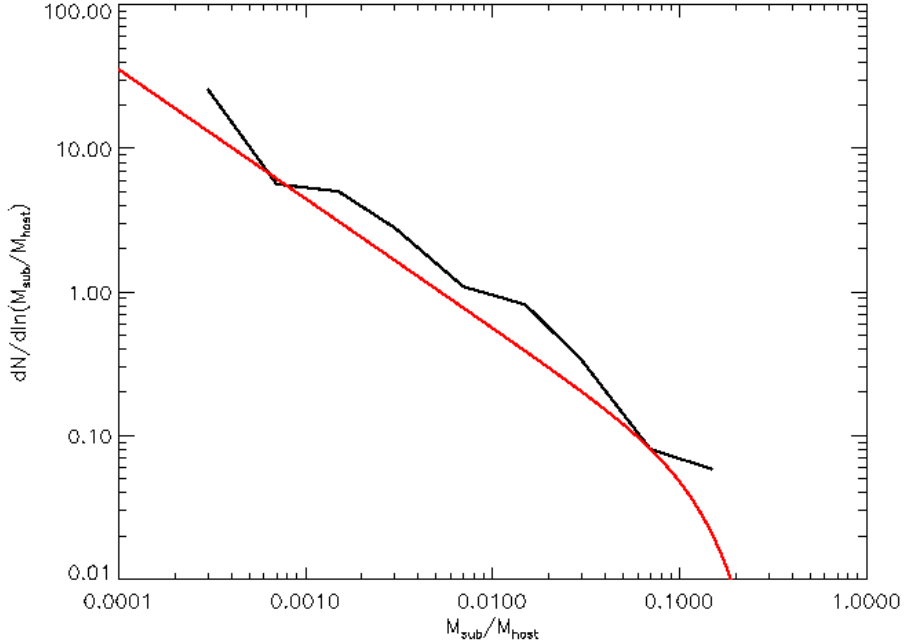


Figure 6.2: Differential number of substructures per host halo as a function of their mass relative to that of the host halo. The red line shows equation (6.2) with values from Angulo et al. (2008). The black line gives results for the SUBFIND groups.

term in this equation is used to correct the usually applied power law fit (see for example Gao et al., 2004) at higher mass ratios, since this power law is only valid for mass ratios below 0.04 at $z = 0$, while for higher mass ratios the subhalo mass function is found to decrease exponentially. We plotted this subhalo mass function for the group halos in the simulation box and found that our subhalo mass function is in general agreement taking statistical errors into account, as shown in Figure 6.2. The deviations might be due to the fact that our simulation has a significantly smaller volume than the millenium simulation, even if the resolution is higher.

Turning to the halos which we identified as groups, Figure 6.3 shows the average number of subhalos of various subhalo masses for the groups. It can be seen that statistically, every group in the SUBFIND sample has one massive subhalo (the central halo) and several significantly smaller halos, especially there exist no subhalos with a mass between $10^{12}M_{\odot}$ and $10^{13}M_{\odot}$. On the contrary, the FOF groups do not show this gap in the distribution of the subhalo mass. At lower mass end both samples behave similarly. It should be noted that the increase with subhalo mass for the lowest masses is caused by the resolution limit.

Following Angulo et al. (2008) we calculate the fraction of the mass of the first, second and third most massive subhalo with the mass of the host halo. The results are shown in Figure 6.4. The most massive substructure contains on average $(8 \pm 4)\%$

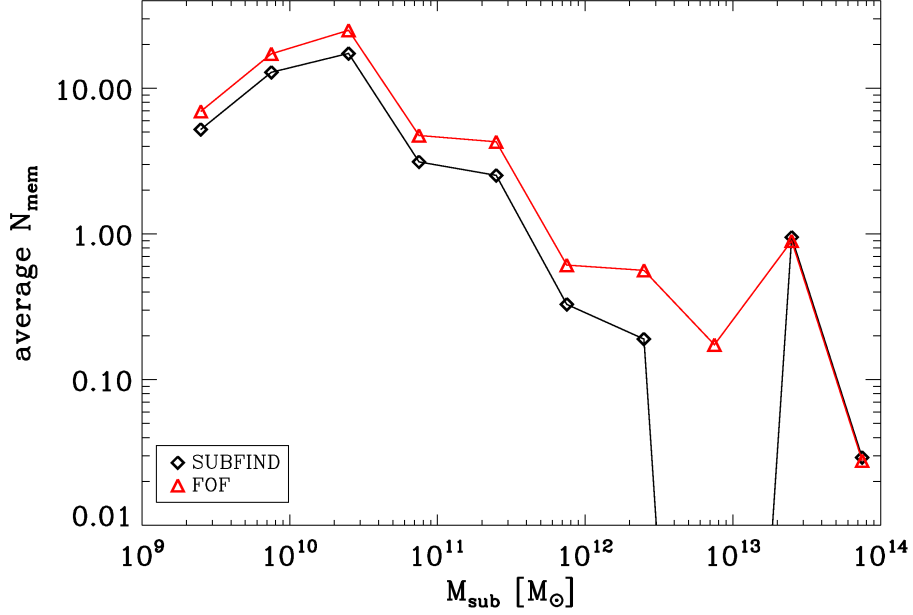


Figure 6.3: Average number of subhalos as a function of the subhalo mass. The black line corresponds to the SUBFIND sample, the red line to the FOF sample.

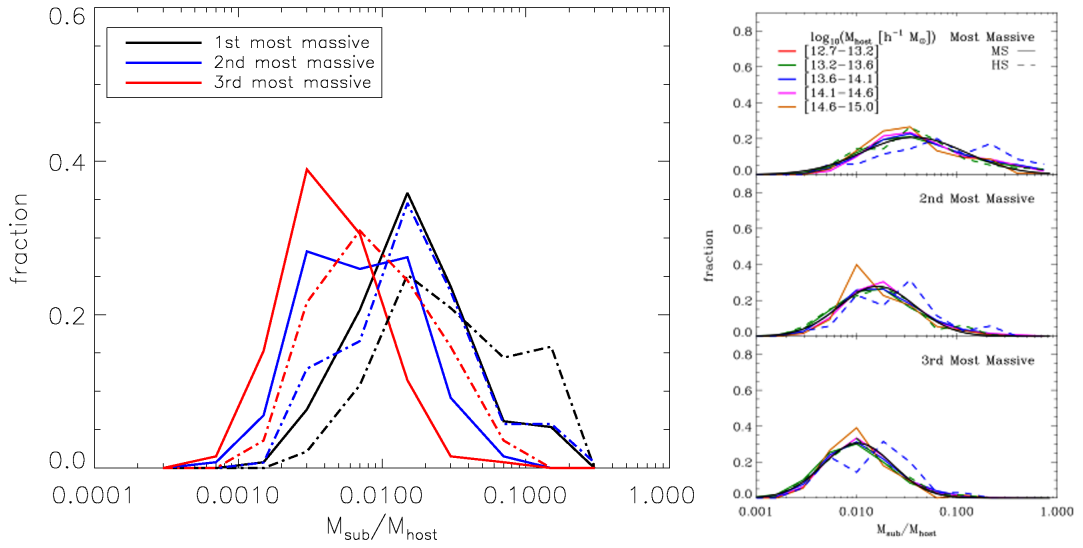


Figure 6.4: Mass fractions of the three most massive subhalos with host halo mass. Left: Mass fractions for our group sample: The figure shows the amount of hosts for a given $M_{\text{sub}}/M_{\text{host}}$, where one of the three most massive subhalos is taken as a reference. Solid lines show the results for the SUBFIND sample while dashed lines show the results for FOF. Right: Figure 2 taken from Angulo et al. (2008). The upper panel shows the distribution for the first most massive subhalo of each group, the central panel shows the distribution of the second most massive and the lower panel the third most massive subhalo.

of the total mass of the host halo for FOF groups and about $(2.5 \pm 1.3)\%$ for SUBFIND groups. The second most massive substructure contains $(2.5 \pm 1.2)\%$ or $(1.0 \pm 0.5)\%$ of the total mass respectively, the third most massive carries $(1.3 \pm 0.7)\%$ or $(0.6 \pm 0.3)\%$. These results are in good agreement with those by Angulo et al. (2008) even though they have better statistics.

The values for the SUBFIND groups are however shifted towards lower values compared to the FOF groups. A reason for this behaviour may be found in the different composition of the FOF and SUBFIND samples: We have seen that a FOF group often contains several SUBFIND groups, so the most massive subhalos of FOF groups correspond to isolated SUBFIND halos, while subhalos of SUBFIND groups are subhalos of subhalos from the FOF-perspective. Therefore we see one more generation of subhalos in the FOF-sample than in the SUBFIND sample. As the SUBFIND groups show the gap in the mass distribution, the mass relative to the host halo is generally lower and therefore the mass fraction peaks are shifted to lower values.

6.3 Phenomenological Description of Subhalo Evolution

In Figure 6.1 we have seen that at $z = 0$ there is a correspondence between the number of subhalos and the final mass of the host halo.

We want to check whether this can also be seen in the evolution of the number of subhalos. As can be seen in the examples given in Figure 6.5, analogue to the archetypes characterised in section 5.1.1, there is a certain correspondence between the mass accretion history and the history of number of subhalos. If a group shows signs of starved behaviour, that is the mass accretion stops at some point in the group's history, the number of subhalos decreases with time.

This is due to the fact that the remaining subhalos are small and get tidally dissolved by the main halo, but since there is no infall from outside anymore the number of subhalos decreases.

6.4 Subhalo-Subhalo Mergers

The properties of the subhalo population of a halo are important for galaxy formation. Subhalos can host small subhalos themselves and mergers between these substructures and the subhalo could cause observable changes like morphological transformations or spontaneous formation of stars. This leads us to the question, whether there are subhalo-subhalo mergers in our groups and how often they occur.

In general, when a smaller halo approaches a larger one, we see that the smaller halo stops accreting mass and particles get transferred to its future host halo. After the infall into the virial radius, the mass of the smaller halo drops dramatically. An example for this scenario can be seen in the lower panel of Figure 6.6.

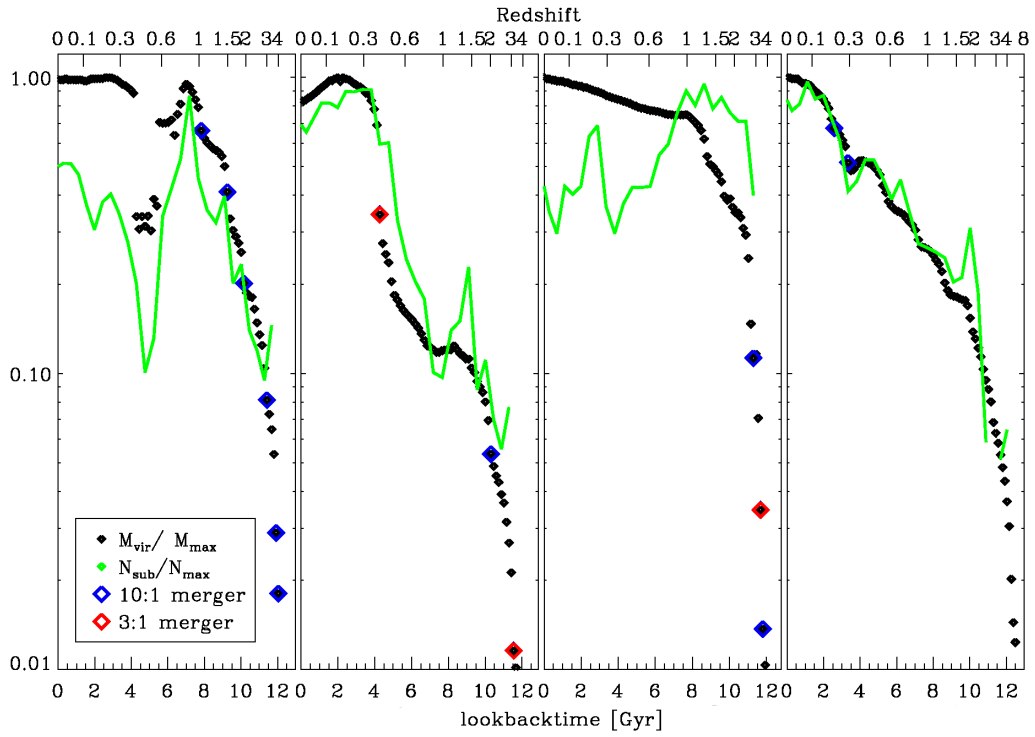


Figure 6.5: Evolution of the number of subhalos for the four different archetypes of mass accretion history. All numbers are relative to the maximum during evolution. The green line represents the number of subhalos. Also shown is the mass development (black) with important mergers highlighted.

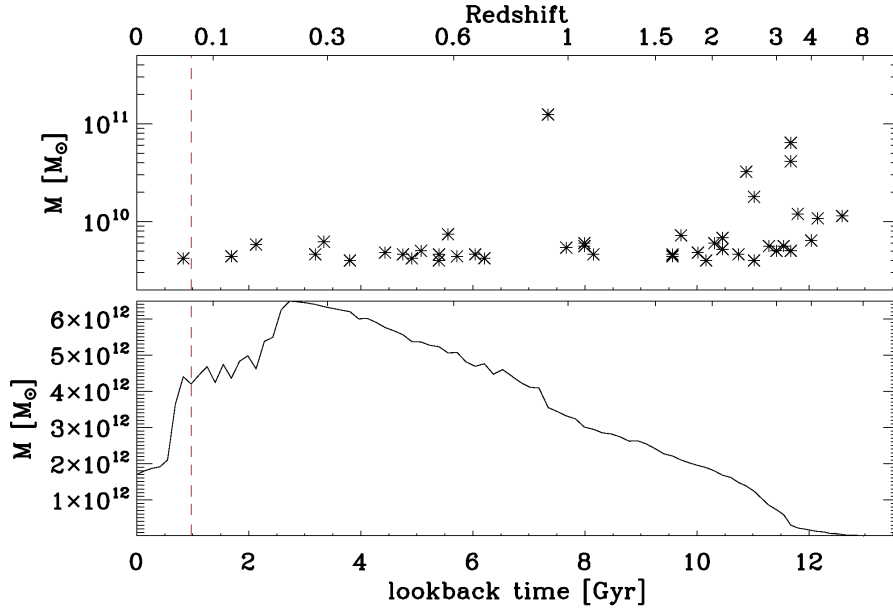


Figure 6.6: Lower panel: Mass accretion history for a halo with a mass $< 10^{13} M_{\odot}$, which merges into a larger host halo at $z = 0.075$ (red dashed line). Upper panel: Mergers into this halo with redshift and mass of the infalling halo. We can see that one merger occurs after the infall into the host halo.

It turns out that there are only a few subhalos that have a merger within the virial radius of their host halos, while the subhalos had a rich merger history before the infall. An example of such behaviour can be seen in the lower panel of Figure 6.6. Figure 6.7 shows the distance from the smaller subhalo S_2 to the larger subhalo S_1 with time for the last merger event in Figure 6.6. As explained before, the merger happens after both halos are within the virial radius of the host halo H . As we can see, the two halos S_1 and S_2 began to interact long before mass stripping by H began. We observe that S_2 starts to orbit S_1 around $a = 0.5$ (that is $z = 1$) and they merge into H at $a = 0.93$ ($z = 0.075$).

The question of subhalo-subhalo mergers was studied by Angulo et al. (2008) for the millenium simulation and their high resolution box. They plotted the mean merger rate of satellite subhalos against the fractional mass of its progenitor and found that it is more likely for a subhalo to merge with the central subhalo than with another more massive subhalo. This is what we see in our studies too, see Figure 6.8.

Since we were just able to study the substructures of the SUBFIND groups in detail, we see one subhalo generation less than Angulo et al. (2008) and therefore we find a significantly lower fraction of subhalo-subhalo mergers. In the range between $z = 0.01$ and $z = 0$ we indeed do not find a single subhalo-subhalo merger. We will investigate FOF-subhalo-trees in the future to be able to make a fair comparison to the results of Angulo et al. (2008).

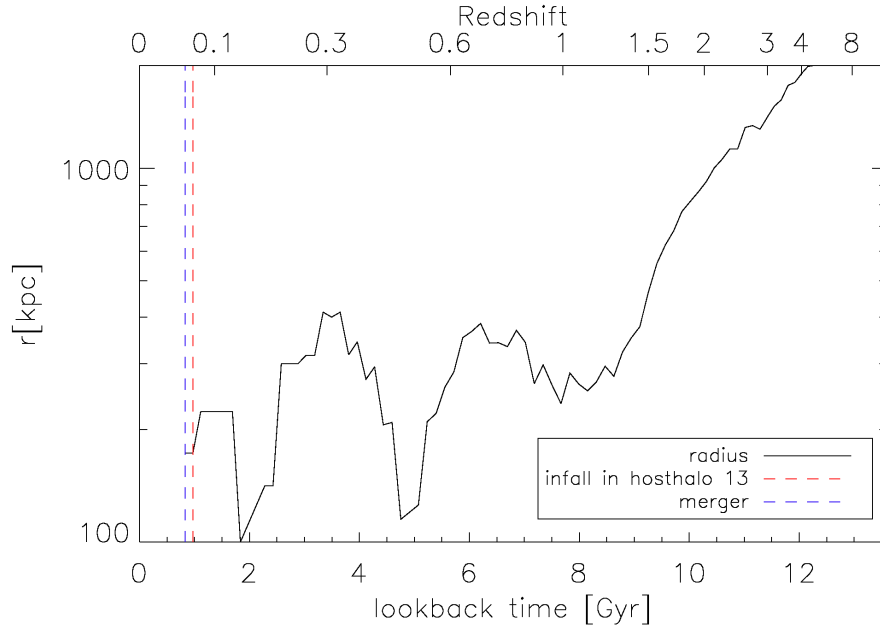


Figure 6.7: Distance between the smaller subhalo S_2 and the larger subhalo S_1 with time. The red dashed line shows the time when S_1 falls into the virial radius of the host halo H , the blue dashed line marks the time of the merger between S_1 and S_2 .

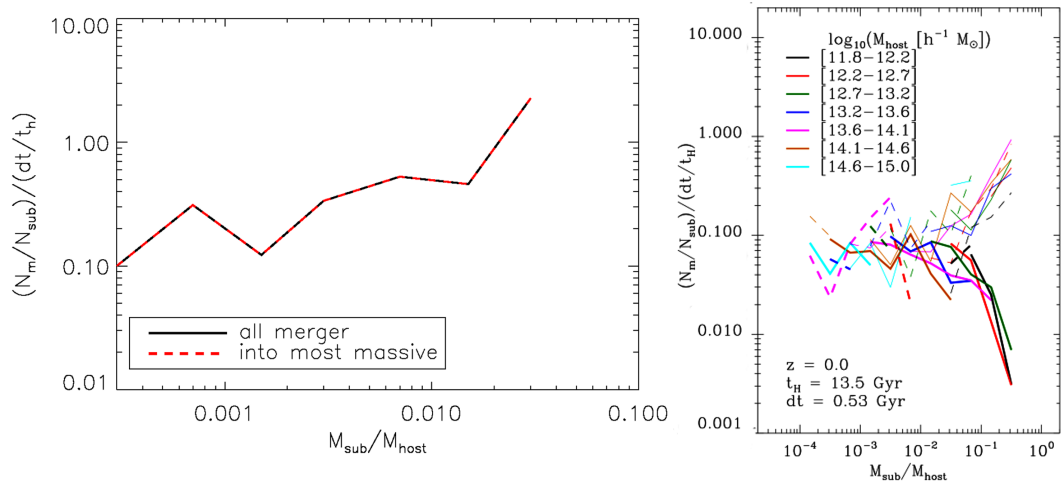


Figure 6.8: Mean number of satellite mergers with the main substructure (the host halo) per unit of time relative to the age of the universe as a function of the mass of the less massive member in the merger with $dt = 0.53\text{Gyr}$ and $t_H = 13.5\text{Gyr}$ according to Angulo et al. (2008). Left: The results from our groups. Since we only study the SUBFIND halos here we have one generation less than Angulo et al. (2008) and therefore we only see merger with main subhalos. Right: The results from Angulo et al. (2008).

Nevertheless we find that 39% of all groups have at least one subhalo-subhalo merger within the virial radius of the host halo. These subhalo-subhalo mergers are generally mergers between a high mass subhalo and a low mass subhalo with a mass fraction of more than 10 : 1. This is in agreement with Angulo et al. (2008) again. Thus we see, subhalo-subhalo mergers are rare but not negligible events in the history of dark matter group halos.

6.5 Projected Velocity Dispersion

We follow Wilman et al. (2005a) who determine line of sight (LOS) dispersions of the velocities of the group members. The LOS velocity dispersion is the standard deviation of the line of sight velocities, calculated as:

$$\sigma = \sqrt{\frac{1}{N} \sum_{i=1}^N (v_i - \bar{v})^2}$$

with

$$\bar{v} = \frac{1}{N} \sum_{i=1}^N v_i,$$

where N is the number of group members and (v_i) the line of sight velocities of the individual group members.

In order to calculate the line of sight velocities of a group we have to choose a line of sight to which the velocities of each subhalo at $z = 0$ are projected. For this LOS we calculate the projected group velocity and the dispersion of the velocities of the subhalos. Figure 6.9 illustrates the result for a single group and a single projection.

Since the choice of the LOS is arbitrary we choose 172 different projections and calculate the mean velocity dispersion for every group. This we plotted against the virial masses of the groups and their number of subhalos, as can be seen in Figure 6.10. We find a correlation between σ and these two parameters. This is to be expected because the velocity dispersion is a measure for the depth of the potential well. We also find that the mean velocity dispersion of the FOF groups is generally lower than that for SUBFIND groups of comparable mass or number of subhalos. This is consistent with the fact, that the FOF groups which are generally more extended allow for higher orbital distances than the SUBFIND groups resulting in lower orbital velocities therefore causing a lower group velocity dispersion.

6.5.1 Comparison with Observed Velocity Dispersions

Since group velocity dispersions are also observed in real galaxy groups, they provide us with an option to compare our results with reality. Dave Wilman from the MPE Munich provided us with data for the groups from the CNOC2 survey analyzed in

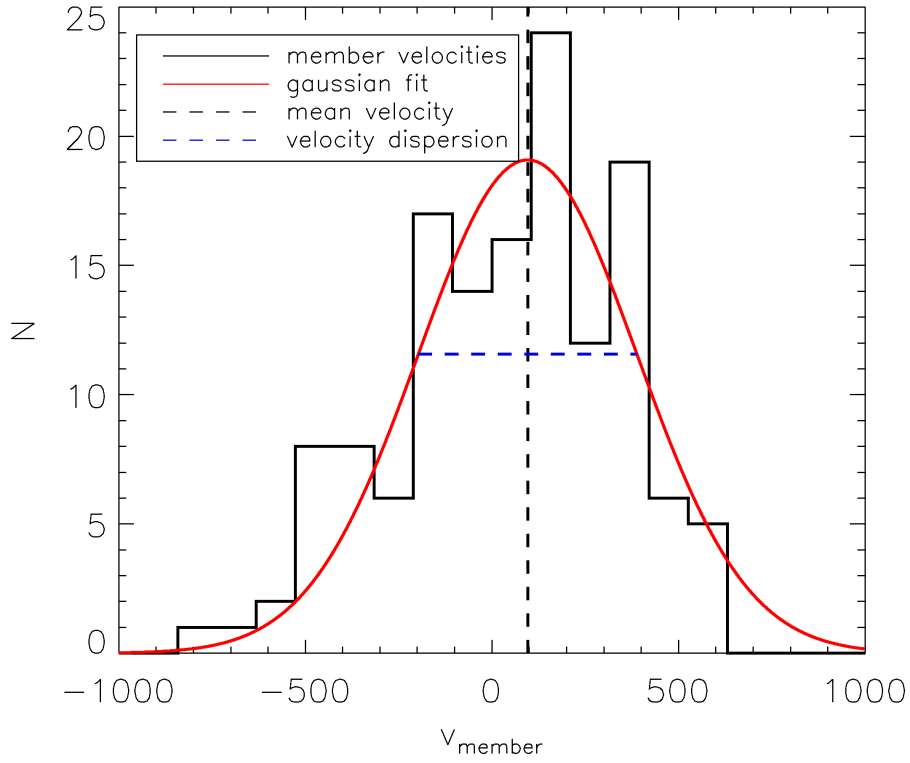


Figure 6.9: Member velocities for a single group and a single projection. The red curve is a Gauss curve with matching mean (black dashed line) and dispersion (illustrated by the blue dashed line). In this case the velocity dispersion is 293km/s.

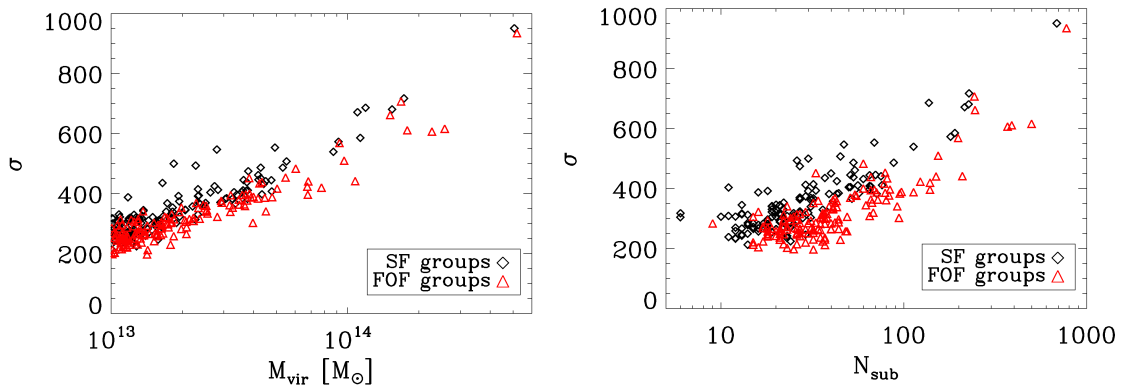


Figure 6.10: Left: Relation between σ and the virial mass at $z = 0$. Right: Relation between σ and the number of subhalos. Red symbols show the FOF groups, black symbols the SUBFIND groups.

Wilman et al. (2005b). Figure 6.11 shows the velocity dispersions for these groups in comparison with the data for our two samples. We can see that all medians

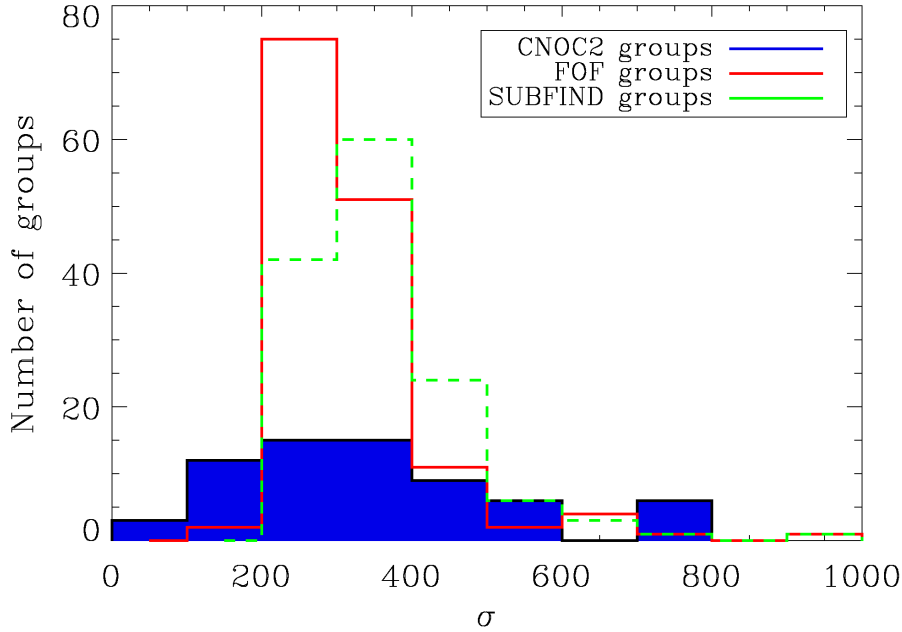


Figure 6.11: Histogram for the velocity dispersion of the FOF group sample (red) and the SUBFIND group sample (green) in comparison with the velocity dispersion of 22 groups from the CNOc2 survey (blue) provided by Dave Wilman. As the number of CNOc2 groups is so low in comparison with the number of groups in our samples we have shifted the histogram to three times its height for better visualization.

are in the same region. In fact for the observed groups we have a mean velocity dispersion of 347km/s as compared to 321km/s for FOF groups and 358km/s for SUBFIND groups. While these values match very well, the spread in the data from Wilman is much larger with a standard deviation of 187km/s while our samples have standard deviations of 70km/s for FOF groups and 83km/s for SUBFIND groups. However it should be noted that the sample of observed groups is naturally incomplete with regard to group detection and especially to substructure detection while in the simulation we do not have to worry about detection thresholds. This might also cause the larger spread in the observed group velocity dispersions.

Studies of the SDSS galaxy groups by McConnachie et al. (2008) also showed a peak at about $300 \frac{\text{km}}{\text{s}}$ as shown in Figure 3.9 in section 3.3.2. The mean velocity dispersion of our groups from the simulation therefore seems to be in good agreement with observations and this indicated that we have really identified galaxy group halos.

It is interesting to note that the luminous matter is a good indication for the dark matter halo dynamics.

6.6 Discussion

In this chapter we have studied the properties of substructures of group halos.

We have found a linear relation between the mass of a group halo and its number of subhalos.

As for the distribution of subhalo masses we are in good agreement with results by Angulo et al. (2008). The mass function of low and intermediate mass subhalos follows roughly a power law. Our studies show, that group mass halos seldomly contain another high mass subhalo, but a large amount of low and intermediate mass halos. Indeed, the most massive subhalo consists of about 8% of the mass of the host halo for FOF groups and just 2.5% of the mass of the host halo for SUBFIND groups. The fraction of mass contained in the second and third most massive subhalo is even smaller. Generally we see that the more massive a host halo, the larger the amount of less and intermediate mass subhalos.

Subhalos tend to merge into the host halo, so the number of subhalos in a group decreases with time, unless mass inflow provides the group with new subhalos. We have seen this behaviour in the previous chapter when we have studied starved groups in an isolated environment. Therefore we found that a starved mass accretion history and a decreasing number of subhalos in a group halo are characteristic of an isolated group environment.

We have found that subhalo-subhalo mergers within the virial radius of a host halo do occur, albeit they do not play a significant role. Usually the high mass subhalos experience a subhalo-subhalo merger with a low mass halo after being accreted by the host halo. Studying the orbits of such low mass halos showed us that these small halos get bound to the high mass halo long before the encounter with the host halo. The mass fraction between the merging partners is never below 10 : 1. However, we are limited in our analysis because we do not have complete FOF merger trees for this analysis up to now.

Finally, we have calculated the mean line of sight velocity dispersion of galaxy groups. We found a correlation between the velocity dispersion and the mass as expected, since the velocity dispersion is a measure for the depth of the potential well. As we have seen, the group mass is correlated with its number of subhalos, therefore we also found a correlation between the number of subhalos and the velocity dispersion. We compared these mean velocity dispersions with CNOC2 observations and found that they fit well.

7 Comparison with Observations

As we deal with a dark matter only simulation, we need a general way to populate dark matter halos with baryons in order to be able to make statements on galactic evolution.

We have seen in section 6.4 that the mass accretion of a halo stops when it falls into a larger halo. Furthermore a large part of its mass gets stripped by interaction. Therefore we cannot simply populate the subhalos based on their dark matter mass alone.

von Benda-Beckmann et al. (2008) found a way to work around this problem. They assume that the baryonic matter within a galaxy is concentrated towards the center of its dark matter halo, where the potential well is deepest, causing the maximum in the rotational velocity. If the halo falls into a larger halo the potential well protects much of the baryonic matter from stripping, and the maximum rotational velocity is conserved.

Therefore they assume the maximum of the rotational velocity v_{rot} to be most tightly related to the baryonic mass. Bullock et al. (2001) propose a mass-velocity relation for baryons of the form

$$\frac{M_{\text{rot}}}{h^{-1}M_{\odot}} = 10^{\alpha} \left(\frac{v_{\text{rot}}}{\text{kms}^{-1}} \right)^{\beta}.$$

The parameters α and β depend on whether the dark matter halo is isolated or a subhalo. For isolated halos Bullock et al. (2001) find $\alpha = 4.3 \pm 0.2$ and $\beta = 3.4 \pm 0.05$, for subhalos they find $\alpha = 2.6 \pm 0.75$ and $\beta = 3.9 \pm 0.25$.

In order to obtain luminosities we need to choose a mass-luminosity relation. Following von Benda-Beckmann et al. (2008) we assume a relation of the general form

$$L(M_{\text{rot}}) = L_0 \left(\frac{M_{\text{rot}}}{M_0} \right)^a \left(b + \frac{M_{\text{rot}}}{M_0} \right)^{\frac{-1}{d}}$$

with $L_0 = 5.7 \cdot 10^9 L_{\odot}$, $M_0 = 2 \cdot 10^{11} M_{\odot}$, $a = 4$, $b = 0.57$, $c = 3.78$ and $d = 0.23$.

von Benda-Beckmann et al. (2008) used this way of populating dark matter halos with baryons to study fossil galaxy groups in a cosmological Λ CDM simulation with $\Omega_0 = 0.24$, $\Omega_{\Lambda} = 0.76$ and $h = 0.73$. Their $80^3 h^{-3} \text{Mpc}^3$ box contains 512^3 particles with a mass of $4 \cdot 10^8 h^{-1} M_{\odot}$. They selected their halos with a FOF algorithm with a linking length of $b = 0.17$. For detecting the substructures within these FOF halos they used the code BDM (Bound Density Maximum) which removes all unbound particles from the halos and the remaining structures are defined as subhalos.

We will apply this population mechanism to our group samples. Populating the halos allows us to compare our groups with the observational classifications, as introduced in subsection 3.2.2.

7.1 Fossil groups

As introduced in 3.2.2 a fossil group is characterized by the large luminosity gap of $\Delta_{mag} \leq 2$ between the most luminous group member L_1 and the second luminous group member L_2 . To decide whether a group is fossil or not, we calculate this magnitude gap from the luminosities we have obtained by using the well known relation

$$\Delta_{mag} = -2.5 \log \left(\frac{L_2}{L_1} \right)$$

If the magnitude gap is greater than $\Delta_{mag} = 2$ we classify the group as a fossil.

We find that in the SUBFIND sample 110 of the 131 groups are fossil, that is 84%, while in the FOF sample only 71 of the 140 groups are fossil, that is 50%. This is in agreement with the results from chapter 6, where we have seen that FOF groups do not show a mass gap in the distribution of the subhalos, while SUBFIND groups have a lack of subhalos at the high mass end.

Figure 7.1 shows the distribution of the magnitude gap for both samples at $z = 0$. The maximum for the SUBFIND sample is between two and three magnitudes, while the FOF sample clearly peaks at less than 2mag. Furthermore, the FOF groups have a generally lower magnitude gap than the SUBFIND groups within their virial radius. In fact, only one single halo has a magnitude gap of $\Delta_{mag} > 10\text{mag}$. All the other highly fossil groups from the SUBFIND sample seem to be surrounded by at least one more massive halo which has not passed the virial radius yet but is near enough to get connected to the halo by the FOF algorithm.

An interesting question is whether the fossilicity of a group is correlated with the formation redshift or not, because fossil groups are usually assumed to be old groups, which have reached the end of their evolution. Thus it is interesting that we can confirm this trend but there are some rather young fossil groups as well, as can be seen in figure 7.2.

This result is in agreement with the results from von Benda-Beckmann et al. (2008), as they also found a generally higher formation redshift for fossil groups than for other groups, but nevertheless some fossil groups that are much younger than expected. On the other hand we have a significant fraction of groups with extremely high magnitude gaps that von Benda-Beckmann et al. (2008) have not found in their sample. This might be due to their different way of detecting subhalos within the FOF groups.

Related to the question of the age of fossil groups is the question how long they are already fossils. Although fossil groups are expected to be old, virialized groups and therefore the fraction of fossil groups is expected to increase with time, we find that the fraction of fossil groups stays nearly constant with time and holds about 75% of

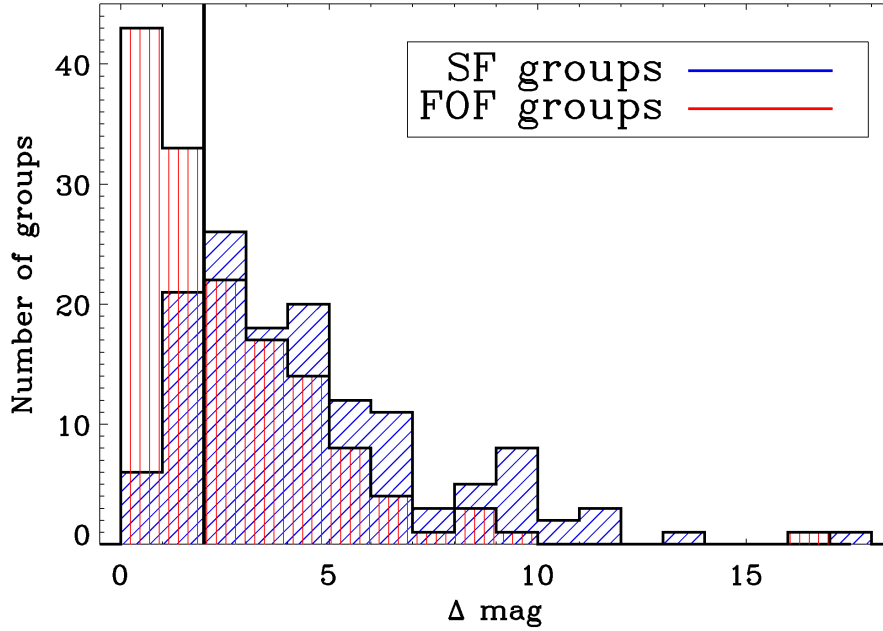


Figure 7.1: This histogram shows the magnitude gap between the most luminous and the second luminous member of the groups at $z = 0$. The red histogram is for the FOF group sample, the blue one is for the SUBFIND sample. The black line marks the fossility border at 2mag.

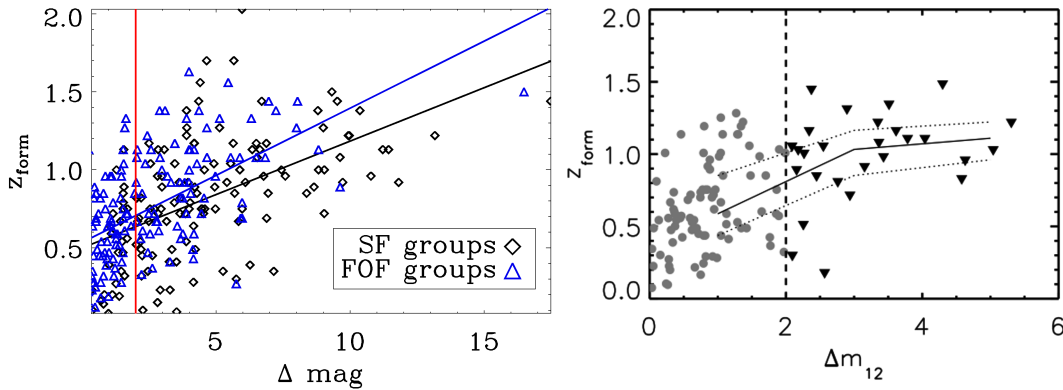


Figure 7.2: In this figure the formation redshift for every group is plotted against its magnitude gap between the two most luminous members. Left: The groups from our simulation. The red line shows the critical value of $\Delta_{\text{mag}} = 2\text{mag}$ with fossils on the right hand side. The blue line is a χ^2 -fitted line to the SUBFIND data with $z_{\text{form}} = 0.07\Delta_{\text{mag}}$, the black line is a χ^2 -fitted line to the FOF data with $z_{\text{form}} = 0.09\Delta_{\text{mag}}$. Right: Figure 3 from von Benda-Beckmann et al. (2008). Triangles are fossil groups, circles the non-fossil groups. The solid line is the mean, the dashed lines are the lower and upper quartiles.

all halos with group mass, as can be seen in Figure 7.3. This is also in accordance with the results by von Benda-Beckmann et al. (2008). A possible explanation for

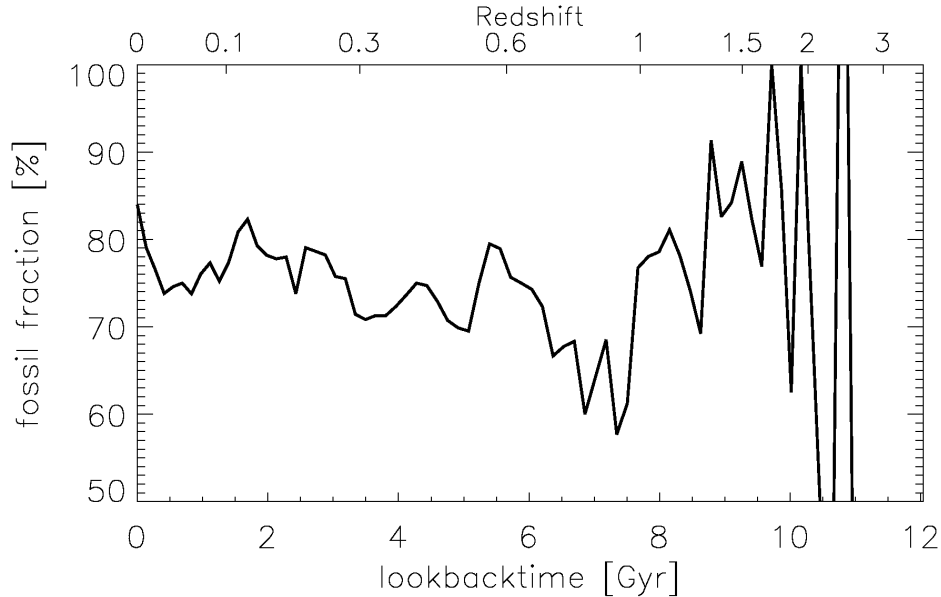


Figure 7.3: Fraction of fossil groups in the SUBFIND sample with redshift.

this behaviour might be that the SUBFIND groups just include the mass within in virial radius of the central halo. When a halo falls into a larger halo, its mass gets stripped and a significant part of it falls into the central halo. Therefore, the central halo grows and the subhalo has a lower mass, so that only very massive infalling halos cause a low enough magnitude gap to create a non fossil group in this catalogue. Since massive merger events are not common for halos with group mass of more than $1 \times 10^{13} M_{\odot}$ most of the groups are identified as fossils.

7.1.1 The Most Fossil Group

As we have seen above there is one group that has an outstanding high magnitude gap in both the SUBFIND and the FOF sample. We were especially interested in the properties of this group. In Table 7.1 the values available from our dark matter analysis for this group are shown.

| | SUBFIND | FOF |
|--------------------------------|----------------------|----------------------|
| Mass [M_{\odot}] | 1.1×10^{13} | 1.1×10^{13} |
| N_{sub} | 6 | 9 |
| z_{form} | 1.44 | 1.50 |
| σ [kms^{-1}] | 304 | 284 |
| Δ_{mag} | 17.5 | 16.5 |

Table 7.1: Values for the most fossil group.

As can be seen the group has a fairly common mass of $1.1 \cdot 10^{13} M_{\odot}$ in both samples and its velocity dispersion is ordinary, too. Everything else about this group is unusual: The number of subhalos is for both samples the lowest number of all halos, and the formation redshift is exceptionally high for a group-sized halo.

Indeed we have already encountered this group in subsection 5.1.1 as the archetype of starved growth. The mass accretion history of this most fossil group can be seen in the right panel of Figure 7.4.

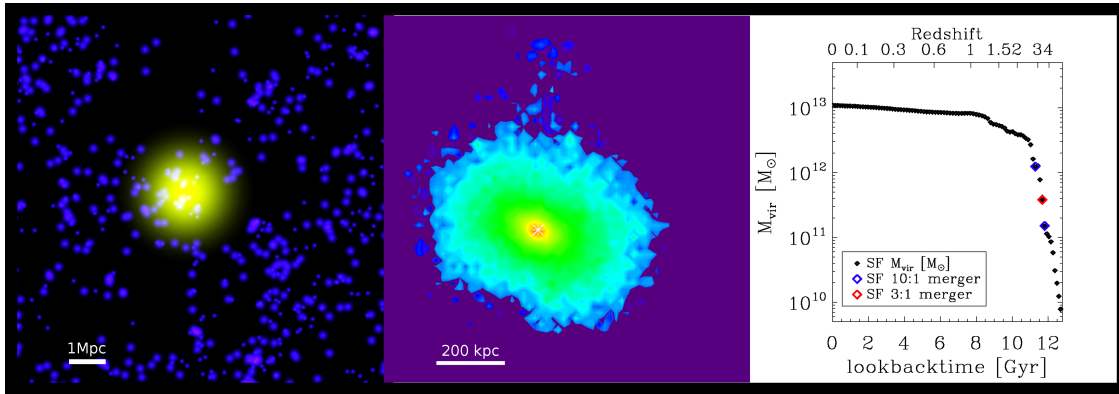


Figure 7.4: The most fossil group in our sample. The left panel shows a $10 \times 10 \times 10 h^{-3} \text{Mpc}^3$ box centered around this fossil group cut from the simulation box at $z = 0$. The blue points are all halos with masses of $10^{10} - 10^{12} M_{\odot}$, while the big yellow halo is the group halo. The size of the halo does not correlate with its virial radius and is just chosen to highlight the object. The central panel shows the density plot of the group. In this case it is exactly the same for both the FOF and the SUBFIND particle distribution. The right panel shows the mass accretion history for the halo. FOF and SUBFIND morphology are indistinguishable.

Its density plot, shown in the central panel of Figure 7.4 shows a single central halo and the FOF and the SUBFIND morphologies are nearly identical. Thus the mass of this object is completely within its virial radius and therefore this group can be assumed to be virialized. This is in agreement with the starved mass accretion history and the high formation redshift, which indicates, that the group has not evolved significantly for a long time.

Another hint at advanced relaxation of this group is the low number of subhalos at $z = 0$ and their decreasing number with time. Together with the fact, that the remaining subhalos have all very low mass this shows, that the group has been isolated enough to not grow furthermore by the infall of other halos.

The lack of infalling material over such a long period of time suggests that this group is located in a low density environment. Therefore, we have cut out a $10 \times 10 \times 10 \text{Mpc}^3$ box centered around this fossil group from the whole box at $z = 0$. The result is shown in the left panel of Figure 7.4. There is no clear sign of any filamental structure around the group and the number of surrounding halos is low.

7.2 Compact Groups

As we have discussed in subsection 3.2.2, Hickson defined a group to be compact if the following criteria are satisfied (Hickson, 1982):

1. Population: $N \geq 4$
2. Luminosity: $m \leq m_{Br} + 3$
3. Isolation: $\theta_N \geq 3\theta_G$
4. Compactness: Mean surface brightness $\mu_G < 26.0 \text{mag/arcsec}^2$

We tried to apply these observational constraints to our group sample. In order to test these we have to take projectional effects into account. Every group with at least four members, that satisfy the luminosity criterion 2, was projected to 172 different planes in the same way we used to calculate the mean projected velocity dispersion for our groups. Then we calculated the surface brightness within the smallest circle encompassing all group members (the algorithm for determination of this circle is described in Appendix C). For practical reasons the isolation criterion was ignored.

At $z = 0$ we found no compact groups in our SUBFIND group sample, but in the FOF sample we found at least 3 groups that fulfill all criteria and 17 groups that are classified as compact when we lower the population criterion from four to three. One of the three compact groups is shown in Figure 7.5. The left panel shows the environment of the compact group. As can be seen the environment of this group is very dense and there are several filamental structures leading towards the group. The group itself is shown in the central panel of figure 7.5 and consists of several substructure cores. Instead of the oval structure that is typical for the groups that consist of only one central halo this group is elongated. Its mass accretion history shows the difference between the evolution of the most massive substructure and the whole group.

This study has shown that compact groups can only be found by the Friends of Friends algorithm and not by the SUBFIND algorithm. A possible explanation for this is that a large fraction of the mass of a dark matter halo gets stripped when it

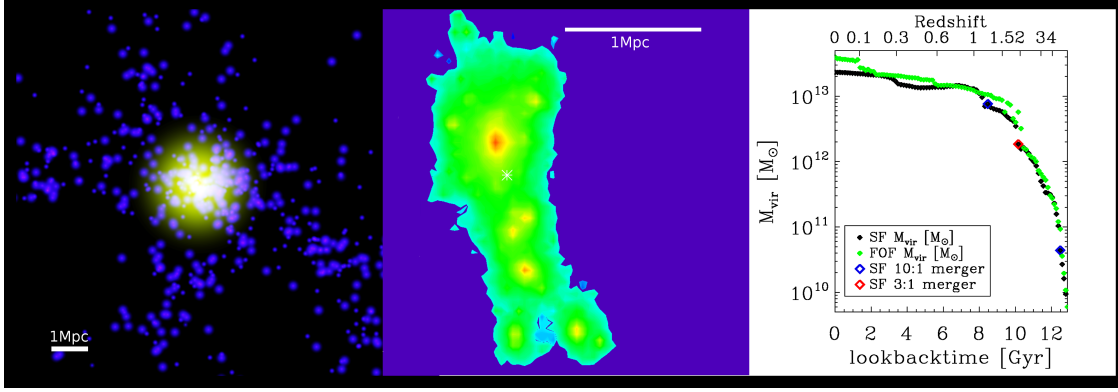


Figure 7.5: A typical compact group from the FOF group sample. The left panel shows a $10 \times 10 \times 10 \text{Mpc}^3$ box centered around the compact group cut from the whole simulation box at $z = 0$. The blue points are all halos with masses of $10^{10} - 10^{12} M_{\odot}$, while the big yellow halo is the group halo. The size of the halo is not correlated with its virial radius and is just chosen to highlight the object. The central panel shows the density plot of the group. The right panel shows the mass accretion history for the halo. The green symbols show the mass accretion of the FOF halo, the black symbols show the mass accretion history of the FOF-groups most massive SUBFIND halo.

falls into another larger halo. Since SUBFIND just finds halos within a virial radius, all substructures are less massive than the substructures of the FOF groups that are isolated SUBFIND halos.

Another reason for this might be that the population of the halos with baryons by the maximum circular velocity is not a good fit. We will test this in the following section by comparing the luminosity directly with observed velocities.

7.3 Luminosity of the Most Luminous Group Member

Up to now we have just studied differences between the calculated luminosities of our groups. We now want to compare the absolute luminosity values available with the populating mechanism explained above. Therefore we want to compare with observational results from the CNOC2 survey. We use again the data for 22 galaxy groups in a redshift range of $0.3 \leq z \leq 0.5$ provided by Dave Wilman (Wilman et al. (2005b)).

Since we got the absolute magnitude M_B of the brightest group member from the CNOC2 observations we are able to calculate the absolute luminosity L for the brightest group member by using:

$$L = 10^{-\frac{M_B - 4.74}{2.5}} [L_{\odot}].$$

The results can be seen in Figure 7.6. The observational data are more widely

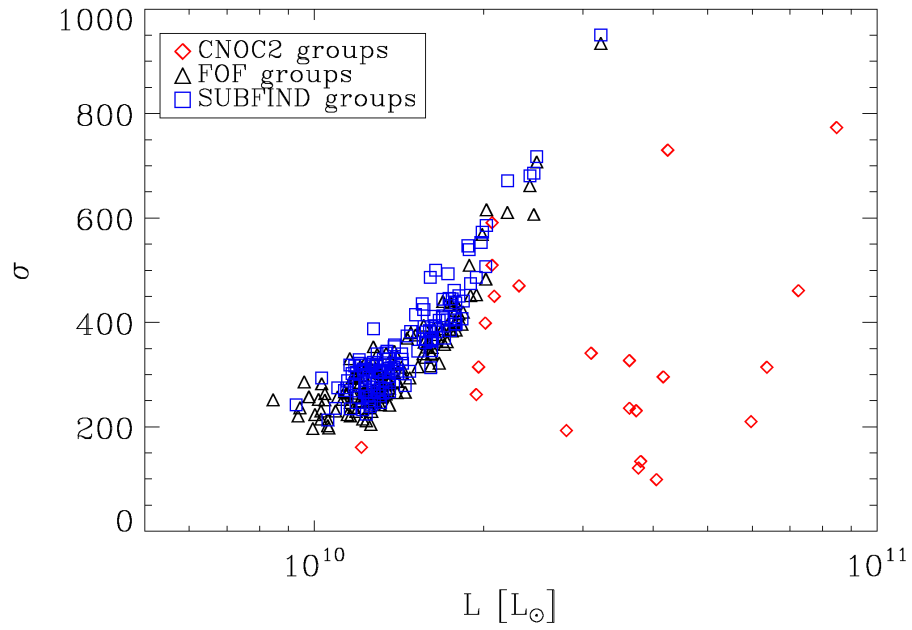


Figure 7.6: Group velocity dispersion σ versus the luminosity of the brightest group member. The red points are the observational data from the CNOC2 survey provided by D. Wilman, the black symbols are the results for our FOF-group sample, the blue ones are the results for our SUBFIND groups.

spread and show a generally higher luminosity. Obviously our population mechanism provides us with terribly bad luminosities.

7.4 Discussion

We have tried to populate our dark matter halos with baryons by a simple relation between the maximum rotational velocity of the subhalos and their baryonic mass. This was just a first test to see whether our results could fit observations or not. This population mechanism provided us with a set of luminosities which fit observations not very well. The calculated luminosities for the brightest galaxy in a group lie at the lower border of the luminosity range found for the sample of 22 CNOC2 groups that we compared with.

Therefore this simple relation does not fit reality well enough to use it for populating dark matter halos with baryons. We will explore other population models like the halo occupation distribution (HOD) models (see for example van den Bosch et al., 2007) and study hydrodynamic simulations.

In summary we can say that this populating mechanism is not a good choice for calculating the baryonic mass within dark matter group halos and subhalos.

Nevertheless, we found that the groups characterized as fossils are the same we found in chapter 5 to be characterized by a single large halo and a starved mass accretion history for both the FOF and the SUBFIND sample. Therefore we can assume that there might be a correlation between this kind of galaxy group and the starved mass accretion. The same applies to the compact groups. We only classified halos as compact groups that belong to the FOF catalogue and therefore are not lying within the virial radius of the most massive group member. In particular, the group halos classified as compact halos are all protoclusers or aggregation groups in the archetype classification of section 4.2.

This is a further evidence that the two catalogues FOF and iso-SUBFIND do find different types of groups and therefore a combined study of both catalogues is necessary.

8 Summary: the Evolution of Groups of Galaxies

In the Λ CDM scenario galaxies are supposed to form in extended dark matter halos, while the dark matter halos themselves grow hierarchically, that is large structures are assembled by smaller halos. Since groups of galaxies are objects with high masses they are supposed to form at low redshifts. It is still an open question whether galaxy groups have a global dark matter halo or if they are just an assembly of mass in the course of merging to form a larger dark matter structure with several baryonic galaxy cores interacting within the halo.

Mass Accretion History

In order to understand the nature of groups in Λ CDM cosmologies, we studied the mass accretion history and the evolution of subhalo number of both group halos within a global dark matter halo defined by its virial radius (SUBFIND catalogue) and groups consisting of several of these global halos linked simply by spatial association (FOF catalogue).

We compared the global properties of these halos with studies by Li et al. (2007) and Angulo et al. (2008) and found that they are in good agreement with their results. By studying the group mass halos in detail we find interesting differences in the mass accretion history of individual groups. These mass accretion histories depend on their environment and the choice of the catalogue.

The typical evolution path of a group in a global dark matter halo can be split in two phases: an early phase dominated by the infall of a large number of subhalos, and a later phase with nearly no mass accretion and a strongly decreasing number of subhalos caused by tidal stripping disruption. These groups consist of one single, massive central halo and show a gap in the subhalo mass function at medium mass of the order of $10^{12}M_{\odot}$.

About 20% of the groups within a global dark matter halo at $z = 0$ however show signs of active development with ongoing mergers or flyby events and therefore their number of subhalos and their mass accretion history still evolves. These groups have been found to live in a dense environment with filamental structures, from which a continuous inflow of new smaller halos occurs.

The variety of mass accretion histories of groups identified by their particles distances (FOF) is even larger. They show a large amount of groups with still increasing mass accretion histories and mergers. More than half of the groups are still assembling mass, while the others consist of a global dark matter halo with some small

substructures linked to it. This indicates that not all of the groups with a global dark matter halo are frozen in this state but still live in an environment where accretion is going on, even when it is not as strong as for the high density environment halos.

In summary we find that the classification of a group can be a difficult task because group halos undergo different evolutionary stages in their life time and a huge fraction of these objects are still very active systems with ongoing accretion. Their accretion history depends strongly on their environment and is dominated by the continuous accretion of small masses.

The Formation Epoch

An important prediction of the Λ CDM model is that massive objects form at later stages of the universe. To test the time of formation for the halos in our simulation we calculated the formation redshift defined as the time a halos has assembled 50% of its present-day mass. We find that halos of group mass generally form later than smaller halos, their mean formation redshift is $\bar{z}_{form} = 0.75$ in agreement with Li et al. (2007) compared to a mean formation redshift for the whole sample of halos in our box of $\bar{z}_{form} = 1.26$.

We also investigated the rate at which group halos are produced. This rate peaks at relatively low redshift of about $z = 1$ with a production rate of 22 halos per Gyr per $100^3 h^3 \text{Mpc}^3$ box and flattens for lower redshifts to about 12 halos per Gyr per $100^3 h^3 \text{Mpc}^3$. In agreement with predictions from hierarchical growth there are no group halos at redshifts earlier than $z = 2$.

Merger Events in Group Halos

Furthermore we studied major merger events since these are very violent events that are supposed to create for example central elliptical galaxies of groups. We find that major mergers of a ratio of less than 3 : 1 do not play a significant role in the formation of galaxy groups with global dark matter halos, since only half of the groups have one major merger in their main branch. For the linked groups (FOF) the fraction of major mergers is higher, the typical group halo has about three major mergers into its main branch of the tree during its formation history. There is no correlation between the present-day mass of the group and its number of major mergers, but the total number of mergers is correlated with the present-day mass.

From our study of group mergers and the multiple merger fraction we find that the definition of a mass ratio of 3 : 1 is not a good choice for analysing galaxy group dark matter halos, since even the merger of a less massive with a medium massive group halo does not count as major merger, although this is a fairly massive event. 20 : 1 mergers and multiple mergers are still found today in a significant amount, and since a halo with about $10^{12} M_{\odot}$ still hosts a galaxy of Milky Way mass these could be encounters observers see in galaxy groups.

The Substructure of Galaxy Groups

We also studied mergers of subhalos within such a group halo. We find that this kind of merger only occurs for the most massive substructures in groups which accrete a small halos, therefore these events are never more massive than a 10 : 1 merger. These subhalo-subhalo mergers are rare for our group sample, but since the smaller merging partner of these mergers is a low mass halo this might result from the resolution limit. A dark matter halo hosting a galaxy comparable to the Milky Way can therefore still accrete a companion galaxy of the order of the mass of the magellanic clouds if it is part of a galaxy group. Limited by the resolution of our simulation box we cannot study subhalo-subhalo mergers with merging partners of the mass of a satellite galaxy like Sculptor, which only has a mass of about $3 \cdot 10^7 M_{\odot}$ (Łokas, 2009). We will try to analyse such subhalo-subhalo mergers in resimulations with higher resolution in the future.

9 Outlook

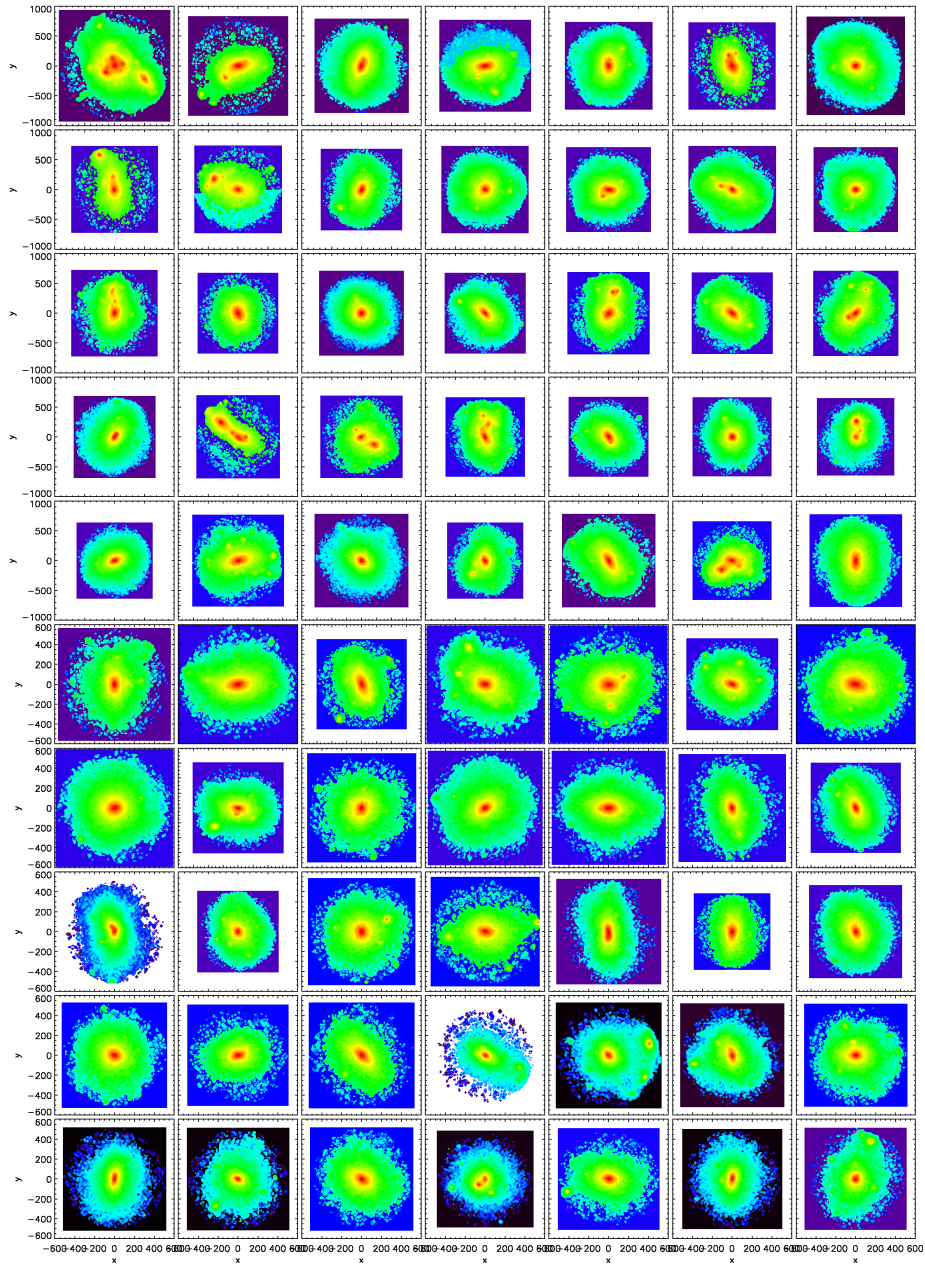
So far we have studied the properties of dark matter group halos in detail. Nevertheless there are still some problems to be solved in the future.

First we want to take a closer look at the impact of the multiple merger fraction on the evolution of the group halos and compare this with the fraction for halos in different mass ranges to better understand these processes. Since galaxy groups are an environment with strong galaxy interactions and mergers we expect the multiple merger fraction to be important for groups.

Another open question concerns the study of subhalo-subhalo mergers in groups. We will continue studying these mergers for FOF group halos so that we obtain one more generation of subhalos and compare this to the results by Angulo et al. (2008). Furthermore we have seen that we are limited by the resolution limit of our box and since in the case of subhalo-subhalo mergers one of the halos is always a very small halo we expect the resolution limit to actually reduce the rate significantly. We are resimulating group halos with interesting mass accretion histories and examine the impact of higher resolution on the subhalo-subhalo merger rate.

Finally we will explore other ways to populate our dark matter halos with baryons, since our first attempt was not very effective. There are several halo occupation distribution (HOD) models, for example by van den Bosch et al. (2007); Vale and Ostriker (2004, 2006) which provide a way to connect the galaxy groups mass to its luminosity. Another possible way to study the baryons within the dark matter galaxy groups will be to analyze the hydrodynamics simulation which is available now for the dark matter box we have used.

A The SUBFIND Groups



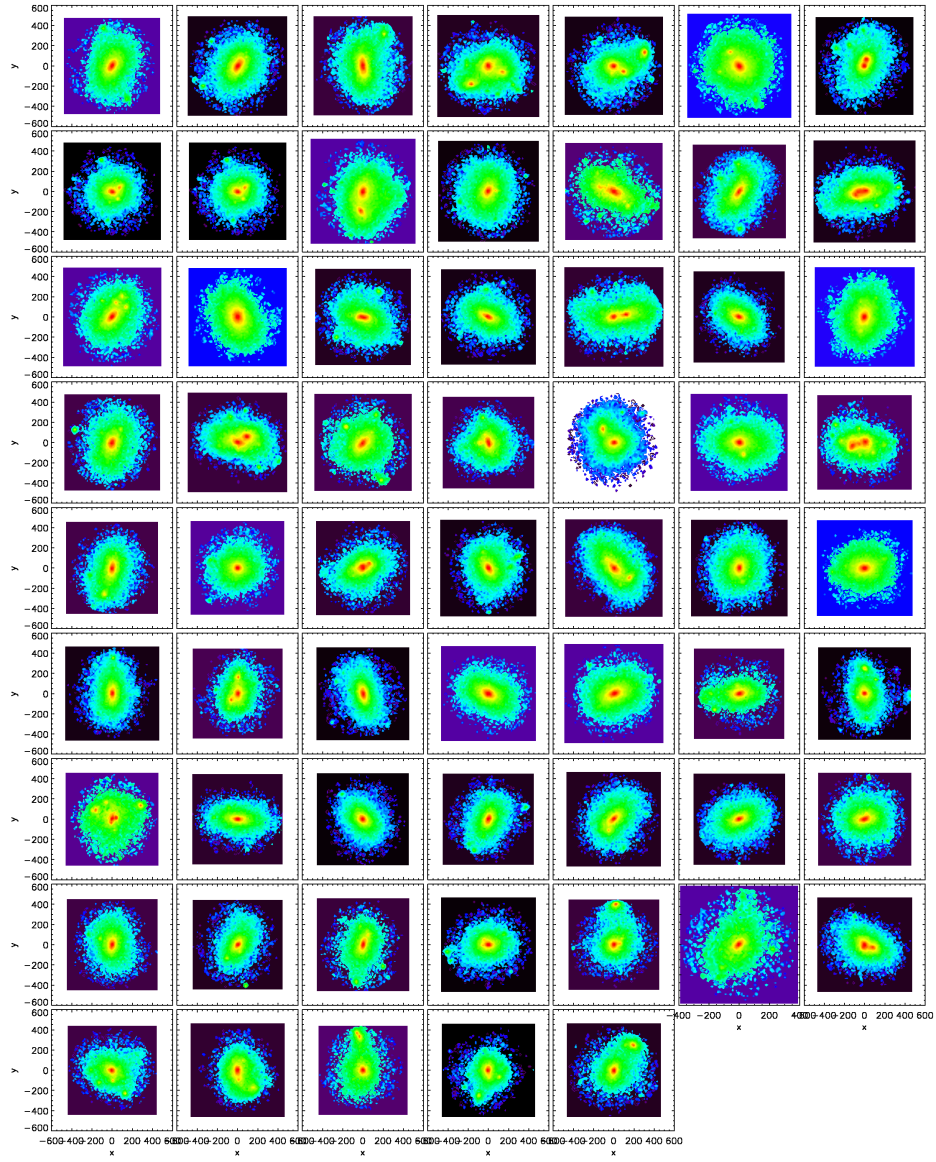
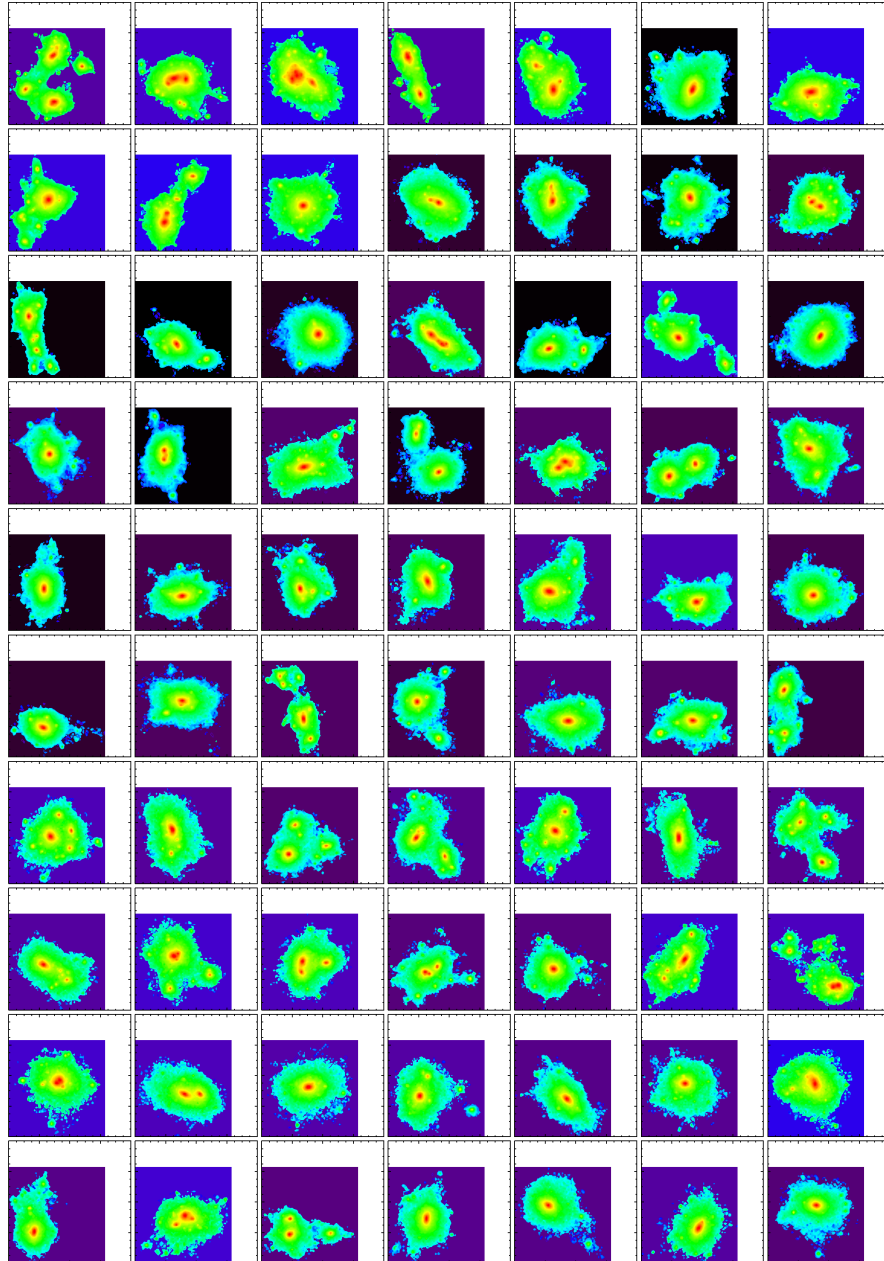


Figure A.1: Density plots for all halos identified as groups in the SUBFIND halo catalogue at $z = 0$.

B The FOF Groups



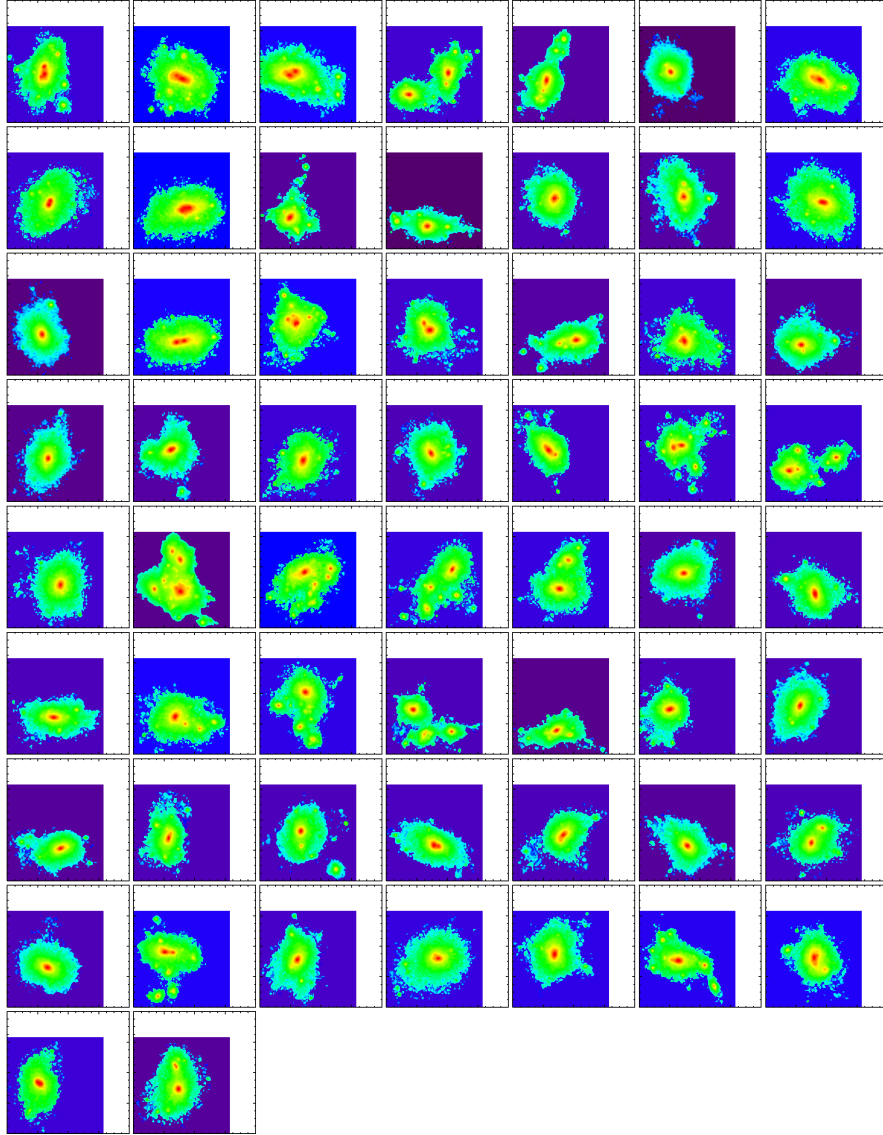


Figure B.1: Density plots for all halos identified as groups in the FOF halo catalogue at $z = 0$.

C Calculating the Group Radius

Let M be a finite subset of \mathbb{R}^2 . We are looking for a point $p \in \mathbb{R}^2$ such that $r(p) = \max_{x \in M} d(p, x)$ is minimal where d is the euclidean metric. If M has more than one element, it is obvious that $d(p, x) = r(p)$ must hold for at least two $x \in M$, because otherwise $r(p)$ could be reduced by moving p closer to the point furthest away from p . Therefore p must lie on one of the perpendicular bisectors of the connections of two points of M . Moving p around even further we see that p is either directly in the middle of two points of M or on the intersection of two perpendicular bisectors. These are the candidates for p and for every of these points we need to determine r . Given two points $u, v \in M$, their center is $(u+v)/2$. For the intersection of two perpendicular bisectors, assume we have four points, $u, v, w, x \in M$. Of those points two might be equal, in this case assume that $v = w$, then everything remains true. The point of intersection is attained, when

$$\frac{1}{2} \begin{pmatrix} u_1 + v_1 \\ u_2 + v_2 \end{pmatrix} + t \begin{pmatrix} u_2 - v_2 \\ v_1 - u_1 \end{pmatrix} = \frac{1}{2} \begin{pmatrix} w_1 + x_1 \\ w_2 + x_2 \end{pmatrix} + u \begin{pmatrix} w_2 - x_2 \\ x_1 - w_1 \end{pmatrix}.$$

Solving this linear system yields us

$$t = \frac{(w_1 + x_1 - u_1 - v_1)(w_1 - x_1) - (w_2 + x_2 - u_2 - v_2)(x_2 - w_2)}{4((u_2 - v_2)(w_1 - x_1) - (x_2 - w_2)(v_1 - u_1))}.$$

From this we can compute all the candidates for the group center and choose the one with minimal r . An example of this can be seen in figure C.1

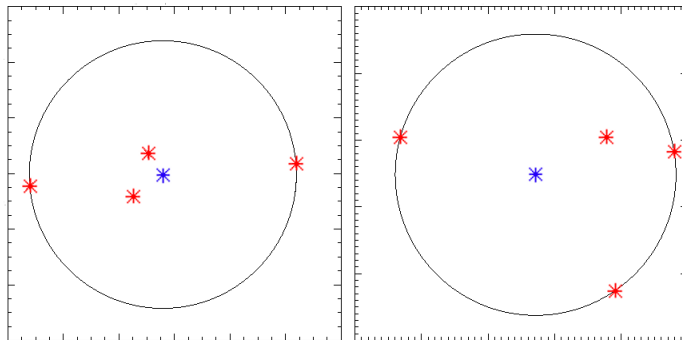


Figure C.1: Left: A group (red points) where p (blue point) is at the midpoint of the line connecting two points. Right: A group where p is in the circumcenter of the triangle defined by three points of the group.

Bibliography

- Angulo, R. E., Lacey, C. G., Baugh, C. M., and Frenk, C. S. (2008). The Fate of Substructures in Cold Dark Matter Haloes. *ArXiv e-prints*.
- Athanassoula, E., Makino, J., and Bosma, A. (1997). Evolution of compact groups of galaxies - I. Merging rates. *Monthly Notices of the Royal Astronomical Society*, 286:825–838.
- Bennett, C., Halpern, M., Hinshaw, G., Jarosik, N., Kogut, A., Limon, M., Meyer, S., Page, L., Spergel, D., Tucker, G., Wollack, E., Wright, E., Barnes, C., Greason, M., Hill, R., Komatsu, E., Nolte, M., Odegard, N., Peiris, H., Verde, L., and Weiland, J. (2003). First year wilkinson microwave anisotropy probe (wmap) observations: Preliminary maps and basic results. *The Astrophysical Journal*, 148.1:1–27.
- Berlind, A. A., Frieman, J. A., Weinberg, D. H., Blanton, M. R., Warren, M. S., Abazajian, K., Scranton, R., Hogg, D. W., Scoccamarro, R., Bahcall, N. A., Brinkmann, J., III, J. R. G., Kleinman, S. J., Krzesinski, J., Lee, B. C., Miller, C. J., Nitta, A., Schneider, D. P., Tucker, D. L., and Zehavi, I. (2006). Percolation galaxy groups and clusters in the sdss redshift survey: Identification, catalogs, and the multiplicity function. *The Astrophysical Journal*, 167.1:1–25.
- Boylan-Kolchin, M., Ma, C.-P., and Quataert, E. (2008). Dynamical friction and galaxy merging time-scales. *Monthly Notices of the Royal Astronomical Society*, 383:93–101.
- Bullock, J. S., Kolatt, T. S., Sigad, Y., Somerville, R. S., Kravtsov, A. V., Klypin, A. A., Primack, J. R., and Dekel, A. (2001). Profiles of dark haloes: evolution, scatter and environment. *Monthly Notices of the Royal Astronomical Society*, 321:559–575.
- Clemens, D. P. (1985). Massachusetts-Stony Brook Galactic plane CO survey - The Galactic disk rotation curve. *The Astrophysical Journal*, 295:422–428.
- Coles, P. and Lucchin, F. (1995). *Cosmology – The origin and evolution of cosmig structure*. Wiley, Chichester.
- Colless, M. (1999a). First results from the 2df galaxy redshift survey. *Royal Society of London Phil Tr A*, 357.1750:105.
- Colless, M. (1999b). Redshift surveys and cosmology. arXiv:astro-ph/9911326v1.

Bibliography

- Da Rocha, C. and Mendes de Oliveira, C. (2005). Intragroup diffuse light in compact groups of galaxies: HCG 79, 88 and 95. *Monthly Notices of the Royal Astronomical Society*, 364:1069–1081.
- Da Rocha, C., Ziegler, B. L., and Mendes de Oliveira, C. (2008). Intragroup diffuse light in compact groups of galaxies - II. HCG 15, 35 and 51. *Monthly Notices of the Royal Astronomical Society*, 388:1433–1443.
- Dekel, A. and Ostriker, J. P., editors (1999). *Formation of structure in the universe*. Cambridge university press.
- D’Onghia, E., Sommer-Larsen, J., Romeo, A. D., Burkert, A., Pedersen, K., Portinari, L., and Rasmussen, J. (2005). The Formation of Fossil Galaxy Groups in the Hierarchical Universe. *The Astrophysical Journal*, 630:L109–L112.
- Dressler, A. (1984). The Evolution of Galaxies in Clusters. *Annual review of astronomy and astrophysics*, 22:185–222.
- Eke, V. R., Baugh, C. M., Cole, S., Frenk, C. S., and Navarro, J. F. (2006). Galaxy groups in the 2dF Galaxy Redshift Survey: the number density of groups. *Monthly Notices of the Royal Astronomical Society*, 370:1147–1158.
- Eke, V. R., Baugh, C. M., Cole, S., Frenk, C. S., Norberg, P., Peacock, J. A., Baldry, I. K., Bland-Hawthorn, J., Bridges, T., Cannon, R., Colless, M., Collins, C., Couch, W., Dalton, G., de Propris, R., Driver, S. P., Efstathiou, G., Ellis, R. S., Glazebrook, K., Jackson, C., Lahav, O., Lewis, I., Lumsden, S., Maddox, S., Madgwick, D., Peterson, B. A., Sutherland, W., and Taylor, K. (2004). Galaxy groups in the 2dFGRS: the group-finding algorithm and the 2PIGG catalogue. *Monthly Notices of the Royal Astronomical Society*, 348:866–878.
- Frenk, C. S., White, S. D. M., Davis, M., and Efstathiou, G. (1988). The formation of dark haloes in a universe dominated by cold dark matter. *The Astrophysical Journal*, 327:507–525.
- Gao, L., White, S. D. M., Jenkins, A., Stoehr, F., and Springel, V. (2004). The subhalo populations of Λ CDM dark haloes. *Monthly Notices of the Royal Astronomical Society*, 355:819–834.
- Genel, S., Genzel, R., Bouché, N., Naab, T., and Sternberg, A. (2008). The halo merger rate in the Millennium Simulation and implications for observed galaxy merger fractions. *ArXiv e-prints*.
- Girardi, M. and Giuricin, G. (2000). The Observational Mass Function of Loose Galaxy Groups. *The Astrophysical Journal*, 540:45–56.
- Goto, T., Yamauchi, C., Fujita, Y., Okamura, S., Sekiguchi, M., Smail, I., Bernardi, M., and Gomez, P. L. (2003). The morphology-density relation in the Sloan Digital Sky Survey. *Monthly Notices of the Royal Astronomical Society*, 346:601–614.

- Governato, F., Tozzi, P., and Cavaliere, A. (1996). Small Groups of Galaxies: A Clue to a Critical Universe. *The Astrophysical Journal*, 458:18–+.
- Götz, M., Huchra, J. P., and Brandenberger, R. H. (1998). Group identification in n-body simulations: Skid and denmax versus friends-of-friends. astro-ph/9811393v1.
- Helsdon, S. F. and Ponman, T. J. (2003). The morphology-density relation in X-ray-bright galaxy groups. *Monthly Notices of the Royal Astronomical Society*, 339:L29–L32.
- Hickson, P. (1982). Systematic properties of compact groups of galaxies. *The Astrophysical Journal*, 255:382–391.
- Hickson, P., Kindl, E., and Huchra, J. P. (1988). Morphology of galaxies in compact groups. *The Astrophysical Journal*, 331:64–70.
- Hunsberger, S. D., Charlton, J. C., and Zaritsky, D. (1998). The Luminosity Function of Galaxies in Compact Groups. *The Astrophysical Journal*, 505:536–557.
- Jeltema, T. E., Mulchaey, J. S., Lubin, L. M., and Fassnacht, C. D. (2007). The Evolution of Galaxies in X-Ray-luminous Groups. *The Astrophysical Journal*, 658:865–883.
- Jenkins, A., Frenk, C. S., Pearce, F. R., Thomas, P. A., Colberg, J. M., White, S. D. M., Couchman, H. M. P., Peacock, J. A., Efstathiou, G., and Nelson, A. H. (1998). Evolution of Structure in Cold Dark Matter Universes. *The Astrophysical Journal*, 499:20–+.
- Jones, L. R., Ponman, T. J., Horton, A., Babul, A., Ebeling, H., and Burke, D. J. (2003). The nature and space density of fossil groups of galaxies. *Monthly Notices of the Royal Astronomical Society*, 343:627–638.
- Kautsch, S. J., Gonzalez, A. H., Soto, C. A., Tran, K.-V. H., Zaritsky, D., and Moustakas, J. (2008). Forming Early-Type Galaxies in Groups Prior to Cluster Assembly. *The Astrophysical Journal*, 688:L5–L8.
- Komatsu, E., Dunkley, J., Nolta, M., Bennett, C., Gold, B., Hinshaw, G., Jarosik, N., Larson, D., Limon, M., Page, L., Spergel, D., Halpern, M., Hill, R., Kogut, A., Meyer, S., Tucker, G., Weiland, J., Wollack, E., and Wright, E. (2008). Five-year wilkinson microwave anisotropy probe (wmap) observations: Cosmological interpretation. 2008arXiv0803.0547K.
- La Barbera, F., de Carvalho, R. R., de la Rosa, I. G., Sorrentino, G., Gal, R. R., and Kohl-Moreira, J. L. (2008). On the Nature of Fossil Galaxy Groups: Are they really fossils ? *ArXiv e-prints*.

Bibliography

- Li, Y., Mo, H. J., van den Bosch, F. C., and Lin, W. P. (2007). On the assembly history of dark matter haloes. *Monthly Notices of the Royal Astronomical Society*, 379:689–701.
- Lin, H., Yee, H., Carlberg, R., Morris, S., Sawicki, M., Patton, D., Wirth, G., Shepherd, C., Ellingson, E., Schade, D., Marzke, R., and Pritchet, C. (1998). Results on galaxy evolution from the cnoc2 field galaxy redshift survey. *ASP Conference Series*, 146:190.
- Lokas, E. L. (2009). The mass and velocity anisotropy of the Carina, Fornax, Sculptor and Sextans dwarf spheroidal galaxies. *Monthly Notices of the Royal Astronomical Society*, 394:L102–L106.
- Longair, M. S. (2008). *Galaxy Formation*. Springer, Berlin Heidelberg New York, second edition edition.
- Lynden-Bell, D. (1967). Statistical mechanics of violent relaxation in stellar systems. *Monthly Notices of the Royal Astronomical Society*, 136:101–+.
- Mamon, G. A. (1992). Are cluster ellipticals the products of mergers? *The Astrophysical Journal*, 401:L3–L6.
- Maulbetsch, C., editor (2007). *The Dependence of the Mass Assembly History of Cold Dark Matter Halos on Environment*.
- Maulbetsch, C., Avila-Reese, V., Colin, P., Gottlöber, S., Khalatyan, A., and Steinmetz, M. (2007). The dependence of the mass assembly history of cold dark matter halos on environment. *The Astrophysical Journal*, 654.1:53–65.
- McConnachie, A., Patton, D., Ellison, S., and Simard, L. (2008). Compact groups in theory and practice - III. Compact groups of galaxies in the Sixth Data Release of the Sloan Digital Sky Survey. *ArXiv e-prints*.
- Mukhanov, V. (2005). *Physical Foundations of Cosmology*. Cambridge University Press.
- Press, W. H. and Schechter, P. (1974). Formation of Galaxies and Clusters of Galaxies by Self-Similar Gravitational Condensation. *The Astrophysical Journal*, 187:425–438.
- Riess, A. G., Filippenko, A. V., Challis, P., Clocchiatti, A., Diercks, A., Garnavich, P. M., Gilliland, R. L., Hogan, C. J., Jha, S., Kirshner, R. P., Leibundgut, B., Phillips, M. M., Reiss, D., Schmidt, B. P., Schommer, R. A., Smith, R. C., Spyromilio, J., Stubbs, C., Suntzeff, N. B., and Tonry, J. (1998). Observational Evidence from Supernovae for an Accelerating Universe and a Cosmological Constant. *Astronomical Journal*, 116:1009–1038.

- Schneider, P. (2006). *Einführung in die Extragalaktische Astronomie und Kosmologie*. Springer, Berlin Heidelberg New York.
- Springel, V. (2005). The cosmological simulation code gadget-2. *Monthly Notices of the Royal Astronomical Society*, 364.4:1105–1134.
- Springel, V., White, S. D. M., Tormen, G., and Kauffmann, G. (2001a). Populating a cluster of galaxies – i. results at $z = 0$. *Monthly Notices of the Royal Astronomical Society*, 328.3:726–750.
- Springel, V., Yoshida, N., and White, S. D. W. (2001b). Gadget: A code for collisionless and gasdynamical cosmological simulations. *New Astronomy*, 6.2:79–117.
- Sulentic, J. W. and Rabaca, C. R. (1994). Optical luminosity functions for compact groups of galaxies. *The Astrophysical Journal*, 429:531–539.
- Vale, A. and Ostriker, J. P. (2004). Linking halo mass to galaxy luminosity. *Monthly Notices of the Royal Astronomical Society*, 353:189–200.
- Vale, A. and Ostriker, J. P. (2006). The non-parametric model for linking galaxy luminosity with halo/subhalo mass. *Monthly Notices of the Royal Astronomical Society*, 371:1173–1187.
- van den Bosch, F. C., Yang, X., Mo, H. J., Weinmann, S. M., Macciò, A. V., More, S., Cacciato, M., Skibba, R., and Kang, X. (2007). Towards a concordant model of halo occupation statistics. *Monthly Notices of the Royal Astronomical Society*, 376:841–860.
- von Benda-Beckmann, A. M., D’Onghia, E., Gottlöber, S., Hoefft, M., Khalatyan, A., Klypin, A., and Müller, V. (2008). The fossil phase in the life of a galaxy group. *Monthly Notices of the Royal Astronomical Society*, 386:2345–2352.
- Warren, M. S., Abazajian, K., Holz, D. E., and Teodoro, L. (2006). Precision determination of the mass function of dark matter halos. *The Astrophysical Journal*, 646:881–885.
- Wechsler, R. H., Bullock, J. S., Primack, J. R., Kravtsov, A. V., and Dekel, A. (2002). Concentrations of dark halos from their assembly history. *The Astrophysical Journal*, 568.1:52–70.
- White, S. D. M. and Rees, M. J. (1978). Core condensation in heavy halos - A two-stage theory for galaxy formation and clustering. *Monthly Notices of the Royal Astronomical Society*, 183:341–358.
- Wilman, D. J., Balogh, M. L., Bower, R. G., Mulchaey, J. S., Oemler, A., Carlberg, R. G., Eke, V. R., Lewis, I., Morris, S. L., and Whitaker, R. J. (2005a). Galaxy groups at $0.3 \leq z \leq 0.55$ - II. Evolution to $z \sim 0$. *Monthly Notices of the Royal Astronomical Society*, 358:88–100.

- Wilman, D. J., Balogh, M. L., Bower, R. G., Mulchaey, J. S., Oemler, A., Carlberg, R. G., Morris, S. L., and Whitaker, R. J. (2005b). Galaxy groups at $0.3 \leq z \leq 0.55$ - I. Group properties. *Monthly Notices of the Royal Astronomical Society*, 358:71–87.
- Wilman, D. J., Balogh, M. L., Bower, R. G., Mulchaey, J. S., Oemler, Jr, A., and Carlberg, R. G. (2005c). The CNOC2 sample of intermediate redshift galaxy groups - the powerhouse of galaxy evolution. *ArXiv Astrophysics e-prints*.
- Wilman, D. J., Oemler, Jr, A., Mulchaey, J. S., McGee, S. L., Balogh, M. L., and Bower, R. G. (2008). Morphological Composition of $z \sim 0.4$ groups: The site of S0 formation. *ArXiv e-prints*.
- Yee, H., Sawicki, M., Carlberg, R., Lin, H., Morris, S., Patton, D., Wirth, G., Shepherd, C., Ellingson, E., Schade, D., and Marzke, R. (1997). The cnoc2 field galaxy redshift survey. arXiv:astro-ph/9710356v1.
- Zabludoff, A. I. and Mulchaey, J. S. (1998). Hierarchical Evolution in Poor Groups of Galaxies. *The Astrophysical Journal*, 498:L5+.

Acknowledgements

I would like to thank Andreas Burkert for giving me the opportunity to write my diploma thesis in his CAST group and for many helpful discussions. Thanks to Ralf Bender as well for evaluating this work. There are several other people I want to thank since this thesis would not have been completed without their valueable help. Especially I would like to thank Roland Jesseit for many helpful suggestions, a lot of patience and so many things I would not have learned without him. I also wish to express my gratitude towards Dave Wilman for interesting discussions about the observational aspects of groups and the group data from the CNOC2 survey and Christano da Rocha for introducing the concept of intra group light to me. Thorsten Naab provided me with interesting ideas and helped me with IDL codes. Ludwig Oser introduced me to the simulation and provided me with some helpful programs. Michaela Hirschmann, Shy Genel and Christian Maulbetsch helped me to understand the difficulties of the merger trees and procured the merger tree files this work is based on. I also want to thank Michaela Hirschmann and Shy Genel for many helpful discussions. Finally I want to say thank you to everybody else I have talked to about my work during the time I have worked on this thesis.

Selbstständigkeitserklärung

Hiermit erkläre ich, dass ich diese Arbeit selbstständig und nur mit den angegebenen Quellen und Hilfsmitteln angefertigt habe.

München, d. 10.03.2009